A WATER TUNNEL FLOW VISUALIZATION STUDY OF THE VORTEX FLOW STRUCTURES ON THE F/A-18 AIRCRAFT

GRANTOR - NASA AMES RESEARCH CENTER

GRANTEE - CAL POLY STATE UNIVERSITY

GRANT NUMBER NCC 2-620

7/1/89 - 3/31/91

Principal Investigator
Dr. Doral R. Sandlin

Student Investigator
Edgar J. Ramirez

Cal Poly State University
San Luis Obispo, CA 93407

July 1991

ABSTRACT

A WATER TUNNEL FLOW VISUALIZATION STUDY OF THE VORTEX FLOW STRUCTURES ON THE F/A-18 AIRCRAFT

Edgar J. Ramirez

November 1990

The vortex flow structures occurring on the F/A-18 aircraft at high angles of attack have been investigated. A water tunnel was used to gather extensive flow visualization data on the forebody vortex and the wing leading-edge extension vortex. The longitudinal location of breakdown of the leading-edge vortex was found to be consistently dependent on the angle of attack. Other parameters such as Reynolds number, model scale, and model fidelity had little influence on the overall behavior of the flow structures investigated. The lateral location of the forebody vortex system was greatly influenced by changes in the angle of sideslip. Strong interactions can occur between the leading-edge extension vortex and the forebody vortex. Close attention was thus paid to vortex induced flows on various airframe components of the F/A-18. Reynolds number and angle of attack greatly affected the swirling intensity, and therefore the strength of the studied vortices. Water tunnel results on the F/A-18 correlated well with those obtained in similar studies at both full- and sub-scale levels. The water tunnel can provide, under certain conditions, good simulations of realistic flows in full-scale configurations.

TABLE OF CONTENTS

Chapter Page

List of Symbols vi

List of Tables ix

List of Figures x

1. Introduction 1

Perspective 1

The Water Tunnel as a Flow Visualization Tool 2

Leading Edge and Forebody Vortices 4

The NASA High Alpha Technology Program (HATP) 5

The Flow Field Surrounding the F/A-18 7

Vortex Flow Studies on the F/A-18 11

Project Justification and Objectives 13

2. Experimental Aspects 16

Flow Visualization Facility 16

Models 17

Data Acquisition Methods 18

Test Conditions 18

Angle of Attack 19

Angle of Sideslip 19

Free Stream Velocity 20

Engine Nacelles Flow Rate 20

Test Plan 21

3. Discussion of Results 23
Examination of Models 23
Identification of the Source of Discrepancy in
LEX Vortex Breakdown Data 25
LEX Vortex Core Breakdown 27
Effect of Angle of Attack 27
Effect of Angle of Sideslip 28
Effect of Reynolds Number 30
Effect of LEX Leading Edge Sharpness and
LEX Surface Smoothness 31
Effect of Model Scale 31
Effect of Model Fidelity 31
LEX Vortex Core Location 32
Effect of Angle of Attack 32
Qualitative analysis 32
Quantitative analysis 33
Effect of Angle of Sideslip 33
Qualitative analysis 33
Quantitative analysis 34
Effect of Reynolds Number 34
Effect of LEX Leading Edge Sharpness and
LEX Surface Smoothness 34
Effect of Scale and Model Fidelity 35
Correlations With Flight Results 35
Qualitative analysis 35

Quantitative analysis 35
Forebody Vortex Core Location 36
Effect of Angle of Attack 36
Effect of Angle of Sideslip 37
Effect of Reynolds Number 38
Effect of Forebody Geometry 38
Effect of Model Scale 39
Correlations With Results From Other Studies.....39
Location of the Forebody Primary Separation Line 40
Effect of Angle of Attack 41
Effect of Reynolds Number 41
Comparison to a CFD Prediction 42
Comparison to Flight Results 42
Interaction Between the LEX and Forebody Vortices 42
Effect of Angle of Attack 43
Effect of Angle of Sideslip 43
4. Conclusions 44
References 47
Appendix A. Computation of Engine Nacelles Flow Rate 52
Appendix B. Vortex Path Reconstruction Method 54
Appendix C. Figures 58

LIST OF SYMBOLS

A_o	capture area, in^2
Alpha	angle of attack, deg
A/C	aircraft
b	aircraft span, ft
BART	Basic Aerodynamic Research Tunnel
CFD	computational fluid dynamics
C_p	coefficient of pressure
FMS	engine flow rate meter setting
F.S., FS	fuselage station, in
FVF	Flow Visualization Facility
HARV	High Alpha Research Vehicle
HATP	High Alpha Technology Program
l, L	aircraft or model length, in
LEX	leading-edge extension
NASA	National Aeronautics and Space Administration
q_1	volume flow rate through one engine nacelle, gal/min
q_2	volume flow rate through both engine nacelles, gal/min

LIST OF SYMBOLS (continued)

Q_{max}	maximum volume flow rate through engine flow meter, gal/min
R	location of Reattachment Line
R_1	primary reattachment line location
R_2	secondary reattachment line location
R_3	tertiary reattachment line location
Re_c	Reynolds number based on mean aerodynamic chord
s	local span distance from LEX fuselage junction to LEX leading edge, in
S_1	location of primary separation line
S_2	location of secondary separation line
UHF	ultrahigh frequency
V_N	normal component of freestream velocity, in/sec
V_o	free stream velocity, in/sec
x, X	longitudinal distance along aircraft or model measured aft from nose, in
X_o	longitudinal world coordinate, in
X_p	horizontal picture coordinate, in

LIST OF SYMBOLS (concluded)

y	lateral or spanwise distance measured outboard from LEX fuselage junction, in
Y	lateral or vertical distance measured outboard or vertically from aircraft or model x axis, in
Y_o	vertical world coordinate, in
Y_p	vertical picture coordinate, in
Z_o	lateral world coordinate, in
α	angle of attack, deg
β	angle of sideslip, deg
θ	forebody, cross-sectional circumferential angle, deg

LIST OF TABLES

		Page
Table 1.	Engine Flow Rate Meter Settings as Percentage of the Maximum Meter Flow	21
Table B.1.	Example of Format Used to Arrange Data for the V.INIT File	55
Table B.2.	Example of Format Used to Arrange Data for the VORTEX.IN File	57

LIST OF FIGURES

		Page
Figure 1.	Vortex Flow Structures on the F/A-18. Angle of Attack: 30 Degrees; Angle of Sideslip: +6 Degrees	59
Figure 2.	The F/A-18 High Alpha Research Vehicle (HARV)	60
Figure 3.	The NASA Ames-Dryden Flow Visualization Facility	61
Figure 4.	Geometry Details of the F/A-18 Aircraft (Figure From Reference 38)	62
Figure 5.	Model of the Cross-Sectional Flow About the LEX of the F/A-18	63
Figure 6.	Model of the Cross-Sectional Flow About the Forebody of the F/A-18	63
Figure 7.	Pressure Distributions on the LEX and Forebody of the F/A-18 HARV (Data and Figures From Reference 32)	64
Figure 8.	Location of LEX Vortex Core Breakdown From Flight and Ground Facilities	65
Figure 9.	Schematic of the NASA Ames-Dryden Water Tunnel	66
Figure 10.	F/A-18 Models Tested	67
Figure 11.	Location of Reference Points Used to Attain a Zero-Degree Angle of Attack	68
Figure 12.	Typical Drawing Used to Determine the Angle of Sideslip	69

LIST OF FIGURES (continued)

		Page
Figure 13.	Comparison of LEX Local Span Between Water Tunnel Models	70
Figure 14.	Forebody Cross-Sectional Geometry (48A Model and MD Drawing)	71
Figure 15.	Forebody Cross-Sectional Geometry (32A Model and MD Drawing)	71
Figure 16.	Location of LEX Vortex Core Breakdown From the 48A Model and Other Flight and Ground Facilities.	72
Figure 17.	Water Tunnel Results of LEX Vortex Core Breakdown Using 1/48-scale Models of the F/A-18	73
Figure 18.	LEX Vortex Core Breakdown on the 48A Model. Alpha = 15 Degrees; Beta = 0 Degrees	74
Figure 19.	LEX Vortex Core Breakdown on the 48A Model and the 32A Model	75
Figure 20.	Longitudinal Variation in the Location of the LEX Vortex Core Breakdown With Increasing Angle of Sideslip	76-77
Figure 21.	LEX Vortex Breakdown Lateral and Longitudinal Location as a Function of Angle of Attack α, and Angle of Sideslip β	78
Figure 22.	Effect of Reynolds Number on the Location of LEX Vortex Core Breakdown Using the 32A Model	79

LIST OF FIGURES (continued)

		Page
Figure 23.	Comparison of LEX Vortex Core Breakdown Location Between the Modified and Unmodified 48A Model	79
Figure 24.	Effect of Model Scale on the Location of LEX Vortex Core Breakdown	80
Figure 25.	Effect of Model Fidelity on the Location of LEX Vortex Core Breakdown	80
Figure 26.	Variation in the Location of the LEX Vortex Core With Increasing Angle of Attack	81-83
Figure 27.	Effect of Angle of Attack (α) on the Vertical Location of the LEX Vortex Core. Angle of Sideslip $\beta = 0$ Degrees	84
Figure 28.	Effect of Angle of Attack (α) on the Lateral Location of the LEX Vortex Core. Angle of Sideslip $\beta = 0$ Degrees	85
Figure 29.	Effect of Angle of Sideslip on the Lateral Location of the LEX Vortices. Alpha = 25 Degrees; Beta= 5.5 Degrees	86
Figure 30.	Effect of Angle of Sideslip (β) on the Vertical Location of the Leeward LEX Vortex Core. Angle of Attack $\alpha = 30$ Degrees	87

LIST OF FIGURES (continued)

		Page
Figure 31.	Effect of Angle of Sideslip (β) on the Lateral Location of the Leeward LEX Vortex Core. Angle of Attack α = 30 Degrees	88
Figure 32.	Comparison of the LEX Vortex Core Location Between Water Tunnel and Flight Results	89
Figure 33.	Comparison of the LEX Vortex Core Vertical Location Between Water Tunnel and Flight Data. Angle of Attack α = 25 Degrees; Angle of Sideslip β = 0 Degrees	90
Figure 34.	Comparison of the LEX Vortex Core Lateral Location Between Water Tunnel and Flight Data. Angle of Attack α = 25 Degrees; Angle of Sideslip β = 0 Degrees	91
Figure 35.	Comparison of the LEX Vortex Core Vertical Location Between Water Tunnel and Flight Data. Angle of Attack α = 30 Degrees; Angle of Sideslip β = 0 Degrees	92
Figure 36.	Comparison of the LEX Vortex Core Lateral Location Between Water Tunnel and Flight Data. Angle of Attack α = 30 Degrees; Angle of Sideslip β = 0 Degrees	93

LIST OF FIGURES (continued)

		Page
Figure 37.	Location of Forebody Vortices. Alpha = 25 Degrees; Beta = 0 Degrees	94
Figure 38.	Location of Forebody Vortices (Effect of Angle of Sideslip). Alpha = 25 Degrees; Beta = 4.0 Degrees	95
Figure 39.	Location of Forebody Vortices (Effect of Forebody Geometry). Alpha = 30 Degrees; Beta = 0 Degrees	96
Figure 40.	Location of Forebody Vortices (Effect of Model Scale). Alpha = 25 Degrees; Beta = 0 Degrees	97
Figure 41.	Location of Forebody Vortices (Effect of Model Scale). Alpha = 30 Degrees; Beta = 0 Degrees	98
Figure 42.	Comparison of Forebody Vortex Location Between Water Tunnel and Flight Results [Ref. 23]. Alpha = 30 Degrees; Beta = 0 Degrees	99
Figure 43.	Forebody Surface Flow Visualization. Alpha = 20 Degrees; Beta = 0 Degrees	100
Figure 44.	Effect of Angle of Attack on the Location of the Forebody Primary Separation Line	101
Figure 45.	Effect of Reynolds Number on the Location of the Primary Separation Lines of the Forebody	101

LIST OF FIGURES (concluded)

		Page
Figure 46.	Comparison of the Location of the Primary Separation Line Between Water Tunnel Results and a Laminar Flow CFD Prediction [Ref. 34]. Alpha = 30 Degrees; Beta = 0 Degrees	102
Figure 47.	Location of Separation Lines From Water Tunnel and Flight Results	103
Figure 48.	Longitudinal Location of LEX/Forebody Vortex Interaction and LEX Vortex Breakdown	104
Figure 49.	Longitudinal Location of LEX/Forebody Vortex Interaction From Water Tunnel and Flight Results	104
Figure 50.	Comparison Between Flight-measured and Water Tunnel Results of the Longitudinal Location of the LEX/Forebody Vortex Interaction as a Function of the Angle of Sideslip β (α = 33 Degrees)	105
Figure B.1.	Location of Cameras and Dimensions Needed for the Vortex Path Reconstruction Technique	106
Figure B.2.	Relationships Between Distorted (d) and Undistorted (u) Picture Coordinates (All Coordinate Values in Inches)	107
Figure B.3.	Example of Results Obtained From the Vortex Path Reconstruction Algorithm	108

CHAPTER 1

Introduction

Perspective

Fighter aircraft technology has evolved significantly since World War II. More demand has been and will continue to be placed on the aircraft to fly and perform maneuvers under conditions which challenge not only the physiological capabilities of the pilot, but also the operational integrity of the aircraft itself. Because of this trend, future fighter pilots will rely heavily on the ability of their aircraft to quickly maneuver during an engagement, in order to enjoy the first shot advantage. In such an environment, aircraft should normally have the capability for flight at high angles of attack. The flow field about an aircraft flying in the high angle-of-attack regime is typically dominated by extensive three-dimensional separated flow. Powerful, concentrated vortices emanate from various locations of the aircraft, such as the fuselage forebody, wings, canards, wing leading-edge extensions, etc. Studies have shown that considerable benefits can be derived from the presence of the aforementioned vortices in the flow field. For example, leading-edge extensions can provide increases in maximum lift at high angles of attack when regular lifting surfaces are stalled. At the same time, such benefits come with their share of penalties, which are usually paid in the form of reduced aircraft agility at high angles of attack. It has been established that this loss of maneuverability (especially lateral-

directional) can be attributed to the interaction between the different vortices occurring at the high angle-of-attack condition [Refs. 1 through 4]. In response to such a drawback, different alternatives have been explored in an effort to minimize the adverse effects by manipulating these vortices [Refs. 5 and 6]. Nevertheless, because of the highly complex nature of such three-dimensional flow structures, a great deal of basic research on the subject is still needed in order to provide a better understanding of these fluid dynamics phenomena.

The present study addresses several issues pertaining to high angle-of-attack aerodynamics through a water tunnel investigation of the vortex flow structures occurring on the F/A-18 aircraft at high angles of attack. Particular attention is paid to the behavior of leading-edge extension (LEX) and forebody vortices. Vortex flow characteristics, such as vortex location, vortex breakdown, and vortex interactions are examined, as well as their sensitivity to various parameters such as angle of attack, angle of sideslip, and Reynolds number. Correlations to flight test data and to results from wind tunnels and other water tunnels are also presented.

The Water Tunnel as a Flow Visualization Tool

The study of separated flow using flow visualization techniques has traditionally been carried out in wind tunnel and full-scale flight tests. The reason for this trend is the belief that the low Reynolds number (10^3 to 10^4) typically found in water tunnels prevents the achievement of dynamic similarity, a basic requirement for the proper correlation and

extrapolation of results to full-scale configurations. Certain types of flows, however, such as vortex flows occurring at high angles of attack on thin, sharp-edged slender wings show relatively small sensitivity to variations in Reynolds number [Ref. 1]. Fighter-type aircraft which are geometrically characterized by the presence of thin, highly-swept surfaces provide a good example of configurations in which the flow field at high angles of attack is essentially vortex-dominated. In this context, vortex-dominated flows refer to those where the size of the vortices involved is substantially greater than any associated boundary layer. In some cases of particular interest, the vortices originate from separation of the lower surface flow at fixed locations along the leading edges of highly-swept wings, leading-edge extensions, canards, etc. This phenomenon occurs whether the lower surface boundary layer is laminar or turbulent. As a result, the overall behavior of leading-edge vortices is considered to be insensitive to Reynolds number [Ref. 7]. In slender bodies, such as fuselage forebodies, on the other hand, the location of separation does vary with Reynolds number. However, the structure of the vortex at high angles of attack does not change much with Reynolds number [Ref. 1], because the vortex core is located far enough from the surface of the body where viscous effects are significantly reduced.

From the preceding argument, it follows that water tunnels can provide, under certain conditions, good qualitative simulations of high angle-of-attack vortex flows encountered on thin, sharp-edged, highly-swept wings, as well as slender bodies.

Some of the vortex flow characteristics that can be assessed in a water tunnel include vortex core trajectories, vortex core breakdown, interactions among different vortex systems, and interactions of a vortex system with other airframe components.

As with any flow visualization method, water tunnels suffer from some limitations regarding the scope of the investigations that can be conducted in them. Reference 1 suggests that only flow fields that are vortex-dominated, such as those at high angles of attack, can provide good representations of higher Reynolds number flows. By contrast, vortex flows at low angles of attack (10 degrees or lower) occur at locations which are closer to body surfaces. In these regions, the flow is viscosity-dominated, and thus Reynolds number effects can increase and significantly influence vortex flow characteristics.

A thorough discussion regarding the utility of the water tunnel for the study of vortex flows can be found in Reference 1. Additionally, References 8 and 9 describe several flow visualization techniques, including the water tunnel.

Leading Edge and Forebody Vortices

A large number of studies have been conducted on the vortex structures encountered in the flow about slender bodies and highly-swept delta wings positioned at high angles of attack. Typically, the flow field in the high angle-of-attack environment involves the presence of vortex flow which originates upon separation of surface flow [Refs. 10 through 12]. In the case of delta wings, separation takes place along

the leading edge; whereas in slender bodies, separation occurs along a line extending downstream from the nose of the body. The vortices thus formed in delta wings and slender bodies are generally known as leading-edge vortices and forebody vortices, respectively. Results from different studies indicate that the behavior of both leading-edge and forebody vortices exhibits different levels of sensitivity to the variation of known parameters such as angle of attack, angle of sideslip, Reynolds number, geometry of the object, etc. [Refs. 13 through 19]. The knowledge gained from the aforementioned studies has helped explain the overall effect of vortex flow on the aerodynamic characteristics of full-aircraft configurations, both generic-type and existing fighter aircraft.

Different methods have been used to gather information on vortex flow. On the experimental side, wind tunnels, water tunnels, and full-scale aircraft have provided representative results. On the computational side, the rapidly maturing field of computational fluid dynamics (CFD) has made and will continue to make use of experimental results to develop and validate computer codes.

The NASA High Alpha Technology Program (HATP)

Several NASA research centers are currently involved in a program aimed at investigating the high angle-of-attack flight regime. The High Alpha Technology Program (HATP) is pursuing this goal through a close coordination of activities performed by ground-based and flight facilities. The overall objective of the HATP program is to

facilitate the development of technologies required to endow future fighter aircraft with unprecedented capability for flight at high angles of attack. Specific objectives of the program are:

1. The development of flight-validated design methods to accurately predict the aerodynamics and flight mechanics of aircraft flying at high angles of attack.

2. The development of advanced technologies to significantly improve the handling qualities of current and future fighter aircraft.

The Northrop/McDonnell Douglas F/A-18 aircraft configuration was selected as the primary testbed for the HATP program. This decision was made after careful consideration of key aspects pertaining to high angle-of-attack technology and the potential usage of several airplanes for flight validation of results from ground-based research [Ref. 20]. The F/A-18 provides a prime example of the highly vortical nature of the flow typically found in advanced fighter aircraft. The two main vortex systems present in the F/A-18 are the LEX vortex and the forebody vortex (see Figure 1).

Three specific areas of study are contemplated in the HATP program. They are high angle-of-attack aerodynamics, advanced control concepts for high angle-of-attack conditions, and maneuver management.

In the area of aerodynamics, NASA Ames-Dryden Flight Research Facility is contributing to the HATP program in various ways [Ref. 21]. A heavily-instrumented F/A-18 aircraft known as the High Alpha Research Vehicle or HARV (see Figure 2) has been used in

conjunction with a water tunnel facility (see Figure 3) to gather extensive flow visualization data of the vortex flow structures on the F/A-18. Some of the vortex flow aspects investigated on the F/A-18 through the HATP program include: (1) characteristics of the surface flow on the fuselage forebody and LEX, (2) location of forebody vortices, (3) location of the LEX vortices and their breakdown, (4) interaction between LEX and forebody vortices, (5) distribution of the surface pressure on the forebody and LEX, (6) effect of LEX vortex breakdown on empennage buffeting, and (7) effect of forebody and LEX vortices on the stability characteristics of the F/A-18.

The Flow Field Surrounding the F/A-18

The F/A-18 is a single place, twin engine, multi-purpose, high performance aircraft manufactured by McDonnell Douglas Corporation and Northrop Corporation for the US Navy and the US Marine Corps. The aircraft has the capability for flight at high angles of attack, making it a prime candidate for research in this flight regime.

Mounted on each side of the aircraft fuselage are wing leading-edge extensions (LEX's), which are located between fuselage stations 191 and 401. Some cross-sectional views of the aircraft are shown in Figure 4. The fuselage forebody is composed of an ogive nose cone with a circular cross section, which gradually evolves into an oblate, elliptical fuselage.

At high angles of attack, the flow field about the LEX's features a system of vortices as shown in Figure 5. The approaching flow (V_N)

first attaches to the lower surface of the LEX and turns outboard towards the leading edge. Because of the sharp turn at the leading edge, the flow is forced to separate (S_1) forming a shear layer or vortex sheet. A primary vortex is then formed as the vortex sheet rolls up inboard attracted by a low pressure region. Part of the flow coming over the primary vortex reattaches to the upper surface of the LEX (R_1) and begins traveling outboard. The reattached flow is first accelerated and then decelerated until separation occurs (S_2), from which a much weaker counter-rotating secondary vortex develops. An even weaker tertiary vortex rotating in the same direction as the primary vortex is further formed as flow coming from over the secondary vortex reattaches (R_2), migrates inboard, and separates (S_3). The location of the secondary and tertiary vortices can, in turn, influence the location of the primary vortex. Studies have shown that the location of the secondary vortex in slender delta wings is highly dependent on Reynolds number due to the closeness of the vortex to the wing surface where the flow is viscosity-dominated [Ref. 22]. Throughout this report the primary LEX vortex will be referred to as the LEX vortex.

As with the case of the LEX, the flow field about the fuselage forebody of the F/A-18 involves the presence of several vortices. Shown in Figure 6 is a view of the cross-sectional flow about the forebody at high angles of attack. In general, the flow field surrounding the forebody greatly resembles that about an ogive. As the normal component of the flow reaches the windward stagnation point, it splits and runs attached to both sides of the forebody. Eventually, this

boundary layer flow, facing an adverse pressure gradient, separates from the forebody (S_1) as vortex sheets, which roll up to form two counter-rotating primary vortices. Flow then reattaches at the leeward meridian (R). Secondary vortices are then formed on the leeward side of the forebody by a mechanism similar to that which resulted in the LEX secondary vortex. A literature review on the subject showed no evidence as to the existence of a tertiary vortex in the forebody flow field.

In water tunnel flow visualizations of the LEX and forebody vortices, the LEX vortex exhibits greater strength than the forebody vortex. This difference in strength can be discerned by the higher level of swirling in the LEX vortex as compared to that in the forebody vortex. Pressure measurements obtained from the HARV show a greater level of suction on the upper surface of the LEX than that on the leeward side of the forebody for the same flight conditions (see Figure 7). Therefore, it can be inferred that the LEX vortex core has a higher level of suction than the forebody vortex core. Such a difference in core suction could account for the higher swirling of the LEX vortex and thus its greater strength relative to the forebody vortex.

Analogous to the case of the leading edge vortex in delta wings, the LEX vortex increases in diameter in the downstream direction. The LEX vortex core, however, remains unchanged in size from its point of origination at the LEX apex until it undergoes breakdown.

The vortex breakdown phenomenon is generally defined as a sudden deceleration and stagnation of the axial flow along the vortex core. Many theories have been proposed in an effort to explain the

vortex breakdown phenomenon. However, as of yet, none enjoys complete acceptance. All theories agree that vortex swirling, core Reynolds number, and pressure gradient along the core directly affect breakdown. Reference 22 provides a comprehensive compilation of different breakdown theories.

Experimental studies on vortex flow have reported that the longitudinal external pressure gradient is the dominant parameter affecting vortex flows at high angles of attack [Refs. 1, 3, and 25]. This parameter can be simulated well in a water tunnel, thus suggesting that certain vortex flow characteristics, such as vortex core breakdown can also be simulated in a water tunnel.

Several studies have reported strong interactions between the LEX and forebody vortices at high angles of attack [Refs. 2, 5 and 23]. Such interactions are the result of the proximity between the two vortex systems. The forebody vortex, which is located for most of its length above the LEX vortex, is first subjected to a downwash from the LEX vortex. This causes the forebody vortex to curve towards the fuselage. Subsequently, an outboard directed sidewash from the LEX vortex has the effect of further curving the forebody vortex in an outboard direction. The result is the forebody vortex being pulled beneath the LEX vortex [Ref. 23].

The combined effect of the LEX and forebody vortices on the flow field of the F/A-18 is to increase the spanwise flow over the wing of the aircraft.

At high angles of attack, the pressure field about the F/A-18 is such that strong vortex flows occur over the aircraft, along with associated increases in lift over what would exist in the absence of vortex flows.

Vortex Flow Studies on the F/A-18

A significant amount of data on high angle-of-attack aerodynamics of the F/A-18 has been gathered from different studies.

Wind tunnel studies have addressed issues such as the degree to which vortex flows in sub-scale, low speed testing is representative of the full-scale, in-flight flow field [Ref. 24]. Other studies have resulted in disagreements on the stability characteristics of the F/A-18 [Refs. 2 and 25], even when tested at the same Reynolds number in the same or different wind tunnels. This apparent scale effect is still not well understood.

Water tunnel studies have also been conducted on the F/A-18 in an effort to improve the understanding of the physical aspects of vortex flows on the aircraft. For example, Reference 2 documents the effects of different geometrical configurations on forebody and LEX vortex interactions. The study reports large asymmetries in vortex locations due to small changes in sideslip, as well as a high sensitivity of vortex interactions to relatively small variations in geometrical configurations. Another study has also examined the effects of configuration changes on the F/A-18's flow field [Ref. 3]. The study concludes that the breakdown of the LEX vortex produces a highly turbulent region on the aft portion

of the F/A-18, accounting for a severe buffeting phenomenon on the vertical tails of the aircraft, for angles of attack of 25 degrees and higher. Several other investigations have been directed towards enhancing the controllability of the F/A-18 at high angles of attack, by aerodynamically controlling the forebody vortices [Refs. 5, 6 and 26]. Reference 26 reports significant improvements in overall forebody vortex management through the use of blowing, suction, and vortex generation; with good potential applicability to full-scale aircraft configurations. The effect of canopy size (single or double seat F/A-18) on the behavior of LEX and forebody vortices has also been examined [Ref. 27].

In-flight flow visualization studies have been carried out by NASA Ames-Dryden using the F/A-18 HARV. Characteristics of both surface and off-surface flow on the forebody and LEX surfaces have been investigated. References 28 and 29 report results of surface flow investigations on the forebody and LEX of the HARV. Primary and secondary vortex separation lines as well reattachment regions have been identified using an emitted fluid technique [Ref. 30]. Another flow visualization study on the F/A-18 HARV examined the behavior of LEX and forebody vortices [Ref. 23]. A smoke generator system allowed the cores of the vortices to be visualized in flight. The location of LEX vortex breakdown is shown to be a function of both angle of attack and angle of sideslip. Flight results are compared to water tunnel results and show good agreement on LEX vortex breakdown and on the longitudinal location of interaction between the LEX and the forebody

vortices. Pressure measurements on the forebody and LEX of the HARV have also been obtained [Refs. 31 and 32]. Good correlations of forebody primary and LEX secondary vortex separation lines with surface flow visualizations and wind tunnel results are reported.

Numerical predictions of the flow about the F/A-18 using CFD methods have been performed [Refs. 33 and 34]. Results thus far obtained agree well with those gathered from in-flight studies on the HARV and wind tunnel tests using a 6%-scale model of the F/A-18.

Project Justification and Objectives

Prior to the time when the present investigation was first proposed, a number of water tunnel flow visualization studies had been conducted on the F/A-18. Some of these studies resulted in both published and unpublished reports on the LEX vortex and forebody vortex characteristics. One common aspect examined by most of the aforementioned studies was the longitudinal location of the LEX vortex core breakdown at different angles of attack. Concurrent with the water tunnel studies, wind tunnel and flight investigations were assessing the LEX vortex and forebody vortex behavior. For the most part, data on LEX vortex characteristics were correlating rather well between the different facilities involved with F/A-18 high angle-of-attack research. Only two particular cases had shown difficulties in data correlation. One involved a discrepancy in lateral stability between different scale models of the F/A-18 tested in various wind tunnels [Refs. 2]. As of yet, the apparent model scale effect is still not well understood.

Reference 2 suggests that the source of discrepancy may be associated with the location of the primary vortex separation line on the forebody of the F/A-18; which can greatly influence the interaction of the forebody vortices with the flow field on the LEX and wing. The other area of difficulty in data correlation involves conflicting results on the longitudinal location of LEX vortex breakdown at high angles of attack. The results in question had been obtained from a water tunnel study using a 1/48-scale model of the F/A-18 [Ref. 3]. The observed location of LEX vortex breakdown from this study was in conflict with similar data gathered from a variety of sources, such as wind tunnels, flight tests, and water tunnels (see Figure 8). The possible cause for these conflicting results observed in the water tunnel data was believed to be a model scale effect, a Reynolds number effect, differences between different water tunnel models, or a combination of these factors. Consequently, further water tunnel studies were deemed necessary in order to identify the source of discrepancy in the water tunnel data. Resolving this issue would help regain some of the confidence that had been lost on the water tunnel as a valuable tool in helping understand complex three-dimensional flows. Moreover, the need existed for expanding the water tunnel data base on forebody vortices. Lastly, additional correlations of water tunnel results with flight, wind tunnel, and other water tunnel results were also in great need.

The present study addresses these issues through a flow visualization study of the F/A-18 aircraft. Flow visualizations were conducted at the NASA Ames-Dryden water tunnel.

The main purpose of the present study is to investigate the high angle-of-attack vortex flow structures present in the flow surrounding the F/A-18 aircraft. Specifically, the visualization of LEX and forebody vortices through water tunnel testing. The objectives of the project are as follows:

1. Conduct water tunnel tests using scale models of the F/A-18 aircraft. Results from these tests are analyzed to:
    a. Verify the existence of a discrepancy in previously gathered data on LEX vortex breakdown.
    b. Determine the cause for conflicting data by examining the effects of model geometry and model scale effects on the behavior of LEX vortices.
    c. Update the water tunnel data base on F/A-18 LEX vortex breakdown.
2. Expand the water tunnel data base on F/A-18 forebody vortices by documenting primary separation lines, surface flow, vortex core location, and interaction with LEX vortices.
3. Correlate water tunnel test results with flight, wind tunnel, and other water tunnel test results gathered from previous studies.

CHAPTER 2

Experimental Aspects

Flow Visualization Facility

The NASA Ames-Dryden Flow Visualization Facility (FVF) is a closed-loop water tunnel (see Figure 9). The vertical test section has a constant rectangular cross-sectional area measuring 16 inches by 24 inches, and a length of 72 inches. The walls of the test section are made of a two-inch thick transparent acrylic plastic allowing a 360-degree view of the model being tested. The test section is equipped with a side door through which the models can be inserted. The model is held in place by an L-shaped mounting attached in one end to a side wall of the test section. This model support system allows two simultaneous degrees of motion, corresponding to changes in angle of attack and angle of sideslip, which can be controlled from outside the test section by means of hand cranks. The free stream velocity in the test section can be varied from zero to 12 in/sec. Visualization of vortex flow structures in the water tunnel is accomplished by releasing dye into the flow field through small orifices (dye ports) located strategically throughout the exterior surface of the models. The dye reaches such orifices through small dye tubes connected to dye containers located outside of the test section where the dye is pneumatically pressurized. A set of needle valves allow control of the dye flow rate. Additional details about the Ames-Dryden FVF can be found in Reference 37.

Models

Models of the F/A-18 used were constructed from commercially available hobby shop plastic kits. Scales of the models tested were 1/32 and 1/48. Configuration of the models were landing gear up, no stores, wing leading-edge flaps deflected 34 degrees down, and trailing-edge flaps undeflected. This configuration corresponds to flight at angles of attack of 26 degrees or higher. All models used featured flow-through inlets to simulate engine inlet suction.

For the present study, the following four models were used (see Figure 10):

1. An existing 1/48-scale model, which in this report will be referred to as the "48A model." This model was subjected to a modification which involved increasing both the LEX leading-edge sharpness and the LEX upper and lower surface smoothness.
2. Another 1/48-scale model, from which conflicting results on LEX vortex breakdown were obtained in an earlier study [Ref. 3]. In this report, this model will be referred to as the "48B model."
3. A newly-built 1/48-scale model, which is as representative as possible of the full-scale aircraft. This model is referred to as the "48C model."
4. An existing 1/32-scale model used in earlier tests, and which is denoted as the "32A model."

All models, except for the 48B model, were marked with lines at specific fuselage and wing span stations as an aid in identifying the location of LEX vortex breakdown.

Data Acquisition Methods

All water tunnel tests conducted in the present investigation were recorded using two video cameras. Two identical still cameras with the capability for simultaneous triggering were also used. For each test condition, top views perpendicular to the longitudinal axis of the model were obtained along with the corresponding side view. An additional 35 mm. camera was used occasionally to document exceptional features of the flows being visualized.

Because of the highly three-dimensional nature of the flows that were visualized in the water tunnel, it became apparent that a third method was necessary to documents those aspects of the flow that can only be discerned by direct observation. Thus, notes were taken and sketches were drawn of the flow visualizations as each water tunnel test was being carried out.

Test Conditions

The Ames-Dryden water tunnel has the capability to vary four different experimental parameters, even when the facility is operating. These experimental parameters are angle of attack, angle of sideslip, free stream velocity, and flow rate through the engine nacelles.

Angle of Attack

Angle of attack could be varied by turning a hand crank connected to the model support system. A seven-inch radius protractor attached to the inner side of a test section wall was used to read the angle of attack. Typically, before a test was conducted, the model would be positioned at zero angle of attack using a plumb line and two reference points on the model (see Figure 11). This technique assumes that the test section is accurately oriented vertically. With the model positioned at zero angle of attack, a reading was taken from the protractor, which would then be used throughout the test as the zero angle-of-attack reference. For the present investigation, angle of attack was varied between zero and 50 degrees for the 1/48-scale models, and between zero and 45 degrees for the 32A model. This difference was due to test section size limitations.

Angle of Sideslip

Angle of sideslip could be varied also by turning a hand crank connected to the model support system. In order to arrive at the correct setting of sideslip, the following procedure was used. First, the angle of sideslip was drawn on a top-view sketch of the model (see Figure 12). The center of rotation in the drawing was located so as to agree with that on the model support system. A plumb line was then used to place the model at the no-sideslip condition. Subsequently, the model was sideslipped until the orientation of the model with respect to the plumb line agreed with that in the drawing. Angles of sideslip in the 1/48-scale

models varied between zero and nine degrees. Because of the bigger size of the 32A model, angles of sideslip for this model could only be varied between zero and 6.5 degrees.

Free Stream Velocity

Variation of the free stream velocity provided a means to vary the Reynolds number. However, it is important to recognize that increases in free stream velocities can invariably lead to increments in the level of free stream turbulence in the test section of the water tunnel. For the ranges of free stream velocities employed in the present study, it was assumed that the effects of increased free stream turbulence were minimal. Most of the tests in the present study were conducted at a free stream velocity of 3 inches/second, which corresponds to a unit Reynolds number of 2.3×10^4 per foot, and which has been found to produce good flow visualizations. A few selected tests were carried out with a free stream velocity of 9 inches/second, corresponding to a unit Reynolds number of 7.0×10^4 per foot.

Engine Nacelles Flow Rate

In order to realistically simulate the flow patterns about the models, water was drawn through the engine inlets of the models to simulate engine flow. A pair of flexible plastic tubes connected to the exhaust nozzles carried the simulated engine flow to a flow meter gauge located outside of the test section. By changing the setting in the gauge, it was possible to vary the flow through the engine nacelles.The

following table shows the different flow meter settings used in the present study (computations are presented in Appendix A).

Table 1

Engine Flow Rate Meter Settings as Percentage of the Maximum Meter Flow

Free Stream Velocity (in/sec)	Model Scale	
	1/48	1/32
3	22.94[a]	51.62[a]
9	68.83[a]	54.45[b]

[a]Setting using a 1.80 gal/min flow meter

[b]Setting using a 5.12 gal/min flow meter

Test Plan

Water tunnel testing for the present study was divided into three phases:

1. Phase I: Testing conducted on the 48A model and on the 48B model. Objective: Verify the existence of a discrepancy in previously gathered data on LEX vortex breakdown, and investigate the effect of LEX surface smoothness and leading-edge sharpness on the behavior of LEX and forebody vortices.

2. Phase II: Testing conducted on the 32A model. Objective: Examine the effect of model scale, Reynolds number, angle of attack, and angle of sideslip on LEX and forebody vortex characteristics, including location, breakdown, and interaction between the two vortex

systems. Additionally, forebody surface flow visualizations are included in this phase.

3. Phase III: Testing conducted on the 48C model. Objective: Study the effect of model fidelity on LEX and forebody vortex characteristics.

CHAPTER 3

Discussion of Results

Examination of Models

The possibility that conflicting data on LEX vortex breakdown might have been caused by model scale effects and/or model differences necessitated a close examination of the different F/A-18 models. This inspection of the models was performed during the early stages of the present project. At the time when the examination of the models was performed, the 48A model was believed to be the only single-seat 1/48-scale model of the F/A-18 used for testing at the Ames-Dryden water tunnel, and thus the model that had produced the conflicting results. Another 1/48-scale model, the 48B model, was later determined to be the model that caused the discrepancy. Consequently, by error, the 48A model was carefully inspected, as was the 32A model. Nevertheless, some interesting geometrical differences were observed between these two models.

The scales of both models were found to be within +/- 0.44 percent and +/- 0.06 percent of the exact values for the 32A model and the 48A model, respectively.

Inspection of the LEX surface smoothness on both models showed that the 32A model exhibited almost no surface irregularities. The 48A model, on the other hand, showed surface roughness on both the upper and lower LEX surfaces, as well as a considerable lack of sharpness of the LEX leading edges. The geometry of the planform of

the LEX was also studied between the two models. Figure 13 shows a comparison of LEX planforms measured from the two models, from a full-scale F/A-18 aircraft, and from a drawing of the F/A-18 provided by McDonnell Douglas (MD). As can be seen, the models' LEX shape agrees well with that of the aircraft and the drawing.

The forebodies of the models were also examined; again showing that the 32A model exhibited much less surface roughness than the 48A model. A vernier caliper was used to measure the height and width of the forebodies of the two models, as well as that on the MD drawing. Results are presented in Figures 14 and 15. As shown in Figure 14, the forebody cross section in the 48A model evolves from a horizontal ellipse into a vertical ellipse, which disagrees with the MD drawing. For any station on the forebody of the 48A model, the cross section area is larger than that obtained from the MD drawing. Figure 15 shows results for the 32A model. As can be seen, the forebody cross section in the 32A model agrees well with that in the drawing by evolving from a circle into a vertical ellipse. Moreover, for much of the forebody the elliptical cross-sectional area is larger than that in the MD drawing.

Based on the above observations, the decision was then made to study the effect of LEX leading-edge sharpness, LEX surface smoothness, and forebody geometry on some LEX and forebody vortex characteristics. For this purpose, the 48A model was subjected to modifications to study LEX geometry effects, and a 1/48-scale model was built to investigate forebody geometry and overall model fidelity effects.

Identification of the Source of Discrepancy in LEX Vortex Breakdown Data

As part of the investigation to determine the source of conflicting data on the LEX vortex breakdown, the 48A model was tested in the water tunnel at a Reynolds number (Re_c) of 5.5×10^3 based on a mean aerodynamic chord of 2.88 inches in 1/48 scale. This Reynolds number corresponds to that of the test involving the conflicting results. Figure 16 presents results on the location of the LEX vortex core breakdown from the test conducted on the 48A model. As shown, data from the 48A model did not duplicate the discrepant results [Ref. 3], but instead are closer to the results from various other tests. This situation raised questions as to whether the 48A model was in fact that which produced the controversial results. The decision was then made to examine all published water tunnel results on LEX vortex breakdown from 1/48-scale models in an effort to establish the identity of the controversial model. After a thorough review of available photographs from different water tunnel studies on the F/A-18, it was determined that the conflicting data belonged to an earlier water tunnel test for which apparently a different model than the 48A model had been used [Ref. 3]. Having identified the model from which the discrepant results were obtained (the 48B model), it was deemed logical to conduct a separate test using the model in question. Figure 17 shows results of the foregoing investigations. As can be seen, vortex core breakdown results reported in Reference 3 lay close to those obtained by examining photographs of top views of the model, which were taken for the same

study. On the other hand, breakdown locations identified from side view photographs nearly match the results from testing the 48A model. Moreover, results from retesting the 48B model are also close to those of the 48A model.

Based on the above findings, the following conclusion was reached as to the possible source of conflicting water tunnel data. The location of the LEX vortex core breakdown reported in Reference 3 seems to have been interpreted from photographs taken of the top view of the model. However, these results are in disagreement with results from side views of the model from the same study. This difference strongly suggests that parallax was not considered when LEX vortex core breakdown locations were identified in the study reported in Reference 3.

In order to properly interpret the longitudinal location of the LEX vortex core breakdown from a top view of the model, the observer's line of sight must be kept normal to the plane formed by the longitudinal axis and the transverse axis of the model; otherwise parallax must be taken into consideration. Because of this complication, the longitudinal location of the LEX vortex core breakdown is usually identified from side views; while the lateral or spanwise location is interpreted from top views.

LEX Vortex Core Breakdown

Effect of Angle of Attack

The pressure gradient along the LEX vortex core was noted earlier in this report as one of the parameters that greatly influences the location of LEX vortex core breakdown. Thus, angle of attack, which dictates the intensity of the pressure gradient, would be expected to affect considerably the location of the LEX vortex core breakdown. This effect was indeed seen throughout all of the testing conducted in the present study.

As angle of attack was increased, the LEX vortex core breakdown moved longitudinally forward. As the breakdown location moves closer to the LEX apex with increasing angle of attack, the lateral location of the LEX vortex core breakdown moves slightly inboard. These patterns of motion of the LEX vortex core breakdown were consistent whenever angle of attack was increased while holding constant the angle of sideslip.

Figure 18 shows that at an angle of attack of 15 degrees breakdown is occurring aft of the trailing edge of the wing. At this angle of attack, the turbulent region behind the point of breakdown, is affecting approximately less than half of the outboard surface of the vertical tails. At 25 degrees angle of attack, the breakdown point has moved over the surface of the wing, and turbulence aft of the breakdown point is now covering the entire surface of both vertical stabilizers. At an angle of attack of 40 degrees, the breakdown point is

positioned over the upper surface of the LEX. At an angle of attack of 50 degrees, the point of breakdown is very near the LEX apex. At this angle of attack, most of the flow field over the aircraft is affected by the turbulence aft of the breakdown of the LEX vortex cores.

Shown in Figure 19 are results of the LEX vortex core breakdown from the present study, as compared to flight and wind tunnel results. Because of the unsteady nature of the LEX vortex core breakdown, the breakdown locations were obtained from video images by estimating an average location of the breakdown. The correlations in Figure 19 are good despite the enormous differences in Reynolds numbers. Moreover, there seems to be a small parametric trend. As Reynolds number is increased for constant angle of attack, the location of the LEX vortex core breakdown appears to move forward. Because of the scatter of the data points, however, the foregoing trend can only be proposed as probable. Nevertheless, the overall agreement of results is good, suggesting that the water tunnel can properly simulate LEX vortex core breakdown.

Effect of Angle of Sideslip

Variation in the angle of sideslip had the following effect on the longitudinal location of the LEX vortex core breakdown. For constant angles of attack, increase in the angle of sideslip caused the windward LEX vortex core breakdown to travel forward, while the leeward LEX vortex core breakdown moved aft. This trend is graphically depicted in Figure 20. At an angle of attack of 25 degrees, the asymmetric location

of LEX vortex core breakdown with sideslip causes the windward wing panel to experience a decrease in its spanwise flow, since the swirling in the turbulent region aft of the point of breakdown is lower than forward of the point of breakdown. The opposite situation takes place in the leeward wing panel, where the vortex flow with greater swirling in front of the point of breakdown affects a larger area of the leeward wing panel than its counterpart on the windward wing panel. In addition, the reported vortex breakdown asymmetry would be expected to produce, in turn, asymmetric lift forces between the LEX's, thus affecting the lateral stability characteristics of the F/A-18.

Flow around the vertical tails would also be expected to be affected by asymmetric LEX vortex core breakdown, especially at moderately high angles of attack (20 degrees to 35 degrees). As angle of sideslip increases, the longitudinal proximity of the leeward LEX vortex core breakdown to the leeward vertical tail increases, while the opposite takes place on the windward side; i.e. LEX vortex core breakdown on the windward side moves longitudinally away from the windward vertical tail with increasing angle of sideslip. This differential effect would be expected to induce differential side forces on the vertical tails, thus affecting the lateral-directional stability of the F/A-18.

The longitudinal and lateral locations of the LEX vortex core breakdown have been plotted in Figure 21 for various angles of attack and sideslip. As reported above, breakdown location on the windward side moves forward with increased sideslip, while on the leeward side breakdown location moves aft. Moreover, increases in angle of sideslip

causes the windward breakdown point to move inboard, whereas the opposite happens to the leeward breakdown point, i.e. breakdown moves outboard. Increases in angle of attack are seen to decrease the longitudinal and lateral asymmetry of the location of breakdown.

Effect of Reynolds Number

As explained earlier in this report, Reynolds number was increased in the water tunnel by increasing the free stream velocity in the test section. Plotted in Figure 22 are the locations of the LEX vortex core breakdown for two different Reynolds number. For angles of attack between 15 and 40 degrees, the higher Reynolds number breakdown locations are slightly forward of the lower Reynolds number locations of breakdown. This difference cannot be explained, although it is believed by the author that increased free stream velocity may be accompanied by higher free stream turbulence, which could promote early breakdown. Further experimentation might be necessary to address this issue. For angles of attack higher than 40 degrees, the trend apparently is reversed. No definitive statements can be made about such a reversal in the trend, because the model used for this particular investigation was the 32A model, which at angles of attack of 45 degrees and higher is almost in contact with one of the test section walls. Such a proximity to the wall may cause adverse effects which could influence the quality of the flow visualizations.

Effect of LEX Leading Edge
Sharpness and LEX Surface Smoothness

Increasing the LEX leading-edge sharpness and surface smoothness produced no appreciable changes in the location of the LEX vortex core breakdown, as shown in Figure 23. LEX surface smoothness was expected to produce negligible effects on the LEX vortex core breakdown, since the LEX vortex core is located far enough from the LEX upper surface so that changes in the LEX upper surface boundary layer would be unnoticed by the LEX vortex. Increased sharpness of the LEX leading edge provided a more fixed flow separation location. However, Reynolds number effects which become noticeable on rounded leading-edge, highly-swept surfaces [Ref. 1], did not show in a clear manner. These observations further emphasize that the adverse pressure gradient is one of the dominant parameters affecting LEX vortex core breakdown.

Effect of Model Scale

Shown in Figure 24 is the effect of model scale on the location of LEX vortex core breakdown. As can be seen, results from two different scale models agree well, suggesting no influence of model scale in the location of the LEX vortex core breakdown.

Effect of Model Fidelity

Results on LEX vortex core breakdown from the unmodified 48A model and the 32A model are compared in Figure 25 to those obtained

from the 48C model. Again, no significant differences are observed in the location of the LEX vortex core breakdown.

LEX Vortex Core Location

Effect of Angle of Attack

Qualitative analysis. At an angle of attack of 15 degrees, the LEX vortex cores are symmetric to each other (see Figure 26). When viewed from the side of the model, the forward portion of the vortex core alongside the canopy is below the line of junction between the canopy and the fuselage. The aft portion of the LEX vortex cores are located outboard of the vertical tails. This suggests that the outboard side of the vertical tails is subjected to downwash flow from the vortices. At an angle of attack of 25 degrees, the portion of the LEX vortex core located over the LEX surface has experienced no noticeable lateral displacements. Vertically, however, the LEX vortex core has moved away from the LEX upper surface, and now is almost at the level of the canopy/fuselage junction. At an angle of attack of 35 degrees, the LEX vortex core still shows no evidence of changes in its lateral location. When viewed from the side of the model, the LEX vortex core appears to be slightly above the canopy/fuselage junction. It is interesting to note that for any angle of attack, the portion of the LEX vortex core located over the LEX upper surface does not rise higher than the top surface of the fuselage.

Quantitative analysis. Using a vortex path reconstruction computer program (see Appendix B), the lateral and vertical locations of the LEX vortex core were accurately placed on a body axis coordinate system. Figures 27 and 28 show results of these computations. As clearly seen in the enlarged areas, the qualitative observations of the effect of angle of attack on the LEX vortex core location made in the previous section are valid. First, on the side view of Figure 27, a definite upwards motion of the vortex core occurs as angle of attack increases. The reason for this vertical displacement of the vortex core cannot be explained, although it is believed by the author that as the angle of attack is increased, the cross-sectional diameter of the LEX vortex increases, in effect displacing upwards the LEX vortex core. The top view in Figure 28 confirms the observation of no lateral motion of the vortex core with increasing angle of attack. It should be pointed out that the most aft discrete point of each of the vortex paths shown does not correspond to the vortex core breakdown.

Effect of Angle of Sideslip

Qualitative analysis. For a constant angle of attack of 25 degrees, the following observations were made for various angles of sideslip. First, at the no-sideslip condition, the LEX vortex cores are essentially symmetric. A few minor differences in the linear shape of the cores can be seen, though. As angle of sideslip is increased to 5.5 degrees (see Figure 29), the aft portion of the vortices begin showing evidence of core lateral displacements. The windward LEX vortex core appears to

be closer to the center line of the model than the leeward LEX vortex core. No discernible differences can be visually detected between the lateral location of the forward portion of the LEX vortex cores; probably because of the small angle of sideslip.

Quantitative analysis. Using again the vortex path reconstruction computer algorithm, locations of the leeward LEX vortex core for three sideslip conditions and for an angle of attack of 30 degrees were obtained. Results are presented in Figures 30 and 31. First, the side view shows hardly any changes in the vertical location of the vortex core with increasing angle of sideslip. The top view, on the other hand, does show an outboard motion of the leeward vortex core as sideslip increases.

Effect of Reynolds Number

No appreciable changes could be observed in the location of LEX vortex core with increased Reynolds number.

Effect of LEX Leading-Edge
Sharpness and LEX Surface Smoothness

No visible variations could be identified in the location of the LEX vortex core, after the LEX's of the 48A model were modified. A line of reasoning similar to that used to explain the insensitivity of the LEX vortex core breakdown to geometrical modifications of the LEX could also be used here to explain why the LEX vortex core location is also insensitive. The behavior of the vortex core is not affected by disturbances in the boundary layer on the LEX upper surface.

Effect of Scale and Model Fidelity

The scale and degrees of fidelity of the models employed in the present investigation proved to produce no appreciable impact on the location of the LEX vortex core.

Correlations With Flight Results

Qualitative analysis. The following observations have been made by inspecting side views of the LEX vortex core from flight and water tunnel flow visualizations. For angles of attack between 16 degrees and 30 degrees, the vortex core follows essentially a straight path up to a point where it undergoes a change in its linear shape (see Figure 32). This change occurs first as the core turns away from the upper surface of the wing. This effect was observed in tests conducted both in the water tunnel and in flights of the HARV. At an angle of attack of 35 degrees, the change in shape of the core showed only slightly in the flight results, and was hardly noticeable in the water tunnel results. It is believed that the cause for the change in the linear shape of the core can be related to the associated upwash produced by the wings.

Quantitative analysis. Shown in Figures 33 through 36 are comparisons of the location of LEX vortex core from water tunnel results from the present study and preliminary, unpublished flight results [Ref. 35] using vortex core reconstruction for angles of attack of 25 degrees and 30 degrees. Side views show the vortex core in the water tunnel above the in-flight smoke-visualized vortex core for both angles

of attack. The only possible explanation for this disagreement is a difference between the pressure fields on the LEX. Top view correlations are not as consistent. The 25-degree angle-of-attack case shows the flight vortex core farther outboard than the water tunnel vortex core. However, in the 30-degree angle-of-attack case, the results nearly match. Reference 35 indicates that flight results are accurate to +/- 8 inches (full scale), which could account for the above difference in the lateral location of the LEX vortex core between water tunnel and flight results.

Forebody Vortex Core Location

Effect of Angle of Attack

For angles of attack up to 20 degrees, flow on the forebody is attached. For 25 degrees angle of attack, evidence of separated flow on the leeward side of the forebody begins to show (see Figure 37). Two weak primary vortices originate near the nose tip of the forebody, the cores of which extend downstream near the upper surface of the fuselage. When viewed from the side of the model, the vortex looks straight from the nose tip to the highest point of the canopy. Aft of the canopy, the core curves towards the fuselage to the point where it is drawn down towards the upper surface of the wing or the LEX. At moderately high angles of attack (20 to 35 degrees), the core is pulled laterally outboard over the surface of the wing and beneath the swirling turbulent region behind the LEX vortex core breakdown. For angles of attack of 40 degrees and higher, the vortex core is still being drawn

laterally, but now flows over the surface of the LEX. In general, as angle of attack increased, the forebody vortices became stronger as the level of swirling was observed to increase.

Effect of Angle of Sideslip

Variations in the angle of sideslip had an effect on the location of the forebody vortex cores similar to that observed on the LEX vortices. Increase in angle of sideslip caused the windward forebody vortex core to move inboard, while the leeward forebody vortex core traveled outboard (see Figure 38). The displacement of the windward forebody vortex core was found to be considerably more sensitive to changes in the angle of sideslip than that of the leeward forebody vortex core. With no sideslip, and for any high angle of attack, both vortex core remain symmetrical to each other; laterally located on the outer edge of the canopy, aft of which they were positioned close to the model's center line. For angles of sideslip as small as three degrees, the windward forebody vortex core essentially lined-up with the model's center line, while the leeward forebody vortex core experienced a much smaller outboard motion. For angles of sideslip greater than three degrees, the windward forebody vortex core crosses over the model's center line, and the leeward forebody vortex core is drawn into the leeward LEX vortex system. When viewed from the side of the model, the forebody vortex cores underwent the following changes in their location. With no sideslip, the cores were essentially lined-up one behind the other. This condition was kept forward of the canopy for angles of sideslip up to

four degrees and angles of attack up to 30 degrees. As sideslip increased, the windward forebody vortex core moved farther away from the upper surface of the fuselage. The curvature of the forebody vortex core aft of the canopy reported previously (effect of angle of attack section) was reduced. On the other hand, increase in sideslip caused the leeward forebody vortex core to move closer to the top of the model, which resulted in it being susceptible to be drawn into the LEX vortex system.

Effect of Reynolds Number

Increases in Reynolds number were found to produce no visible changes in the location of the forebody vortex cores. However, the forebody vortices exhibited much more strength, which could be discerned by the increased swirling. Additionally, increase in Reynolds number caused the unstable and turbulent portions of the forebody vortex cores to move forward. These changes occurred consistently in all models and for all angles of attack considered in the present study.

Effect of Forebody Geometry

Comparison of the forebody vortices between the 48A model and the 48C model produced the following results. As viewed from the side, no significant differences were observed in the location of the forebody vortex cores. When viewed from the top of the model at an angle of attack of 30 degrees, the forebody vortex cores on the 48A model showed a curvature directed outboard and located approximately halfway between the nose tip and the forward most point of the canopy.

Evidence of such a curvature in the forebody vortex cores could not be seen in the 48C model (see Figure 39). Moreover, the curvature was found to move forward with increasing angle of attack.

Effect of Model Scale

The lateral location of the forebody vortex cores of the 32A model and the 48C model seemed nearly identical for the most part. However, the aft portion of the forebody vortices, near the leading edge of the vertical tails, showed some differences between the two scale models at various angles of attack. For example, for an angle of attack of 25 degrees (see Figure 40), the aft portion of the forebody vortex core flowed completely over the wing surface on the 32A model; while on the 48C model the forebody vortex core flowed mostly through the inboard side of the vertical tails. For angles of attack of 30 degrees and higher (see Figure 41), the foregoing flow pattern shifted between the models, so that now the aft portion of the forebody vortex core on the 48C model was drawn farther outboard than in the 32A model. When observed from the side of the model, hardly any differences could be noticed on the location of the forebody vortex cores for any angle of attack.

Correlations With Results From Other Studies

For angles of attack up to 25 degrees, the forebody vortex core is located very near the upper surface of the forebody. This observation was made from both water tunnel and flight test results [Ref. 36]. Aft of the canopy, however, results from the water tunnel seem to indicate that

the forebody vortex core is farther away from the upper surface of the fuselage than in the flight case. At an angle of attack of 30 degrees, water tunnel data show that the forebody vortex core still remains very close to the forebody for most of the forebody, which agrees with the flight results. Moreover, aft of the canopy the forebody vortex core in the water tunnel results again seemed farther away from the fuselage than in the flight results (see Figure 42). Angles of attack of 35 degrees and higher caused the forebody vortex core to move even further away from the fuselage in both water tunnel and flight results. In addition, the curvature of the forebody vortex core aft of the canopy increased with increasing angle of attack.

Location of the Forebody Primary Separation Line

As part of the effort to expand the water tunnel data base on the F/A-18, surface flow investigations on the forebody of the F/A-18 were conducted.

Before results are presented, it is important to point out that quantitative characteristics of surface flow as documented from a water tunnel possess limited practical utility due to the presence of strong viscous effects near the surfaces of the body [Ref. 1]. Nevertheless, given the current need to improve the understanding of the physics of vortex flow on the F/A-18, any information that can be gathered on F/A-18 vortex flows, even if limited in practical applications, would be of great value.

Lack of knowledge of an effective method to visualize surface flows in water tunnels, coupled with very limited information available on the subject from existing literature, necessitated conducting surface flow experiments to develop an effective surface flow visualization technique. After several trials using different approaches, it was opted for the method of releasing a stream of dye in front of the object from an external dye source.

Using this technique, surface flow patterns on the F/A-18 forebody were revealed. However, the only clear piece of information that could be gathered was the location of the primary separation line. Figure 43 shows an example of forebody surface flow visualization at an angle of attack of 20 degrees.

Effect of Angle of Attack

Shown in Figure 44 are the circumferential locations of the primary separation lines for various angles of attack. As would be expected, the separation lines move closer to the windward side of the forebody with increased angle of attack. The noticeable "dip" seen in the plot is directly attributed to the presence of an antenna cover located on both sides of the forebody, which causes the boundary layer to separate closer to the windward side than anywhere else on the forebody.

Effect of Reynolds Number

Increase in Reynolds number caused the primary separation line to move towards the windward side of the forebody (see Figure 45).

Comparison to a CFD Prediction

Shown in Figure 46 is a comparison of the location of the primary separation line between water tunnel results at $Re_C = 8.1 \times 10^3$ and a laminar flow CFD prediction at $Re_C = 8.1 \times 10^5$ [Ref. 34]. As can be seen, the higher Reynolds number CFD solution places the primary separation line mostly below the $\theta = 120$ degrees line. This difference seems to confirm the effect of Reynolds number described earlier.

Comparison to Flight Results

Since flow separation on the forebody in a water tunnel is laminar, it would be expected to see the location of separation closer to the windward side than in flight results, where separation around the forebody is delayed due to the more energized turbulent boundary layer. This trend is observed in Figure 47 where water tunnel results are plotted along with flight results obtained from Reference 28.

Interaction Between the LEX and Forebody Vortices

The location of the interaction between the LEX and forebody vortices is defined in this report as the point along the fuselage where the forebody vortex core first exhibits a change in its curvature as viewed from either the side or the top of the model. This change in curvature occurs as the more powerful LEX vortex attracts the weaker forebody vortex. This results in the forebody vortex being drawn beneath the LEX vortex system.

Effect of Angle of Attack

Increases in angle of attack caused the location of the interaction to move forward on the model. Shown in Figure 48 are the locations of the interaction as well as the locations of vortex breakdown for the 48A model and the 32A model. As can be seen, for any angle of attack, interaction between the vortex systems occurs aft of the LEX vortex core breakdown. Figure 49 shows a comparison of results on the interaction between LEX and forebody vortices from water tunnel and flight results [Ref. 23]. Good correlation is obtained, suggesting that the interaction, like the breakdown of the LEX vortex core is mainly dependent on the angle of attack and insensitive to large differences in Reynolds number.

Effect of Angle of Sideslip

The longitudinal location of interaction as a function of angle of sideslip is plotted in Figure 50. Opposite to the trend observed in LEX vortex core breakdown location, the location of interaction on the windward side moves aft with increasing angle of sideslip, while on the leeward side, interaction moved forward along the model. Also plotted in Figure 50 are the locations of interaction from flight results [Ref. 23]. The correlation in this case is only fair and could possibly be attributed to differences in the location of forebody vortex cores at sideslip between the water tunnel and flight results.

CHAPTER 4

Conclusions

A flow visualization study has been conducted on the high angle-of-attack vortex flow structures surrounding the F/A-18 aircraft. The NASA Ames-Dryden water tunnel was used to investigate the characteristics of the LEX vortex and forebody vortex systems.

Conflicting results from an earlier water tunnel study involving the longitudinal location of the LEX vortex core breakdown were identified. Results from the present study did not duplicate those from the earlier study. Therefore, an in-depth examination of results from the earlier study led to the conclusion that a possible source for the discrepancy was parallax not being taken into consideration in the interpretation of the location of LEX vortex core breakdown in the earlier water tunnel study.

The water tunnel database on LEX vortex core breakdown has been updated. Angle of attack, and thus, pressure gradient was found to be the main parameter affecting the location of LEX vortex core breakdown. Other parameters, such as scale of the model tested was shown to have no significant effect on the location of the LEX vortex core breakdown. Similarly, LEX leading-edge sharpness and LEX surface smoothness did not vary the location of the LEX vortex core breakdown. Assessments of flow visualizations indicate that both longitudinal and lateral asymmetries in LEX vortex core breakdown

location have the potential to significantly alter the lateral and directional stability of the F/A-18. Additionally, for angles of attack of approximately 25 degrees, the vertical tails of the F/A-18 were immersed in turbulent flow coming from the breakdown of the LEX vortex cores.

Angle of attack and angle of sideslip were observed to have different effects on the vertical and lateral location of the LEX vortex core. Angle of attack produced no significant lateral but vertical displacements of the core. Conversely, angle of sideslip caused the core to displace significantly more laterally than vertically.

Forebody vortex core location was very sensitive to changes in sideslip. The windward forebody vortex core was observed to move laterally more than the leeward forebody vortex core with increasing sideslip. The angle of sideslip also produced changes in the vertical location of the forebody vortex cores.

The swirling intensity and thus the strength of the LEX and forebody vortices became greater whenever angle of attack or Reynolds number was increased.

Primary separation lines on the forebody were observed in the water tunnel to move closer to the windward side of the forebody with increasing angle of attack and Reynolds number. These trends agreed with flight results and CFD predictions, further demonstrating the utility of the water tunnel as a flow simulation facility.

The location of the interaction between the LEX vortex and the forebody vortex moved forward as angle of attack was increased. Angle

of sideslip produced an effect on the location of the interaction opposite to that of LEX vortex core breakdown. As sideslip increased, the windward location of interaction moved aft, while the leeward location of interaction moved forward.

Extensive correlations were performed between results from the present study and results from different flight and ground-based facilities. The best correlations were obtained for those flow characteristics which were independent of Reynolds number. Thus, realistic simulations in the water tunnel of full-scale configurations were successful. This will be the case so long as care is exercised in the selection of the types of flows to be visualized in the water tunnel.

REFERENCES

1. Erickson, Gary E. Vortex Flow Correlation. AFWAL:-TR-80-3143, Wright-Patterson Air Force Base, Ohio, 1980
2. Erickson, Gary E. Water Tunnel Flow Visualization and Wind Tunnel Data Analysis of the F/A-18. NASA CR- 165859 Northrop Corporation, Aircraft division, Hawthorne, California, 1982.
3. Wentz, William H. Jr. Vortex-fin Interaction on a Fighter Aircraft. AIAA Paper #87-2474-CP, Institute for Aviation Research, Whichita State University, Wichita, Kansas.
4. McDonnell Aircraft Personnel "F/A-18 Fin Buffet, Project Briefings on Fin Buffet." Naval Air Developmental Center, May 21, 1986.
5. Malcolm, Gerald N., Skow, Andrew M. Enhanced Controllability Through Vortex Manipulation on Fighter Aircraft at High Angles of Attack. Eidetics International, Inc. Visual Aerodynamics Division, Torrance, California, 1986.
6. Malcolm, G. N., Ng, T.T., Lewis, L.C., and Murri, D.G., Development of Non-Conventional Control Methods for High angle of Attack Flight Using Vortex Manipulation. AIAA Paper 89-2192, AIAA 7th applied Aerodynamics Conference, Seattle, Washington, July 31-August 2, 1989.
7. Erickson, Gary E., Experimental Investigation of Forebody and Wing Leading-Edge Vortex Interactions at High Angles of

Attack. NASA CR- 165859. NASA Langley Research Center, Hampton, Virginia, 1982.

8. Werle, H. Flow Visualization Techniques for the Study of High Incidence Aerodynamics. AGARD Conference Proccedings 342. Aerodynamics of Vortical Type Flows in Three Dimensions, 25-28 April, 1983.
9. Merzkirch, W., Flow Visualization. Second Edition, Academic Press, Inc., 1987.
10. Fartshore, I. S., Djilali, N. Flow Separation - Problems and Possibilities. 9th Australasian Fluid Mechanics Conference, Auckland, New Zealand, 8-12 December, 1986.
11. Peake, David J., Tobak, Murray. Three-dimensional Separation and Reattachment. NASA Ames Research Center, Moffett Field, California.
12. Payne, F.M., Ng, T.T., Nelson, R.C., Schiff, L.B. Visualization and Flow Surveys of the Leading Edge Vortex Structure on Delta Wing Planforms. AIAA-86-0330, AIAA 24th Aerospace Sciences Meeting, January 6-9, 1986.
13. Brandon, Jay M., Nguyen, Luat T. Experimental Study of Effects of Forebody Geometry on High Angle-of-Attack Stability. NASA Langley Research Center, Hampton, Virginia, 1988.
14. Carr, P., Gilbert, W. Effects of Fuselage Forebody Geometry on Low-Speed Lateral-Directional Characteristics of a Twin-Tail Fighter Model at High Angles of Attack. NASA TP 1592, 1979.

15. Brandon, J.M., Nguyen, L.T. Experimental Study of Effects of Forebody Geometry on High Angle of Attack Static and Dynamic Stability. AIAA Paper 86-0331, 1986.

16. Wortman, A. On Reynolds Number Effects in Vortex Flow Over aircraft Wings. AIAA Paper 84-0137, .

17. Keener, Earl R. Flow-Separation Patterns on Symmetric Forebodies. NASA Technical Memorandum 86016, 1986.

18. Erickson, Gary E. "Water Tunnel Studies of Leading-Edge Vortices," J.Aircraft. Vol 19, No. 6, June (1982): 442-448.

19. Wentz, W.H. Effects of Leading-Edge Camber on Low-Speed Characteristics of Slender delta Wings. NASA CR-2002, October, 1972.

20. NASA. High Alpha Technology Program Official Plan. NASA Unclassified Internal Document, March 19, 1990.

21. Scott, William B., "NASA Adds to Understanding of High Angle of Attack Regime". Aviation Week and Space Technology Magazine, 22 May 1989: 36-42.

22. Payne, Francis M. The Structure of Leading Edge Vortex Flows Including Vortex Breakdown. University of Notre Dame, Notre Dame, Indiana, May 1987.

23. DelFrate, John H., Zuniga, Fanny A. In-Flight Flow Field Analysis on the NASA F-18 High Alpha Research Vehicle With Comparisons to Ground Facility Data. AIAA Paper 90-0231, 1990.

24. Erickson, G.E. et al Experimental Investigation of the F/A-18 Vortex Flows at Subsonic Through Transonic Speeds, Invited Paper AIAA Paper 89-2222, 1989.

25. Banks, D.W., Wind Tunnel Investigation of the Forebody Aerodynamics of a Vortex -Lift Fighter Configuration at High Angles of Attack. SAE Paper 881419, October 1988.

26. Ng, T. Terry, Malcolm, Gerald N. Aerodynamic Control of the F/A-18 Using Forebody Vortex Control. Eidetics International Aeronautical Research Division, NASA Contract No. NAS2-13155, TR90-004, 1990

27. Johnson, Steven A., Fisher, David F. Water Tunnel Results of a TF/A-18 and F/A-18 Canopy Flow Visualization Study NASA Document, June, 1989.

28. Fisher, David F., Richwine, David M., Banks, Daniel W. Surface Flow Visualization of Separated Flows on the Forebody of an F-18 Aircraft and Wind-Tunnel Model NASA TM 100436, 1988.

29. Fisher, David F., Del Frate, John H., Richwine, David M. In-Flight Flow Visualization Characteristics of the NASA F-18 High Alpha Research Vehicle at High Angles of Attack SAE Paper 892222, 1989.

30. Fisher, David F., Meyer, Robert R., Jr. Flow Visualization Techniques for Flight Research NASA TM 100455, 1988.

31. Fisher, David F., Banks, Daniel W., Richwine, David M. F-18 High Alpha Research Vehicle Surface Pressures: Initial In-

Flight Results and Correlation with Flow Visualization and Wind-Tunnel Data NASA TM 101724, 1990.

32. Del Frate, John H., Fisher, David F., Zuniga, Fanny A. In-Flight Flow Visualization with Pressure Measurements at Low Speeds on the NASA F-18 High Alpha Research Vehicle NASA TM 101726, 1990.
33. Ghaffari, F., Luckring, J.M., Thomas, J.L., Bates, B.L. Navier-Stokes Solutions about the F/A-18 Forebody LEX Configuration AIAA Paper 89-0338, 1989.
34. Schiff, Lewis B., Cummings, Russell M., Sorenson, Reese L., Rizk, Yehia M. Numerical Simulation of High-Incidence Flow over the F-18 Fuselage Forebody AIAA Paper 89-0339, 1989.
35. Zuniga, Fanny A. Private Communication with NASA Researcher, 1990.
36. Del Frate, John H. Private Communication with NASA Researcher, 1990.
37. Hall, Capt. Robert M., Del Frate, John H. Interaction Between Forebody and Wing Vortices, A Water Tunnel Study AFWAL-TM-85252, 1986.
38. Linn, Don F-18 Hornet in detail & scale Aero Publishers, Inc. 1982.
39. Bjarke, Lisa. Private Communication with NASA Researcher, 1990.

APPENDIX A

Computation of Engine Nacelles Flow Rate

The flow characteristics of the F/A-18 are well represented in a water tunnel if the testing facility provides a means to simulate the air flow through the engine nacelles. The NASA Ames-Dryden Water Tunnel has such a capability, which was used in the present investigation to obtain the best possible simulation of flow about the F/A-18.

The following is a summary of the procedure to determine the settings for the flow rate meters that were used to control the flow through the engine nacelles of the different F/A-18 models.

Data needed for the computation:

1. Capture Area (A_0), which is defined as the cross-sectional area of the freestream being drawn into the engine inlet. For the flight regime under study (high angle of attack), the capture area has an average value of 610.56 in^2 (full scale) for one engine inlet [Ref. 39].
2. Freestream velocity (V_0). For the present study, the freestream velocities used were 3 in/sec and 9 in/sec.
3. Maximum flow through flow meters (Qmax). Two flow meters are currently operational at the Ames-Dryden water tunnel. One can indicate up to 1.8 gal/min, while the other 5.12 gal/min.

Given the above information, the flow rate (q_1) through one engine nacelle of a 1/48-scale model in a freestream velocity of 3 in/sec is:

$$q_1 = (A_o/48^2)*V_o$$

$$q_1 = (610.56 \text{ in}^2/2304)*3 \text{ in/sec}$$

$$q_1 = 0.795 \text{ in}^3/\text{sec} \quad \text{or} \quad q_1 = 0.2065 \text{ gal/min.}$$

Then the flow rate for both engine nacelles of the 1/48-scale model of the F/A-18 will be:

$$q_2 = 2*q_1$$

$$q_2 = 2*0.2065 \text{ gal/min} \quad \text{or} \quad q_2 = 0.4130 \text{ gal/min}$$

Using the 1.8 gal/min flow meter, then the setting (FMS) for such a meter is:

$$FMS = (q_2/Qmax)*100\%$$

$$FMS = [(0.4130 \text{ ga./min})/(1.8 \text{ gal/min})]*100\%$$

or $$FMS = 22.94\%.$$

Following a similar procedure, the engine flow rates can then be computed for the other cases involving the 1/32-scale model and for a freestream velocity of 9 in/sec.

APPENDIX B

Vortex Path Reconstruction Method

A mathematical formulation making use of photogrammetry has been developed at NASA Ames-Dryden for the purpose of mapping out the path followed by the cores of the vortices occurring on the F/A-18 at high angles of attack. Using this technique, the LEX vortex core location on a body axis coordinate system has been determined for the F/A-18 HARV from in-flight flow visualization photographic and video images. The method uses as input picture coordinates corresponding to the path of the vortex core from two different views. Additionally, data regarding the location of the cameras and two different reference points are supplied to the algorithm as input.

For the present investigation, two still cameras were used for LEX vortex path reconstruction, which were positioned facing two adjacent test section walls of the water tunnel. Figure B.1 shows on the left a "primary view" camera and on the right a "secondary view" camera. Using a system of rectangular coordinates X_O,Y_O,Z_O (world coordinates), each camera is assigned a location in space with respect to such a coordinate system. The coordinates of two different reference points are also needed. Such reference points must be chosen so as to be visible through both cameras. Additionally, the coordinates of points in the line of sight of each camera must also be known.

From photographs of each view, the measured horizontal distance in each photograph between the two reference points is obtained.

The data is arranged in the following format and saved as a file named: V.INIT.

Table B.1

Example of Format Used to Arrange Data for the V.INIT File

1	13.5944	37.4055	-2.9375
2	19.4526	28.0175	-10.7023
3	2.175		
4	11.2031	36.0000	-28.8958
5	11.2031	36.0000	-20.0938
6	-5.0780	40.0469	-9.98440
7	28.0000	40.0469	-9.98440
8	2.4438		

where:

1. Line 1 contains the world coordinates of reference point 1.
2. Line 2 contains the world coordinates of reference point 2.
3. Line 3 contains the horizontal distance between the two reference points measured from a primary view image.
4. Line 4 contains the world coordinates of the primary view camera.
5. Line 5 contains the world coordinates of the point in the line of sight of the primary view camera.
6. Line 6 contains the world coordinates of the secondary view camera.
7. Line 7 contains the world coordinates of the point in the line of sight of the secondary view camera.

8. Line 8 contains the horizontal distance between the two reference points measured from a secondary view image.

As the initial data is being gathered and saved in the V.INIT file, the picture coordinates of the vortex core can also be obtained from images of both the primary and the secondary view. For the primary view, an x_p and a y_p coordinate of discrete points of the vortex core are obtained, while for the secondary view only the x_p coordinate of the corresponding points is needed.

Because of the distortion effect described above, it became necessary to correct the values of the picture coordinates read from the "distorted" views of the vortex cores. This correction was done by using relationships between distorted and undistorted picture coordinates. Such relationships were obtained from knowing in advance the location of certain specific points on the F/A-18 such as the LEX apex, the UHF antenna on the top of the fuselage, the intersection of the left vertical tail leading edge with the fuselage, etc. Thus, by working "backwards", the undistorted picture coordinates of such points were obtained and plotted against the distorted values. Figure B.2. shows such plots and the linear relationships obtained. These formulas were then used to correct all the distorted picture coordinates of the vortex cores.

Having corrected the picture coordinates for distortion, the resulting values are then arranged in the following format and saved in a file called VORTEX.IN.

Table B.2.

Example of Format Used to Arrange Data for the VORTEX.IN File

.6673	2.3375	-.8694
.6228	2.1909	-.9388
.5949	2.0763	-.9735
.5382	1.9297	-.9977
.4833	1.7831	-.9977
.4493	1.6479	-1.0026
.3909	1.5022	-.9994
.2924	1.3441	-.9638

999.

where:

1. The first column represents the corrected x_p coordinate from the primary view.
2. The second column represents the corrected y_p coordinate from the primary view.
3. The third column represents the corrected x_p coordinate from the secondary view.

Subsequently, the vortex path reconstruction program (VORTEX) is run. The results are dumped into a file called VXYZ, which contains the world coordinates (X_o,Y_o,Z_o) of the vortex cores.

These coordinates are further transformed to a body axis coordinate system and plotted as shown in Figure B.3.

APPENDIX C

Figures

This appendix contains all the figures. Included are half-tone pictures made from original color photographs, showing F/A-18 water tunnel flow visualizations, as well as various other aspects relevant to the present investigation.

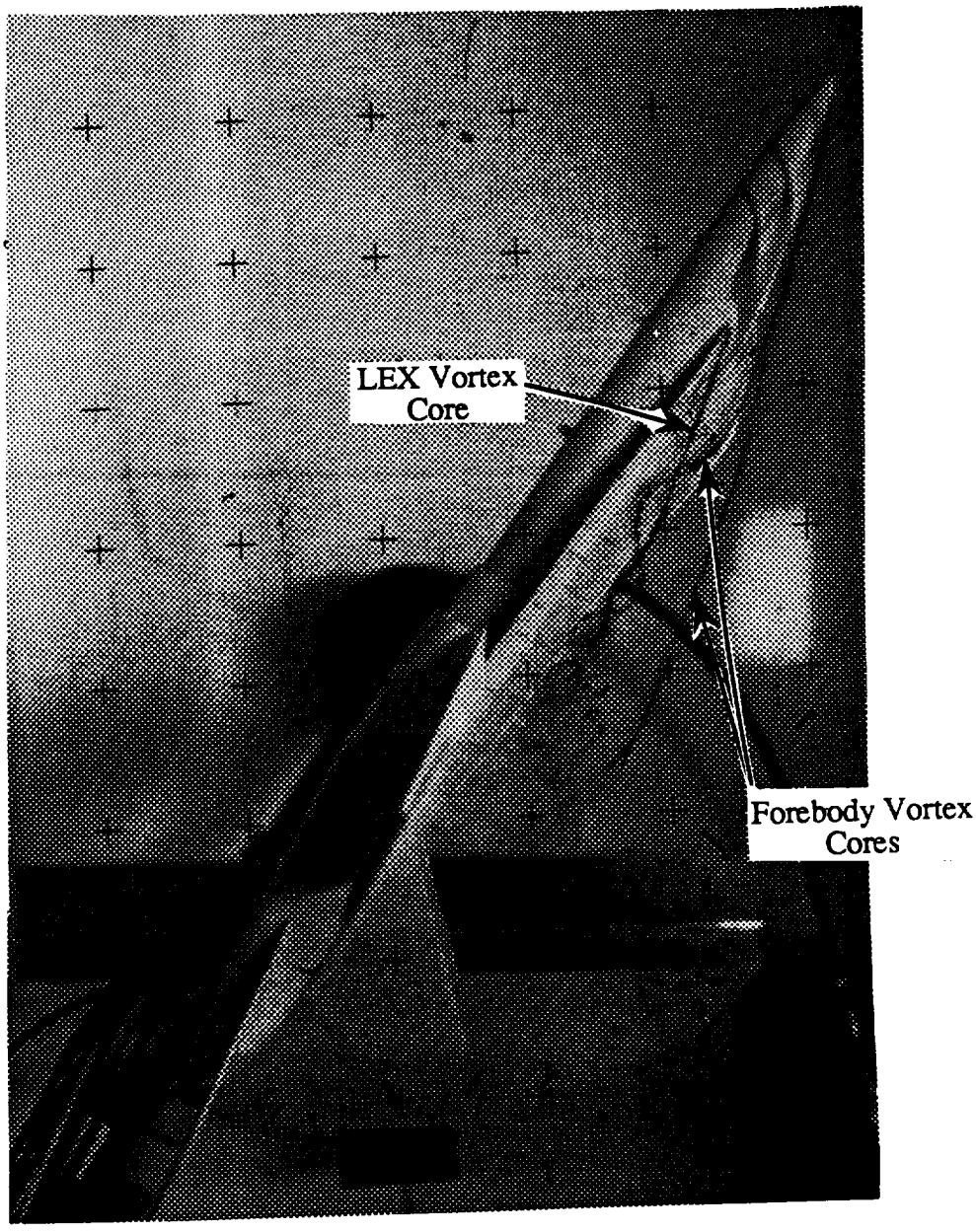

Figure 1. Vortex Flow Structures on the F/A-18. Angle of Attack: 30 degrees; Angle of Sideslip: +6 degrees

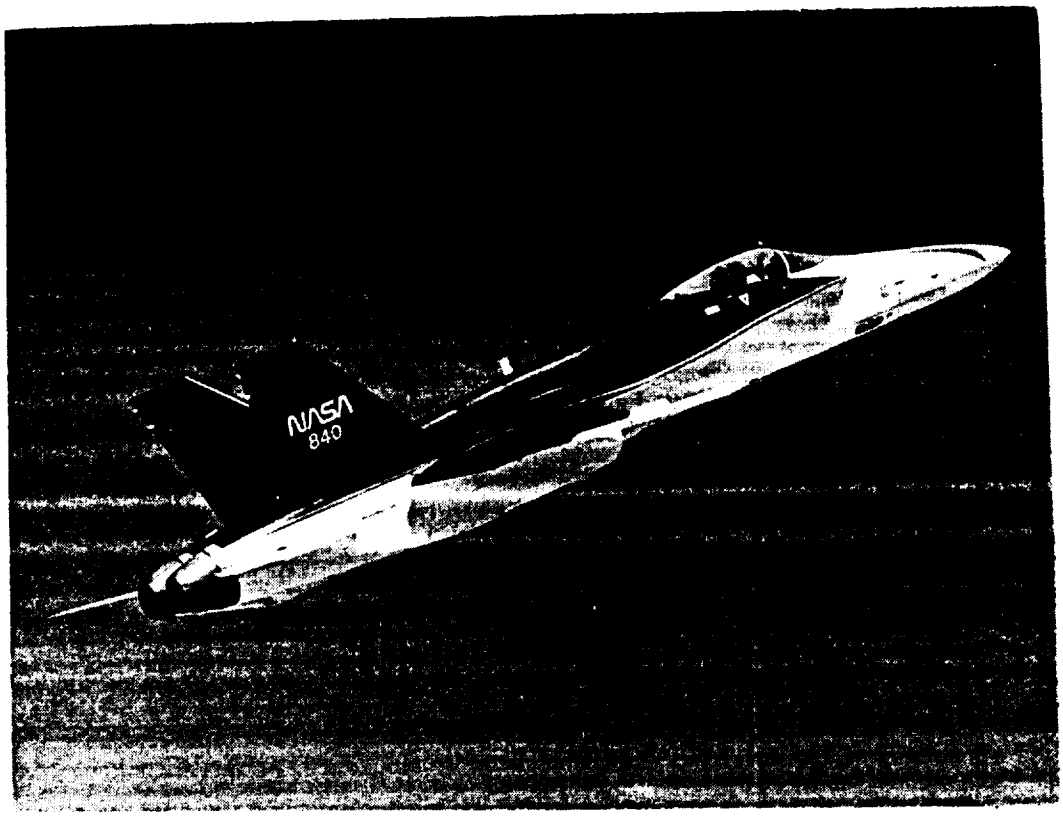

Figure 2. The F/A-18 High Alpha Research Vehicle (HARV)

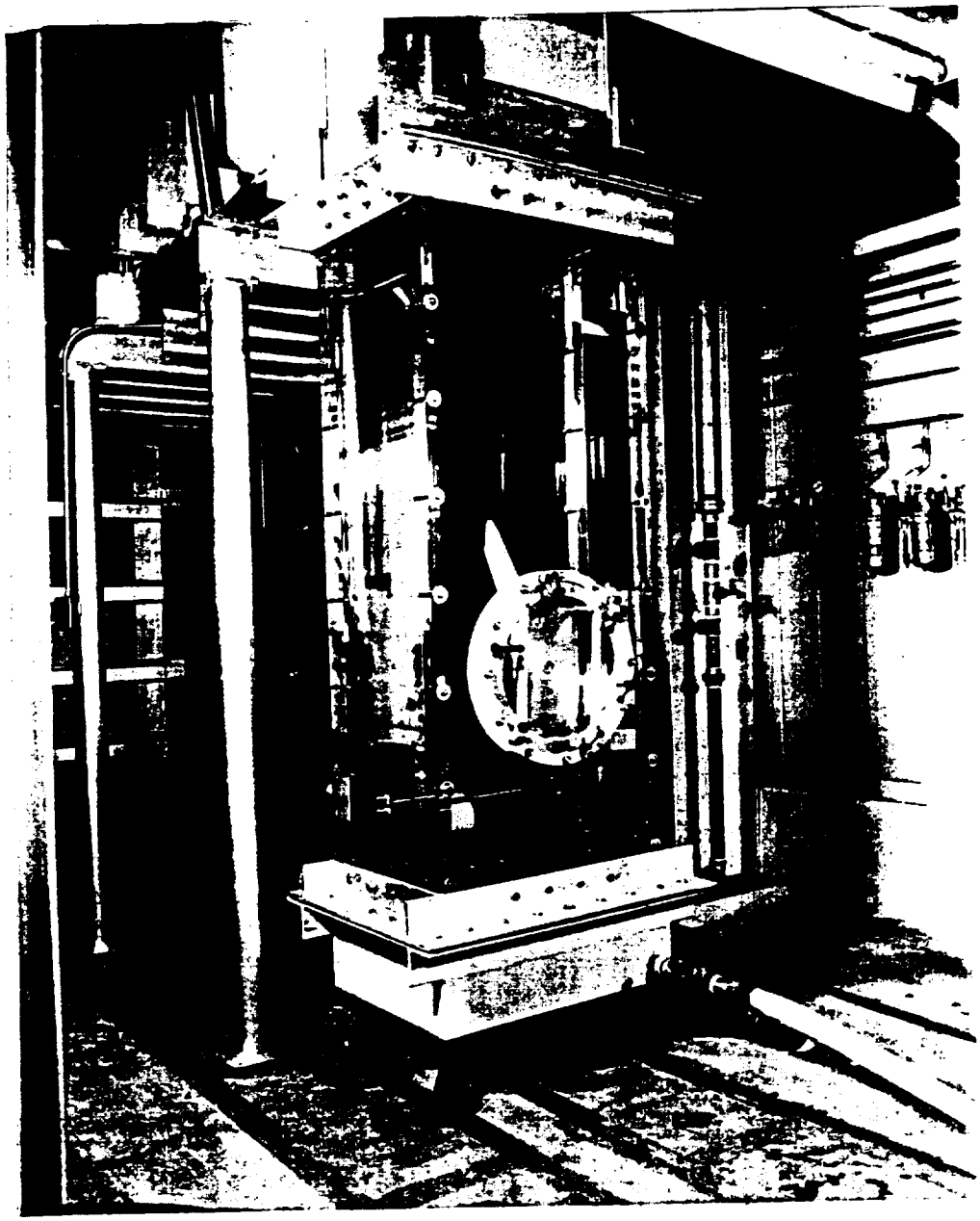

Figure 3. The NASA Ames-Dryden Flow Visualization Facility

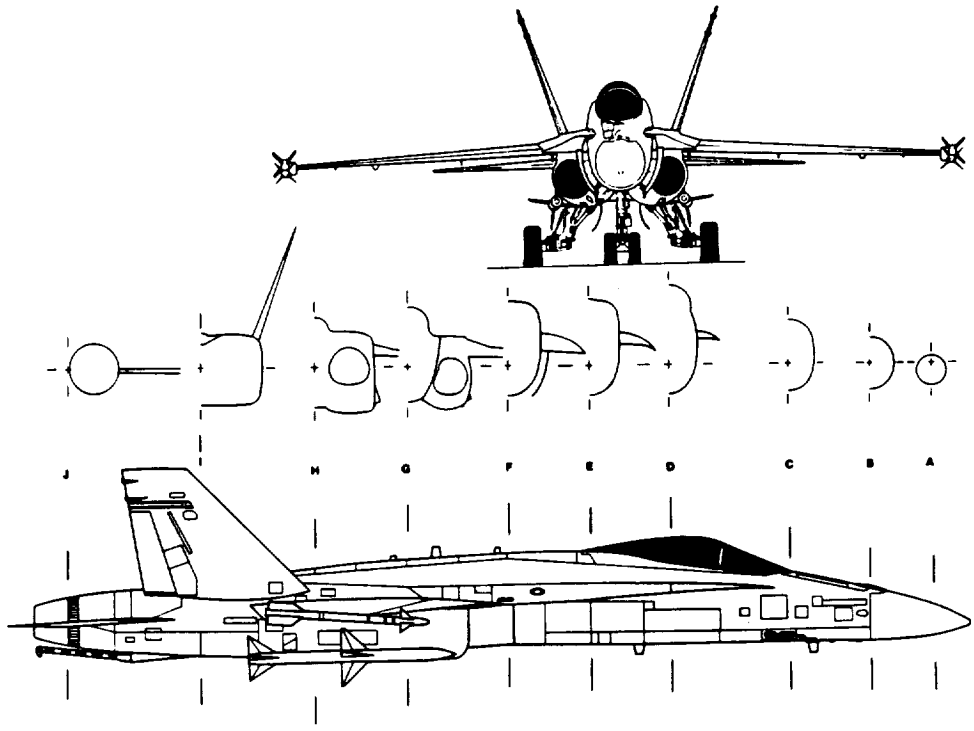

Figure 4. Geometry Details of the F/A-18 Aircraft (Figure From Reference 38)

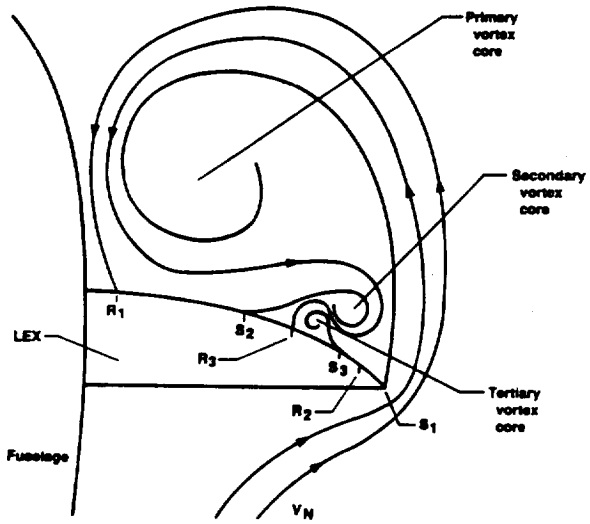

Figure 5. Model of the Cross-Sectional Flow About the LEX of the F/A-18

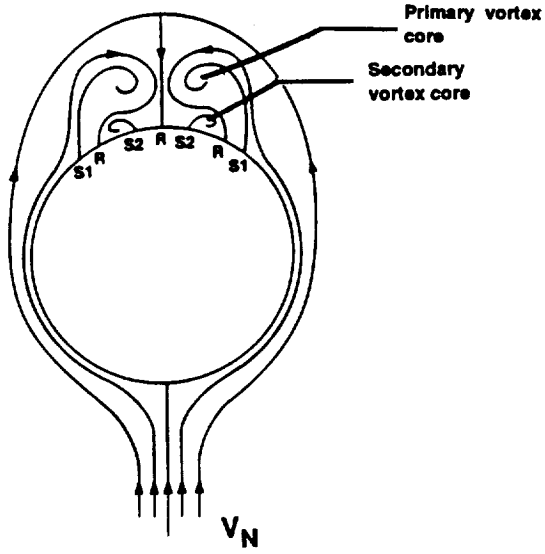

Figure 6. Model of the Cross-Sectional Flow About the Forebody of the F/A-18

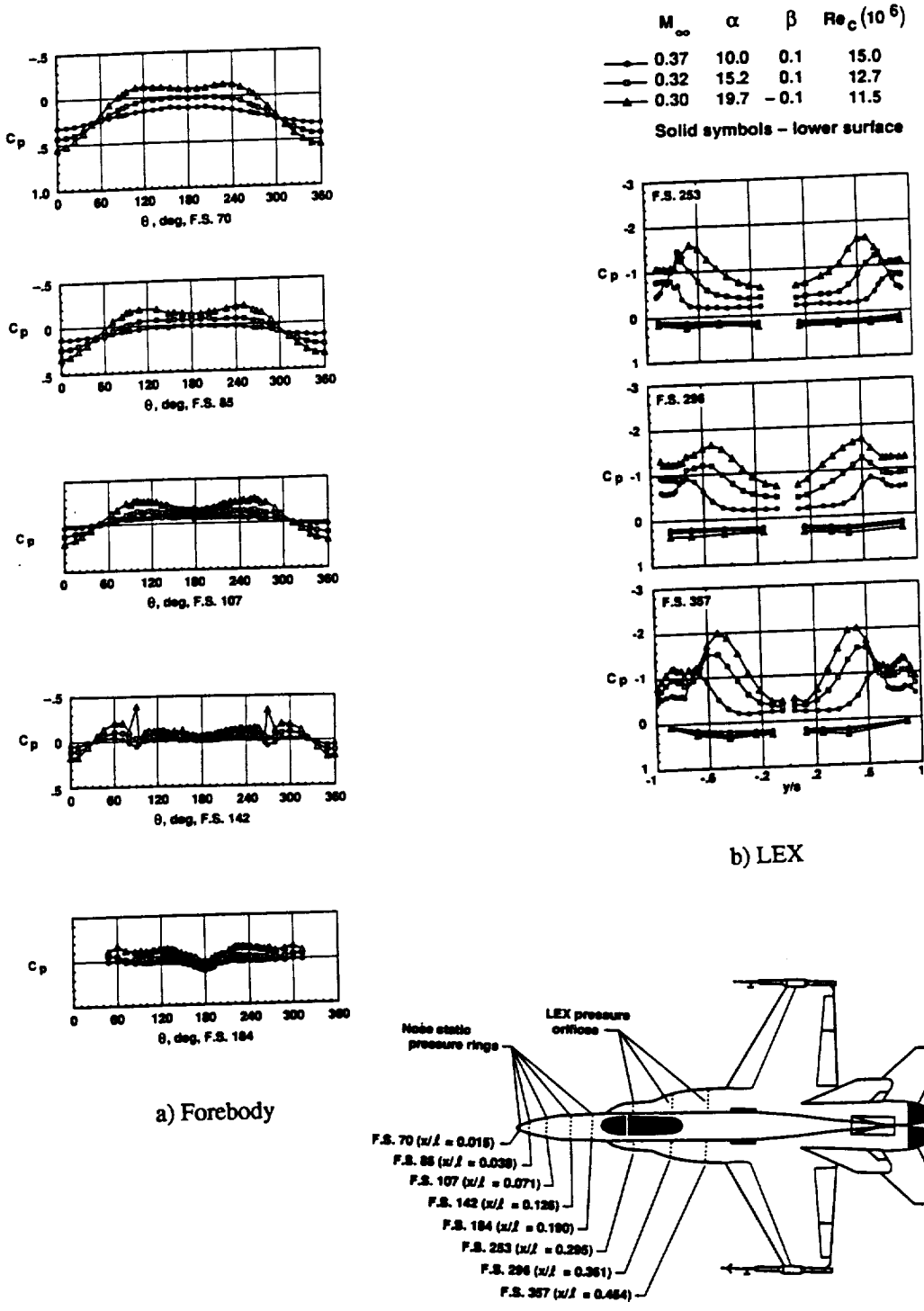

Figure 7. Pressure Distributions on the LEX and Forebody of the F/A-18 HARV (Data and Figures From Reference 32)

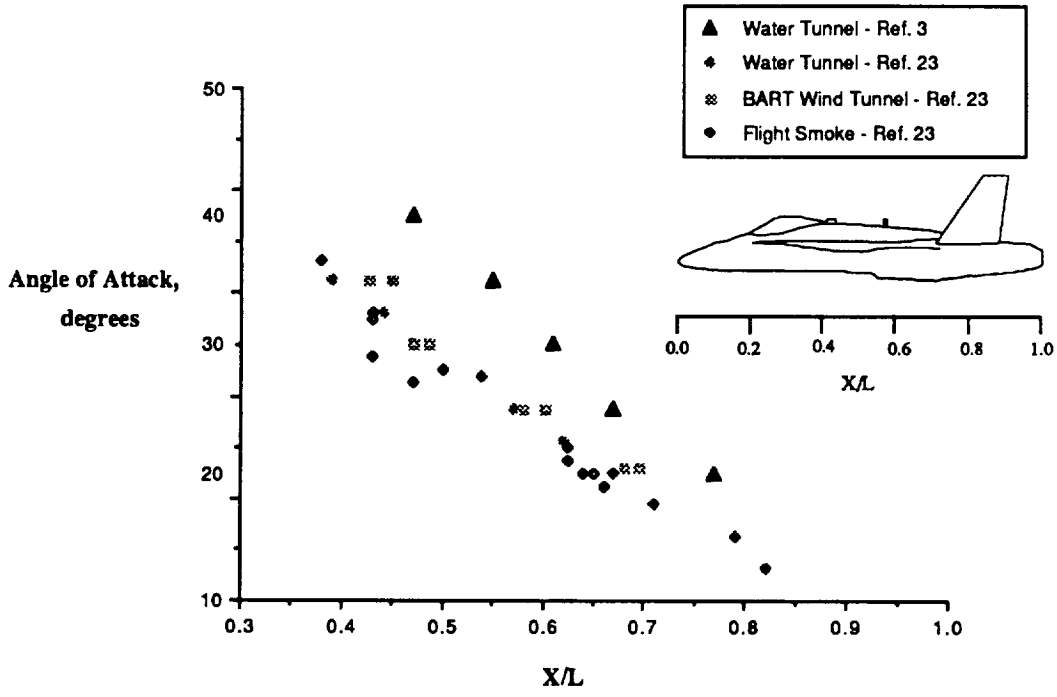

Figure 8. Location of LEX Vortex Core Breakdown From Flight and Ground Facilities

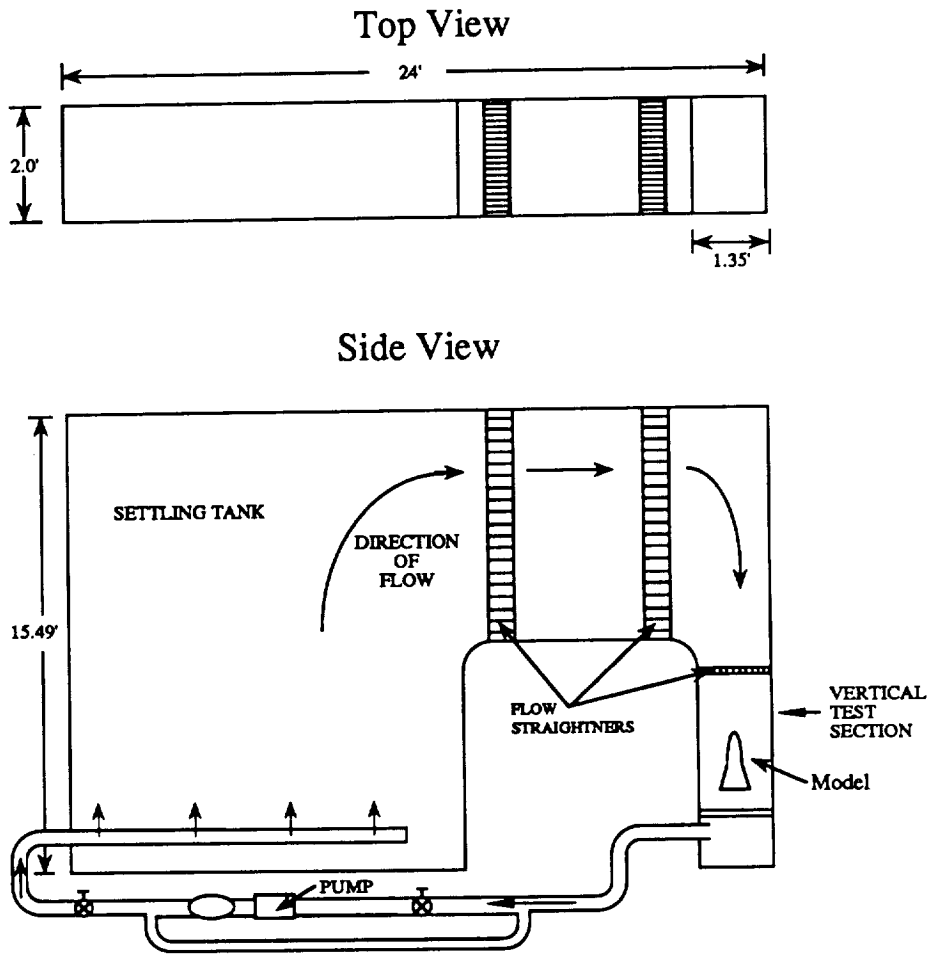

Figure 9. Schematic of the NASA Ames-Dryden Water Tunnel

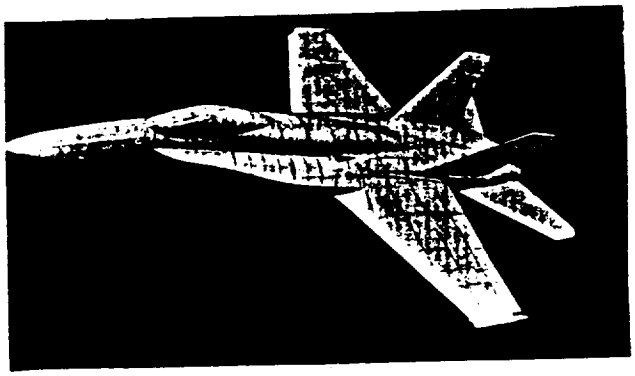

48A Model

48B Model

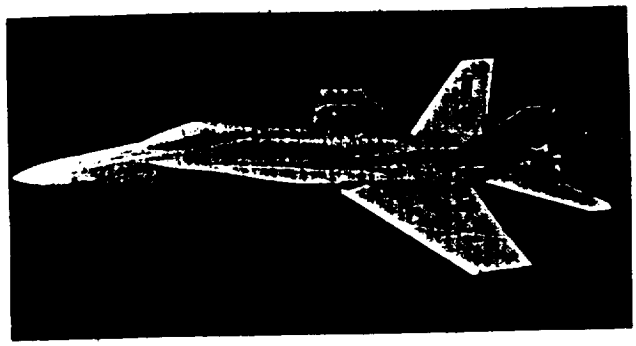

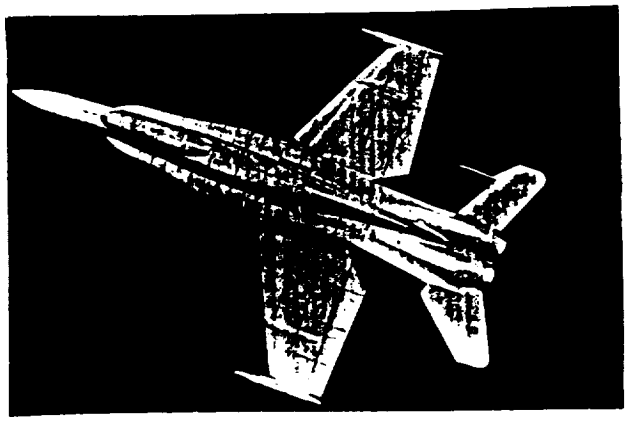

48C Model

32A Model

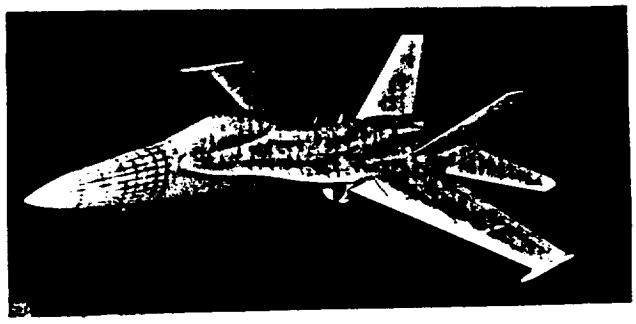

Figure 10. F/A-18 Models Tested

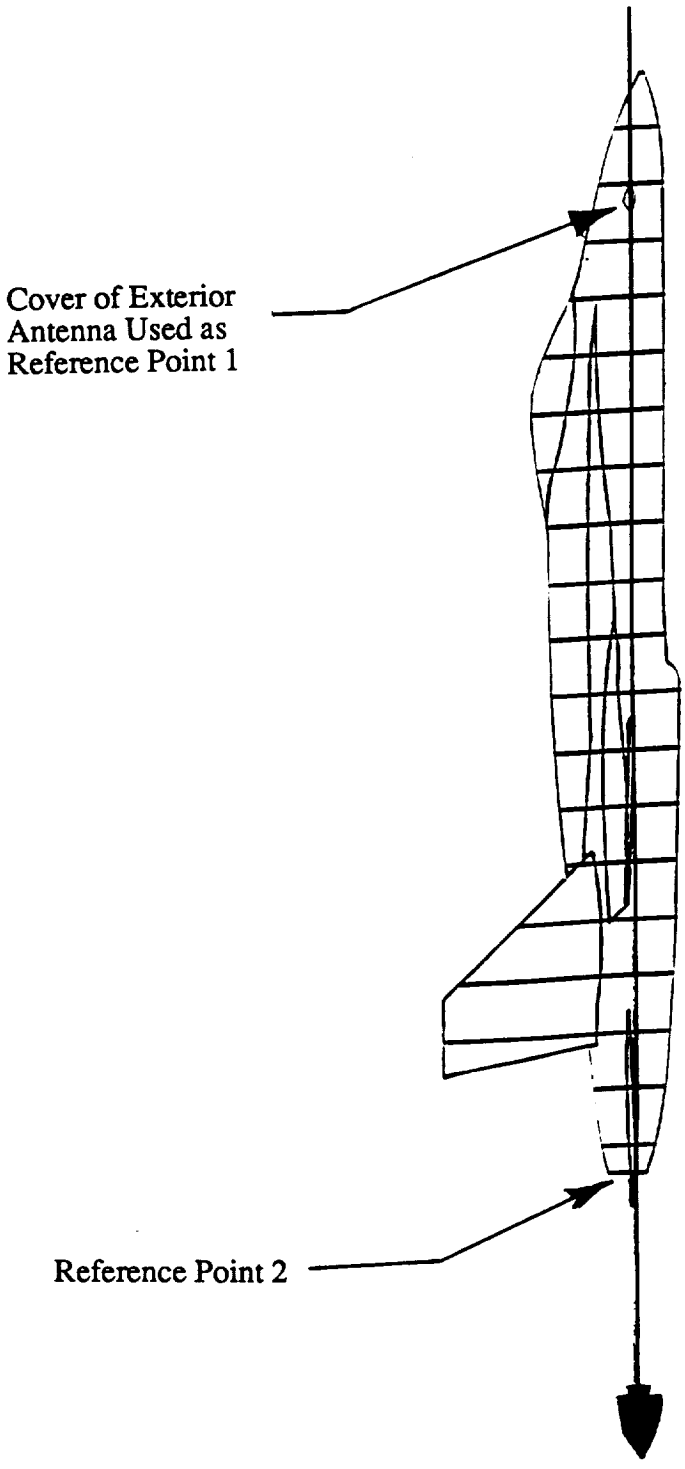

Figure 11. Location of Reference Points Used to Attain a Zero-Degree Angle of Attack

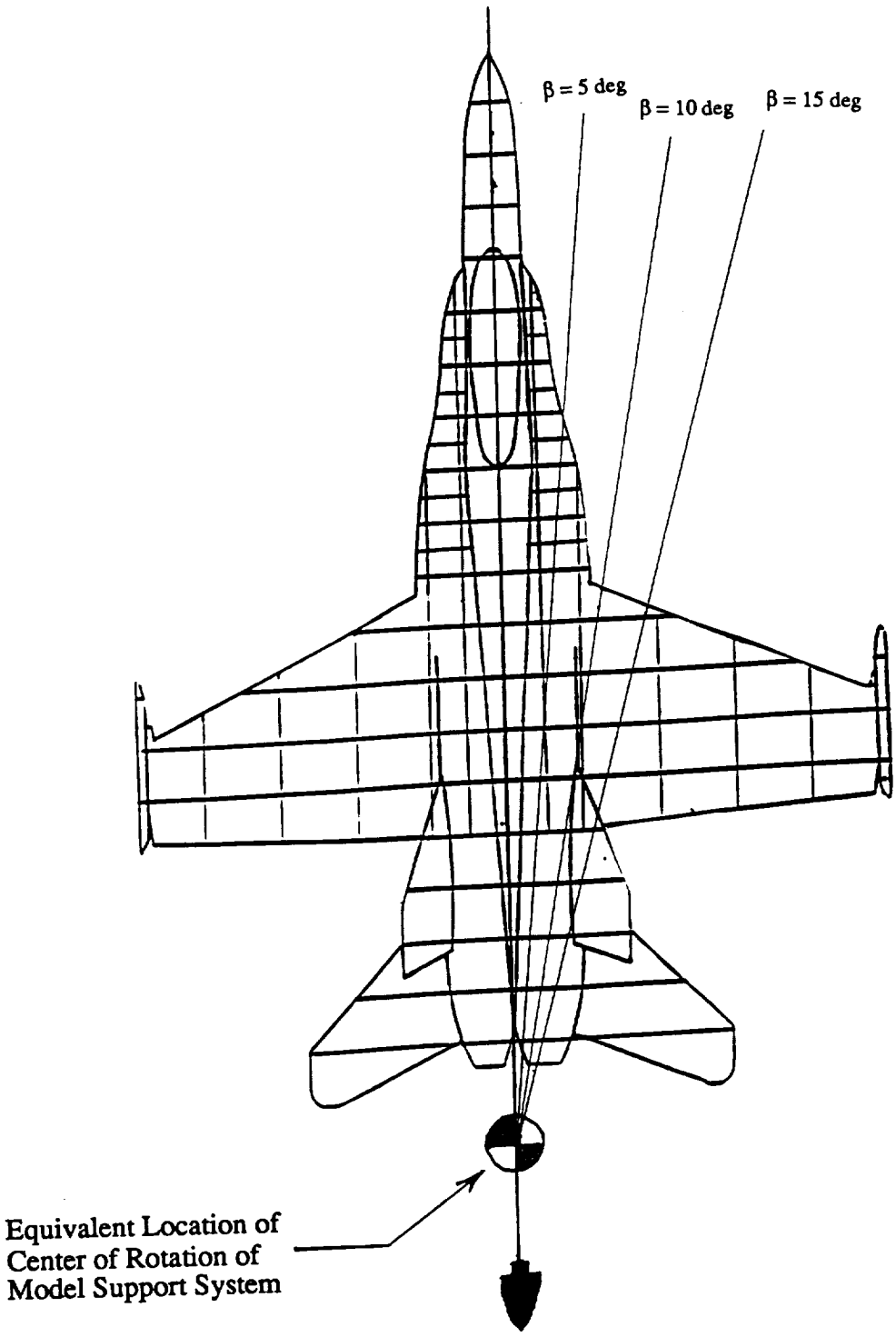

Figure 12. Typical Drawing Used to Determine the Angle of Sideslip

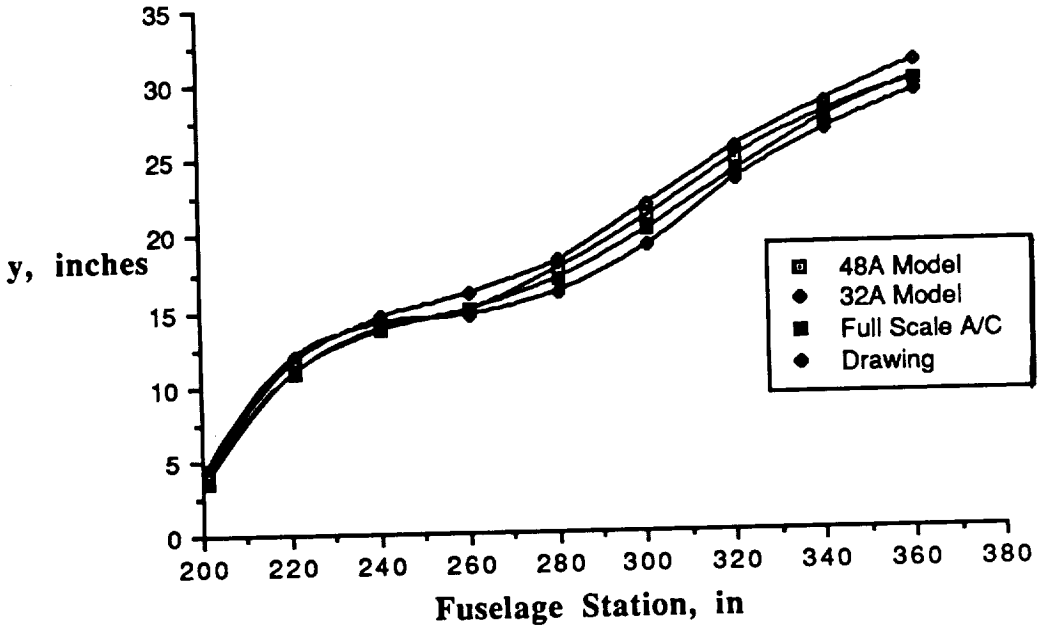

Figure 13. Comparison of LEX Local Span Between Water Tunnel Models

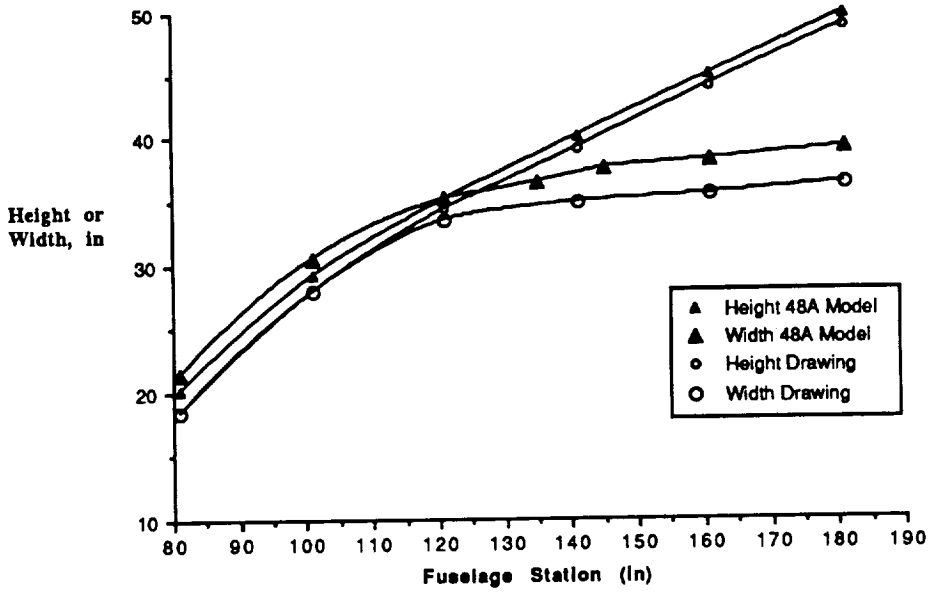

Figure 14. Forebody Cross-Sectional Geometry
(48A Model and MD Drawing)

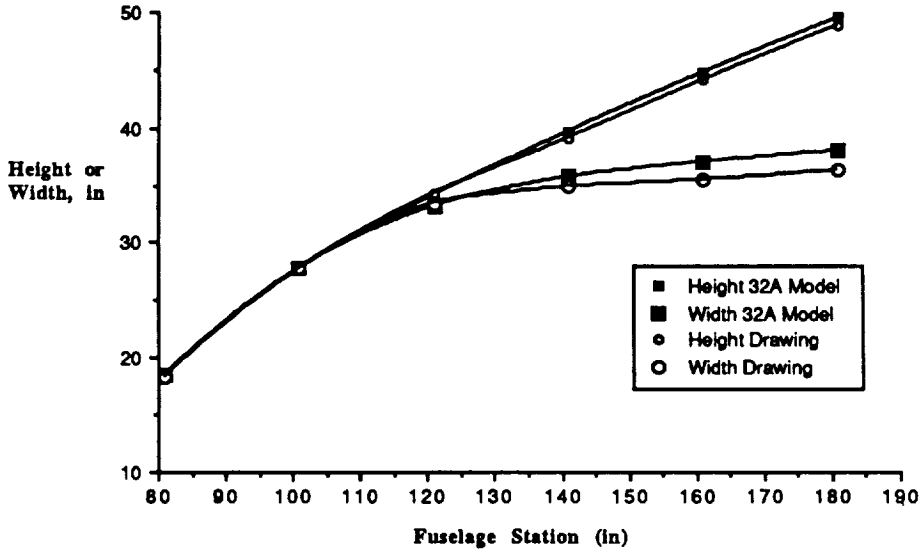

Figure 15. Forebody Cross-Sectional Geometry
(32A Model and MD Drawing)

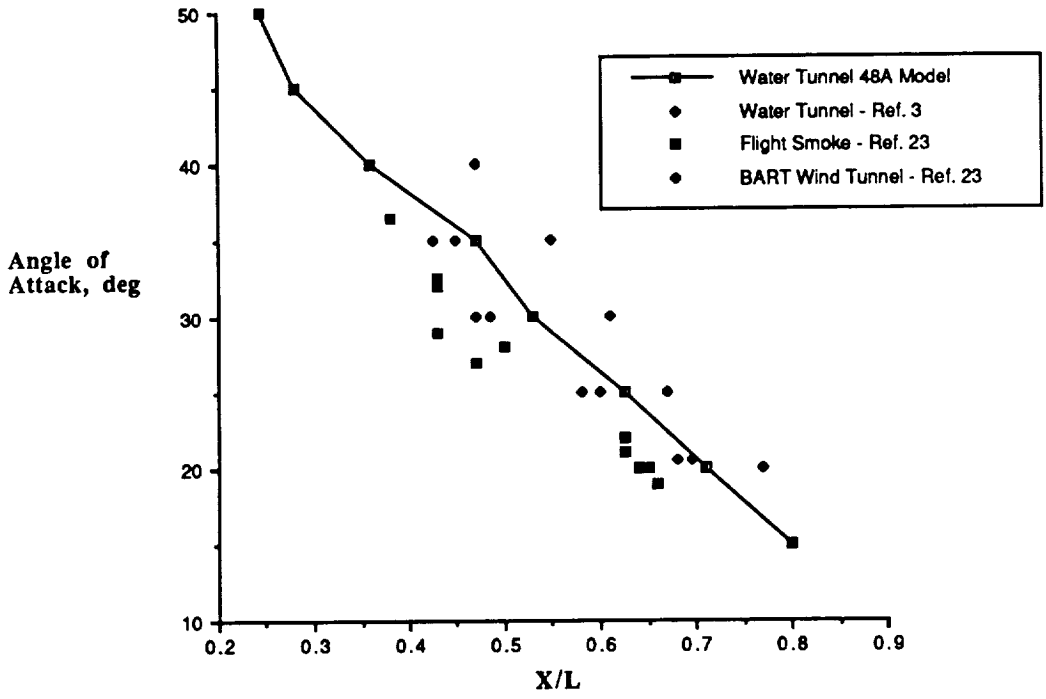

Figure 16. Location of LEX Vortex Core Breakdown From the 48A Model and Other Flight and Ground Facilities

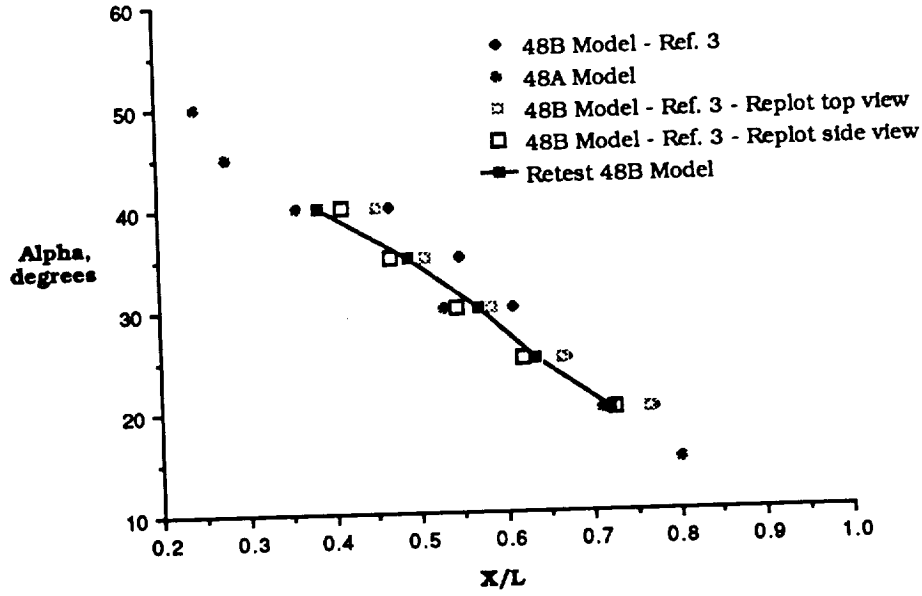

Figure 17. Water Tunnel Results of LEX Vortex Core Breakdown Using 1/48-scale Models of the F/A-18

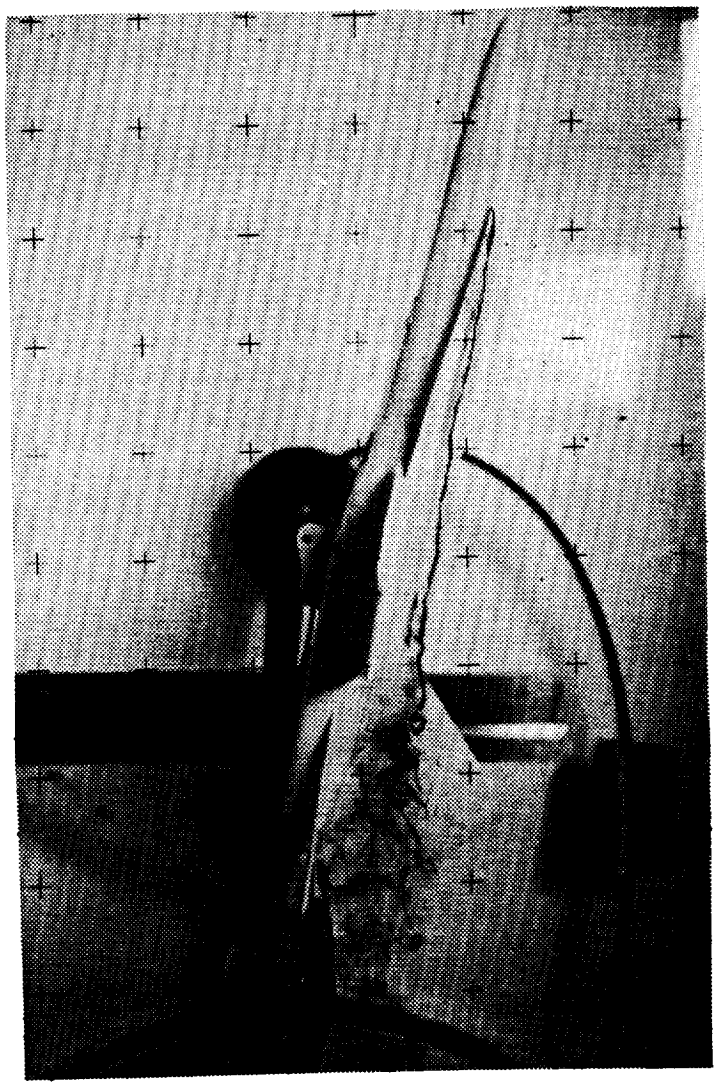

Figure 18. LEX Vortex Core Breakdown on the 48A Model.
Alpha = 15 Degrees; Beta = 0 Degrees

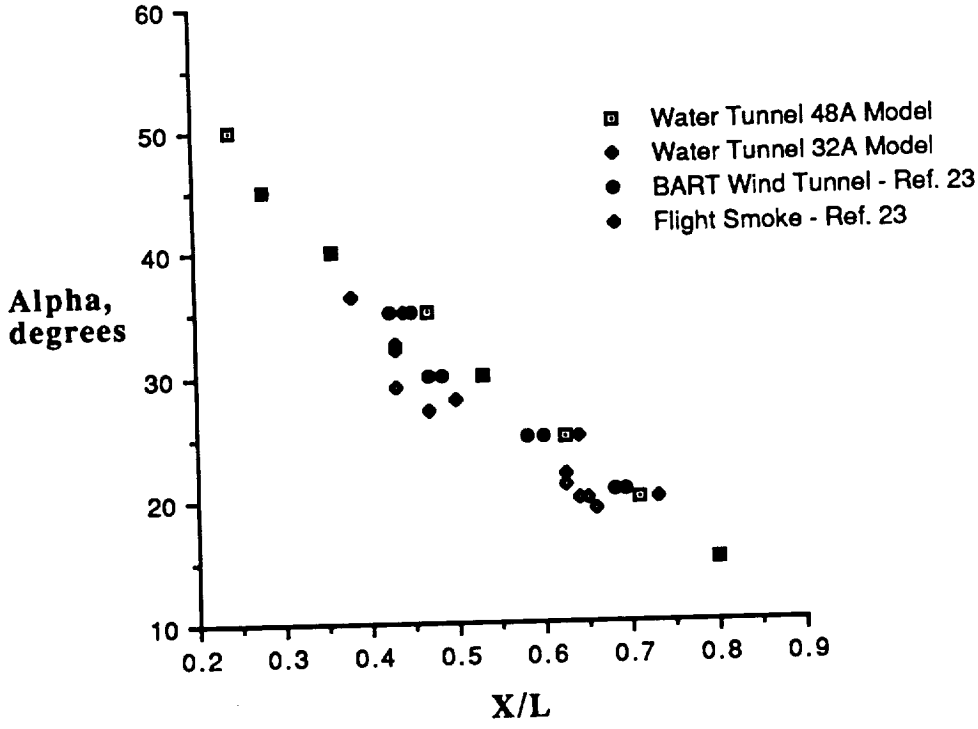

Figure 19. LEX Vortex Core Breakdown on the 48A Model and the 32A Model

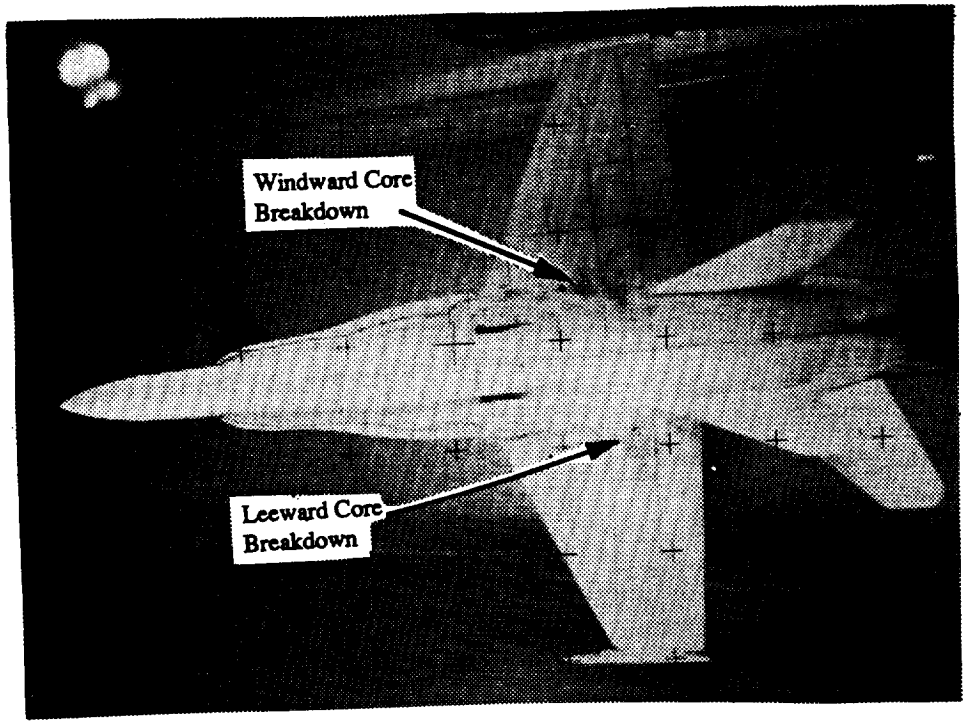

a) Alpha = 25 Degrees; Beta = 3.5 Degrees

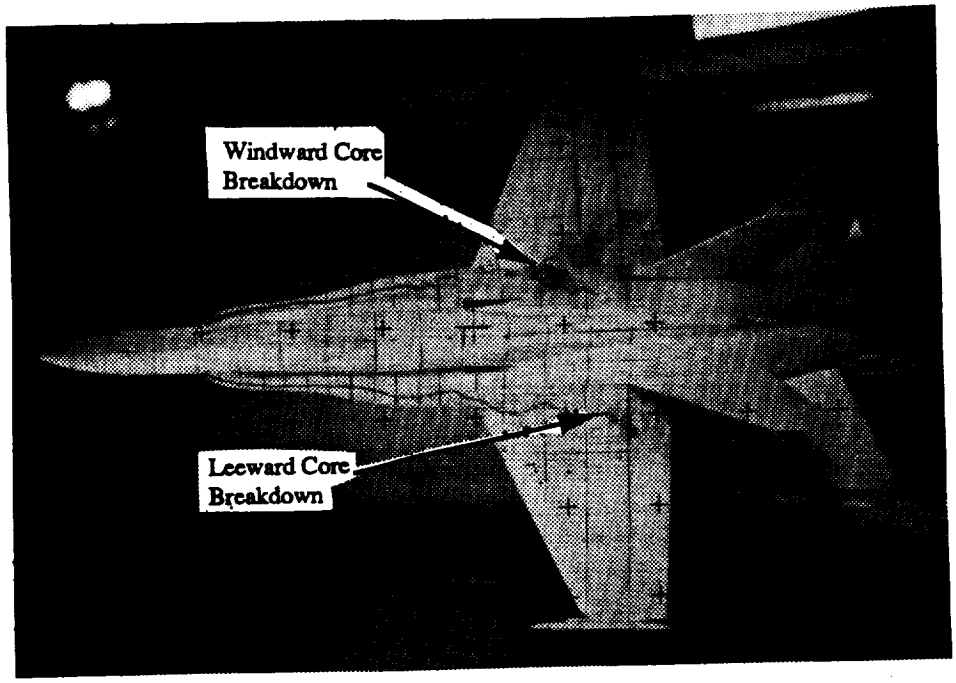

b) Alpha = 25 Degrees; Beta = 4.5 Degrees

Figure 20. Longitudinal Variation in the Location of the LEX Vortex Core Breakdown With Increasing Angle of Sideslip

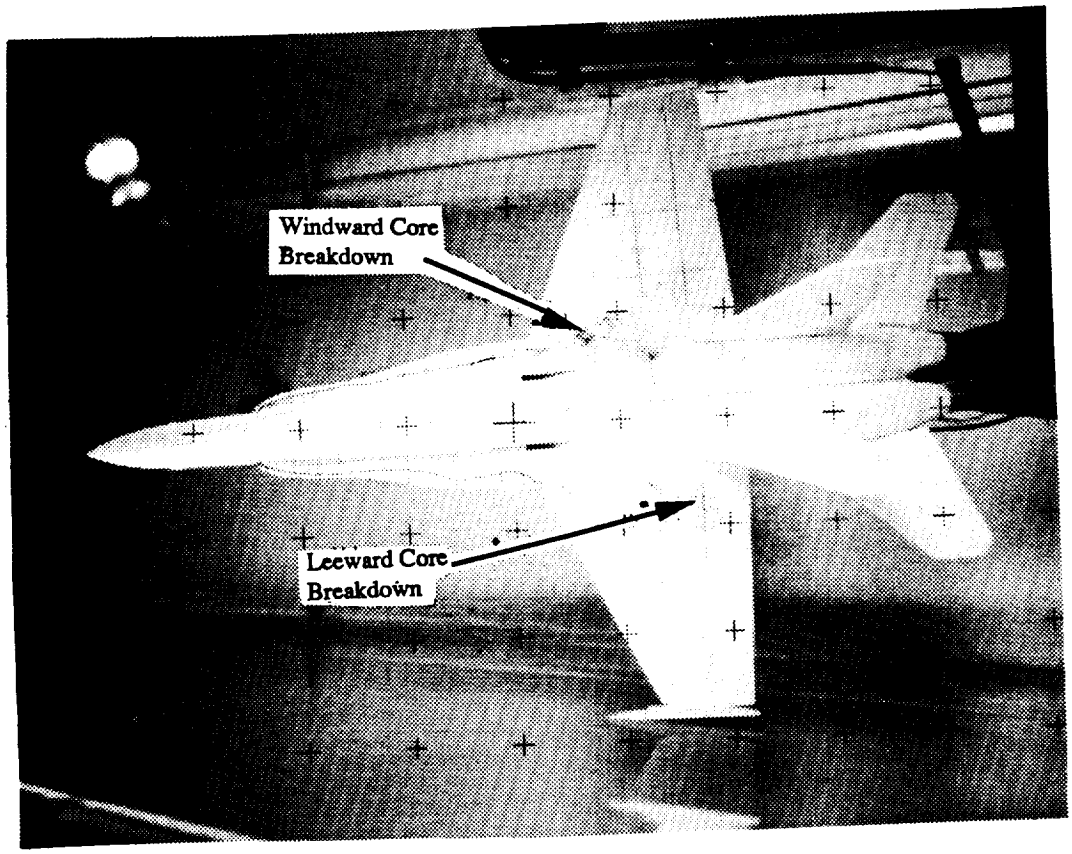

c) Alpha = 25 Degrees; Beta = 5.5 Degrees

Figure 20. Concluded

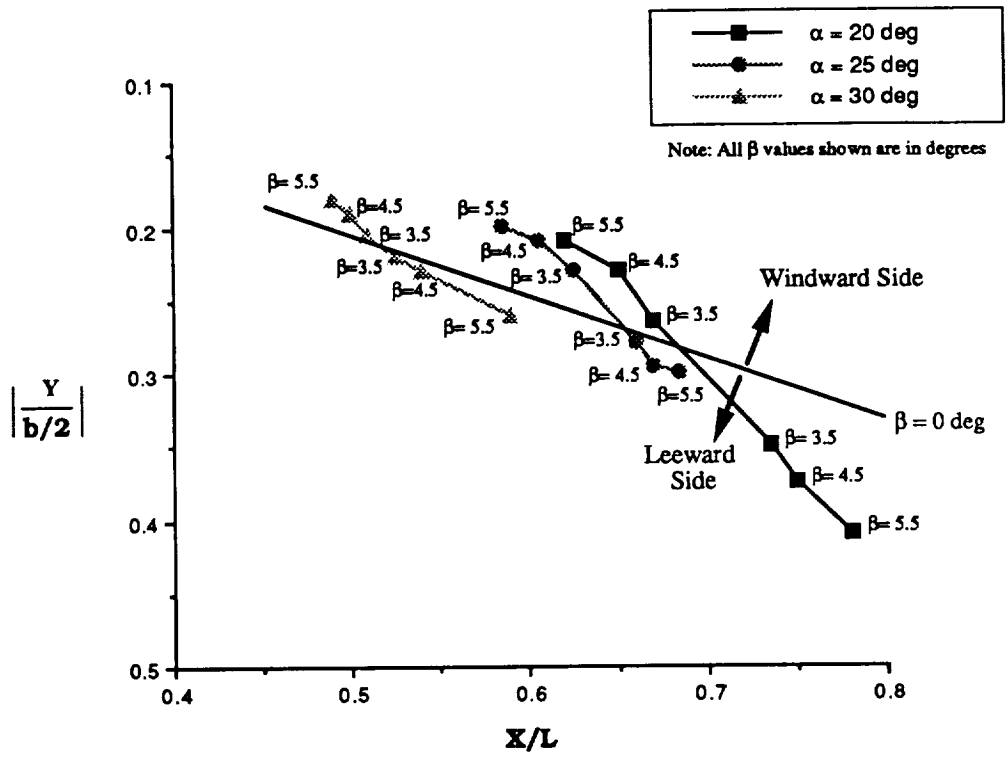

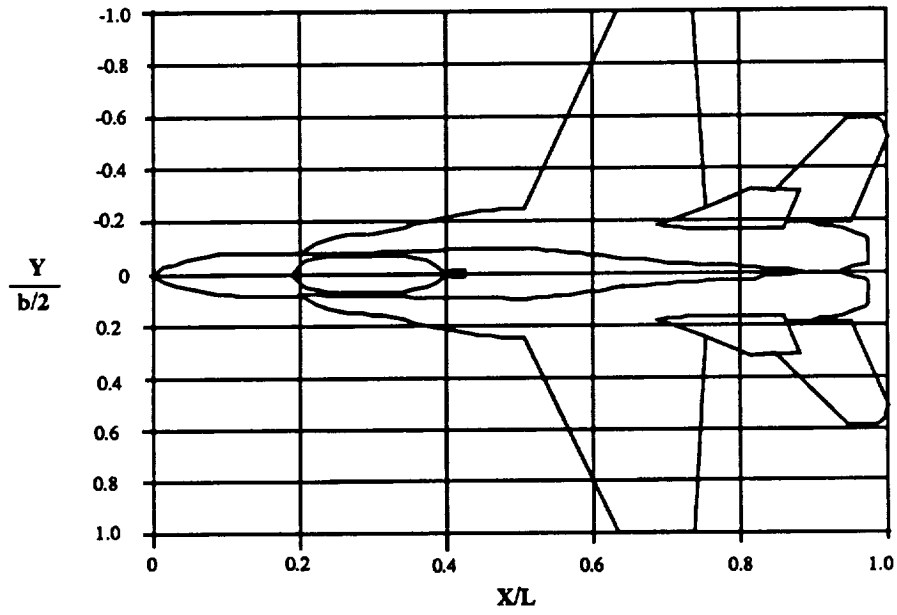

Figure 21. LEX Vortex Breakdown Lateral and Longitudinal Location as a Function of Angle of Attack α, and Angle of Sideslip β

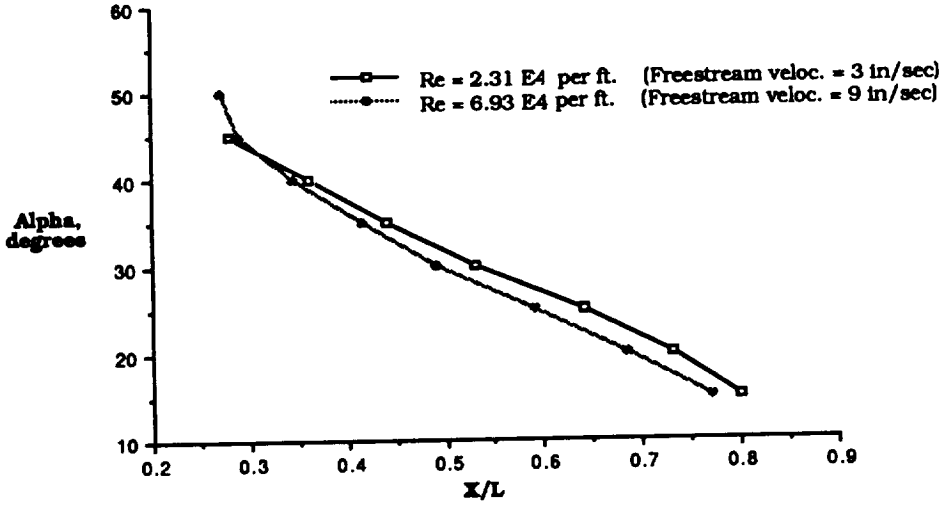

Figure 22. Effect of Reynolds Number on the Location of LEX Vortex Core Breakdown Using the 32A Model

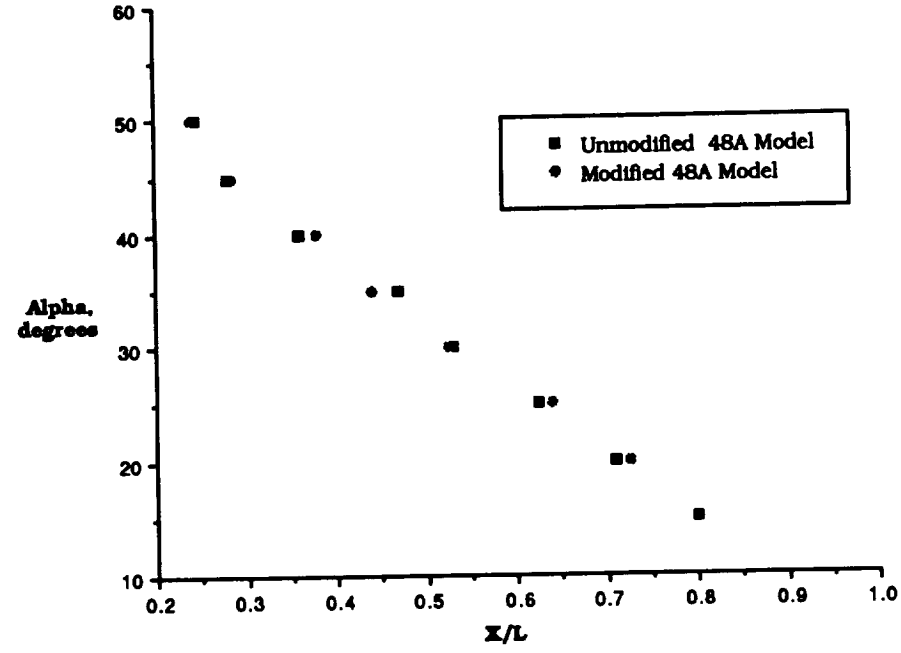

Figure 23. Comparison of LEX Vortex Core Breakdown Location Between the Modified and Unmodified 48A Model

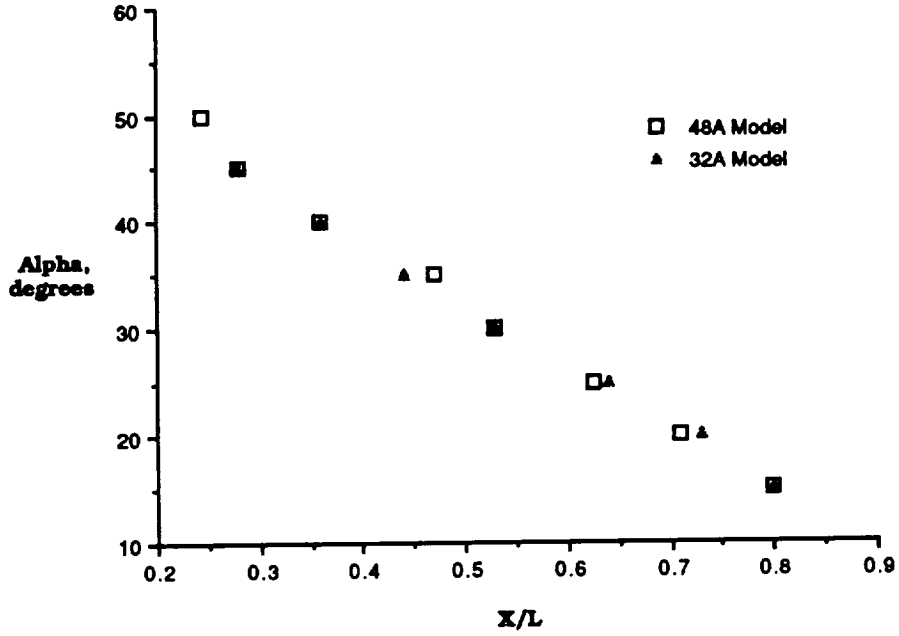

Figure 24. Effect of Model Scale on the Location of LEX Vortex Core Breakdown

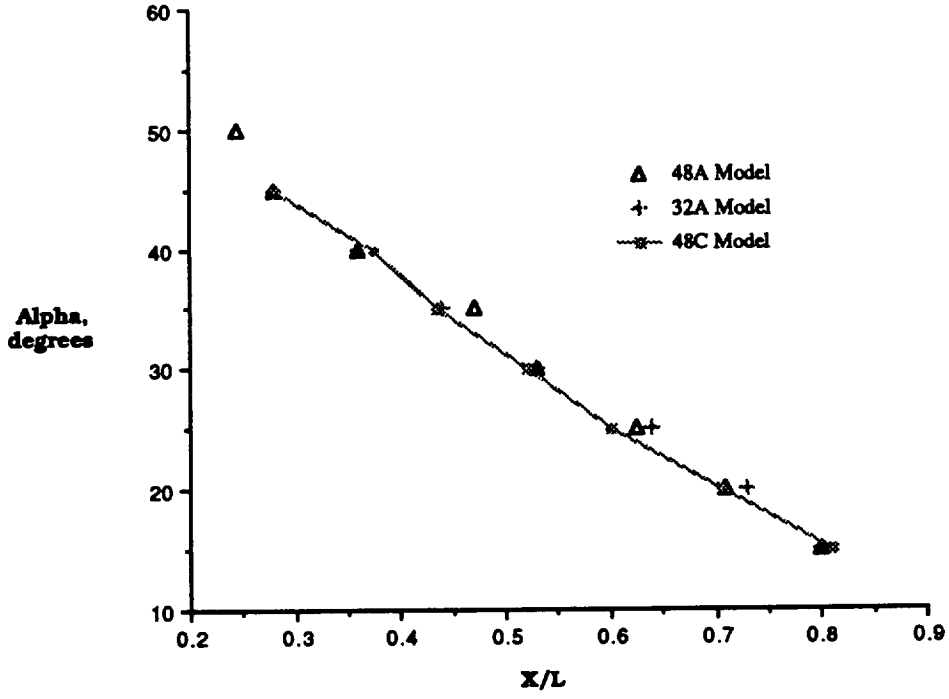

Figure 25. Effect of Model Fidelity on the Location of LEX Vortex Core Breakdown

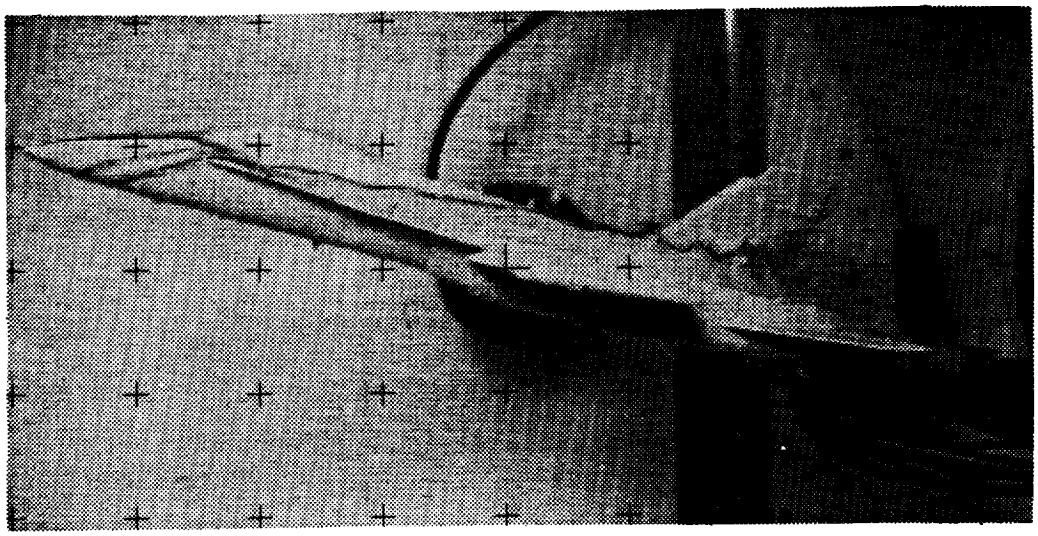

a) Alpha = 15 Degrees; Beta = 0 Degrees

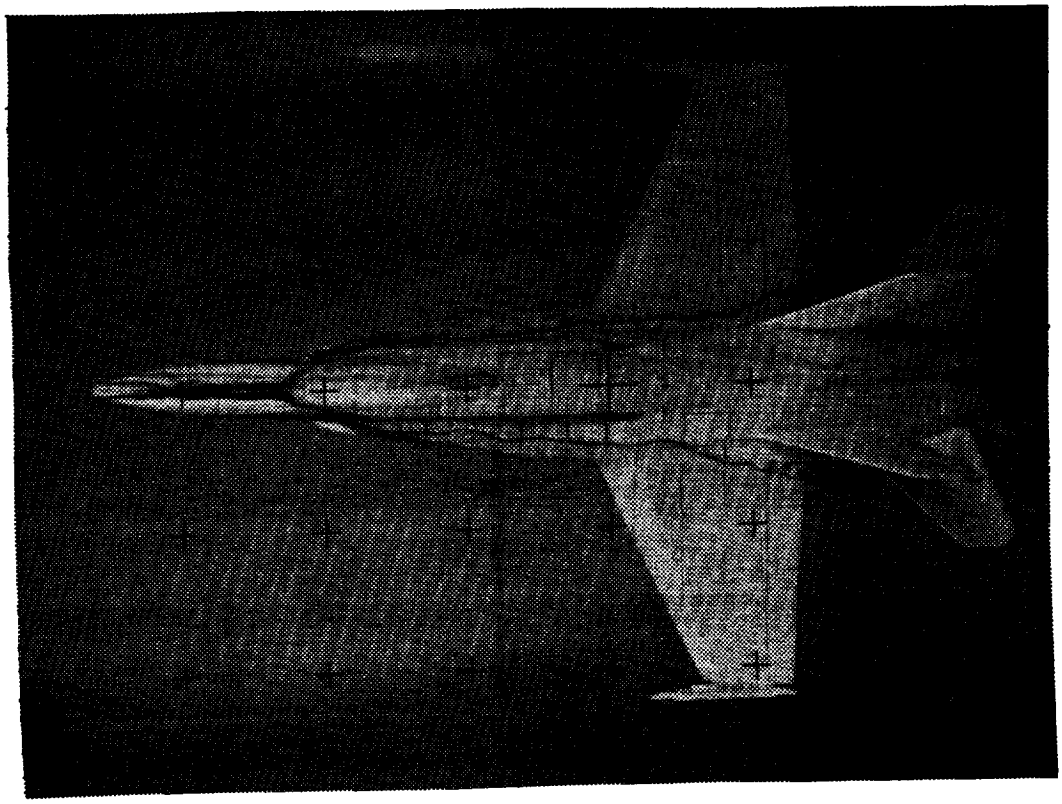

b) Alpha = 15 Degrees; Beta = 0 Degrees

Figure 26. Variation in the Location of the LEX Vortex Core With Increasing Angle of Attack

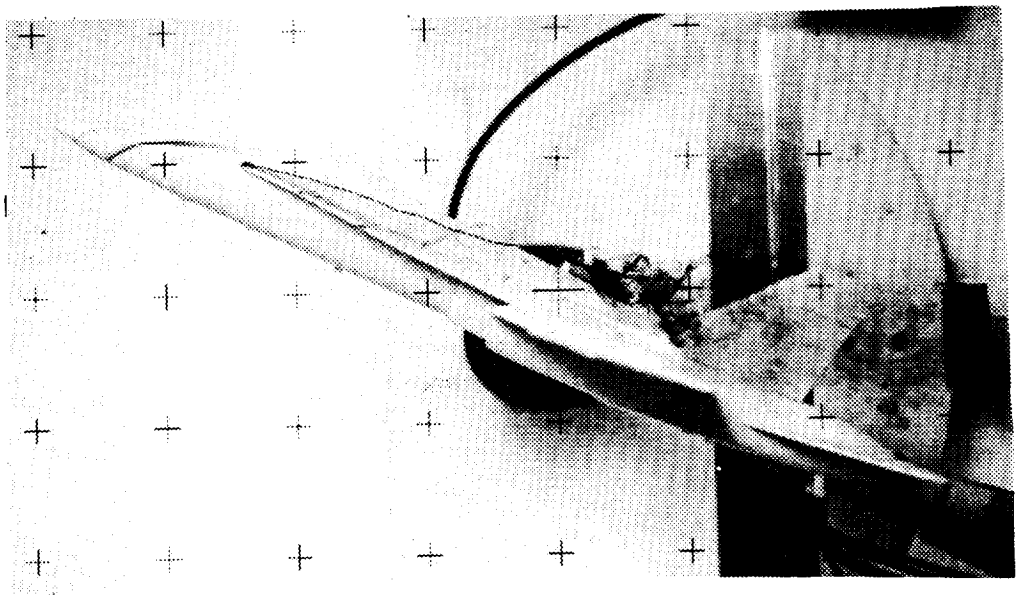

c) Alpha = 25 Degrees; Beta = 0 Degrees

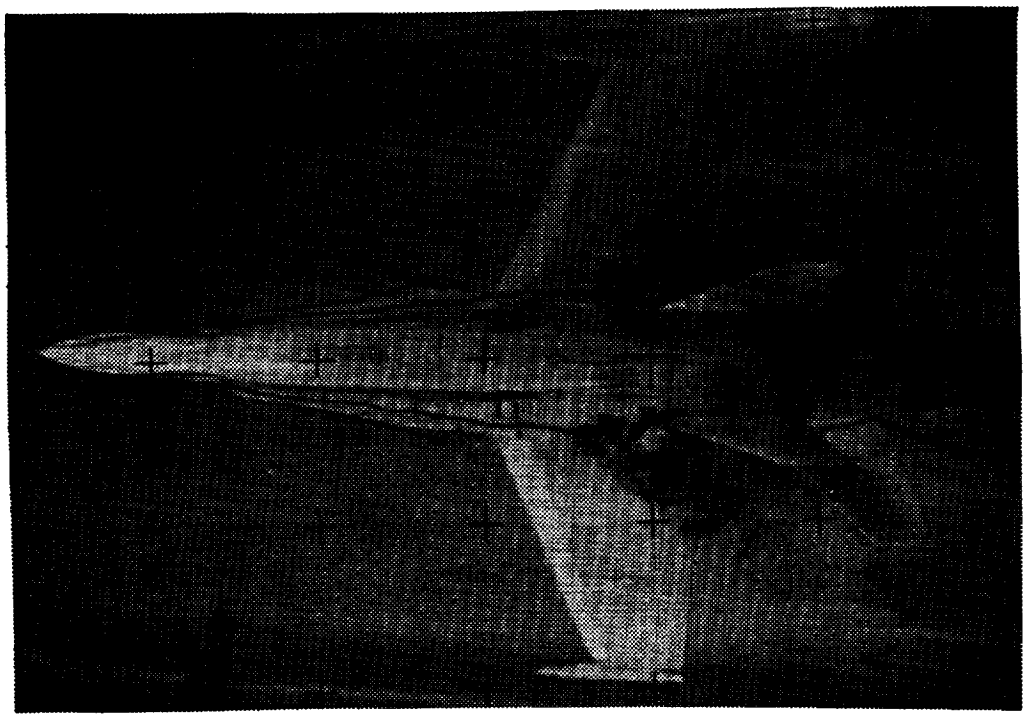

d) Alpha = 25 Degrees; Beta = 0 Degrees

Figure 26. Continued

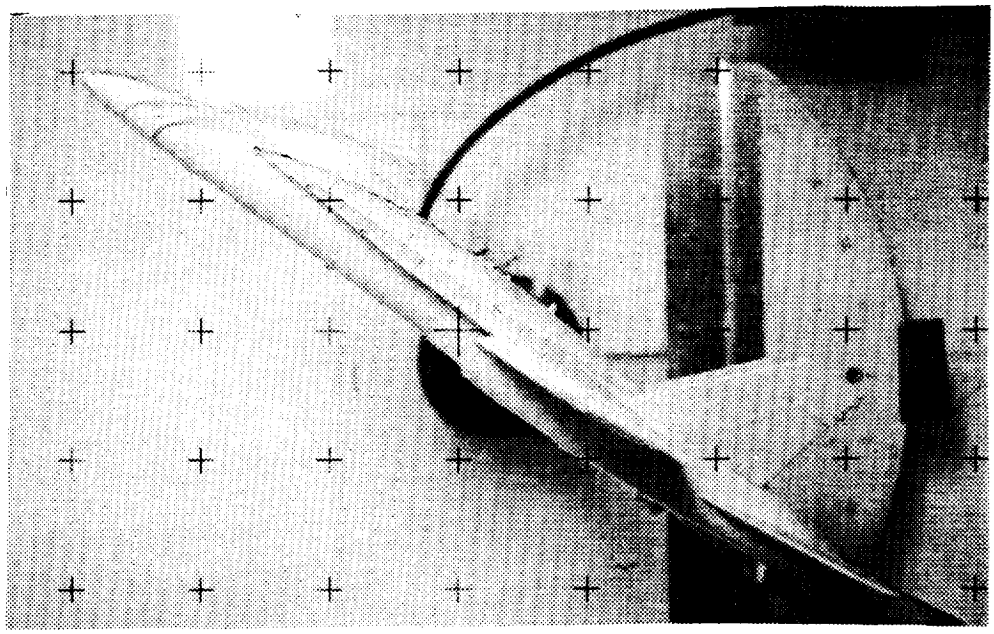

e) Alpha = 35 Degrees; Beta = 0 Degrees

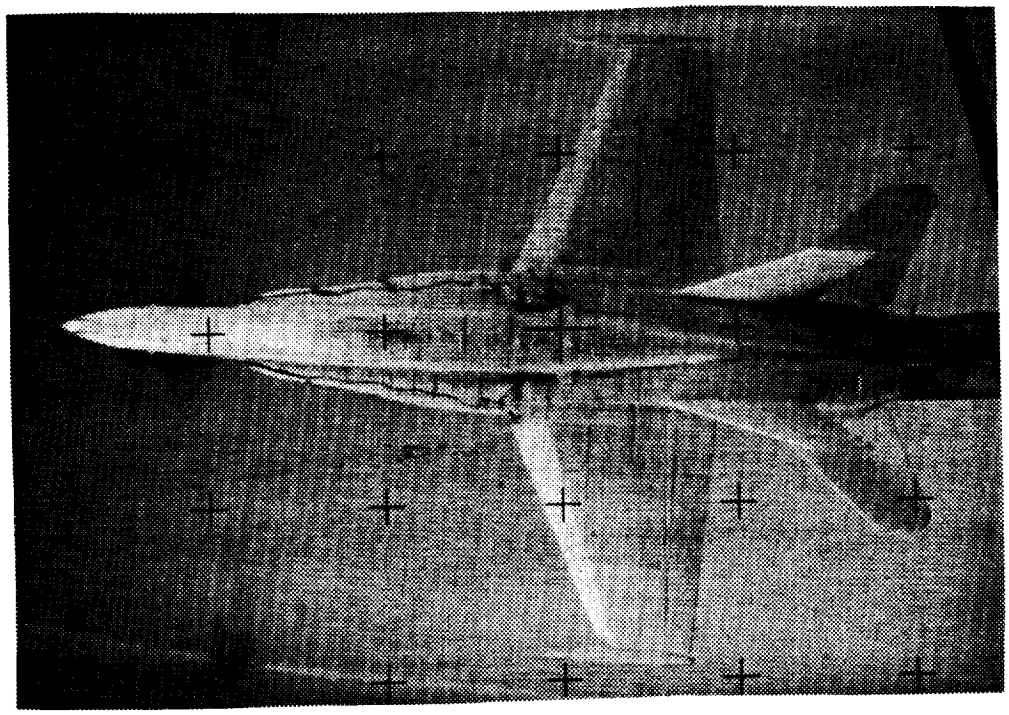

f) Alpha = 35 Degrees; Beta = 0 Degrees

Figure 26. Concluded

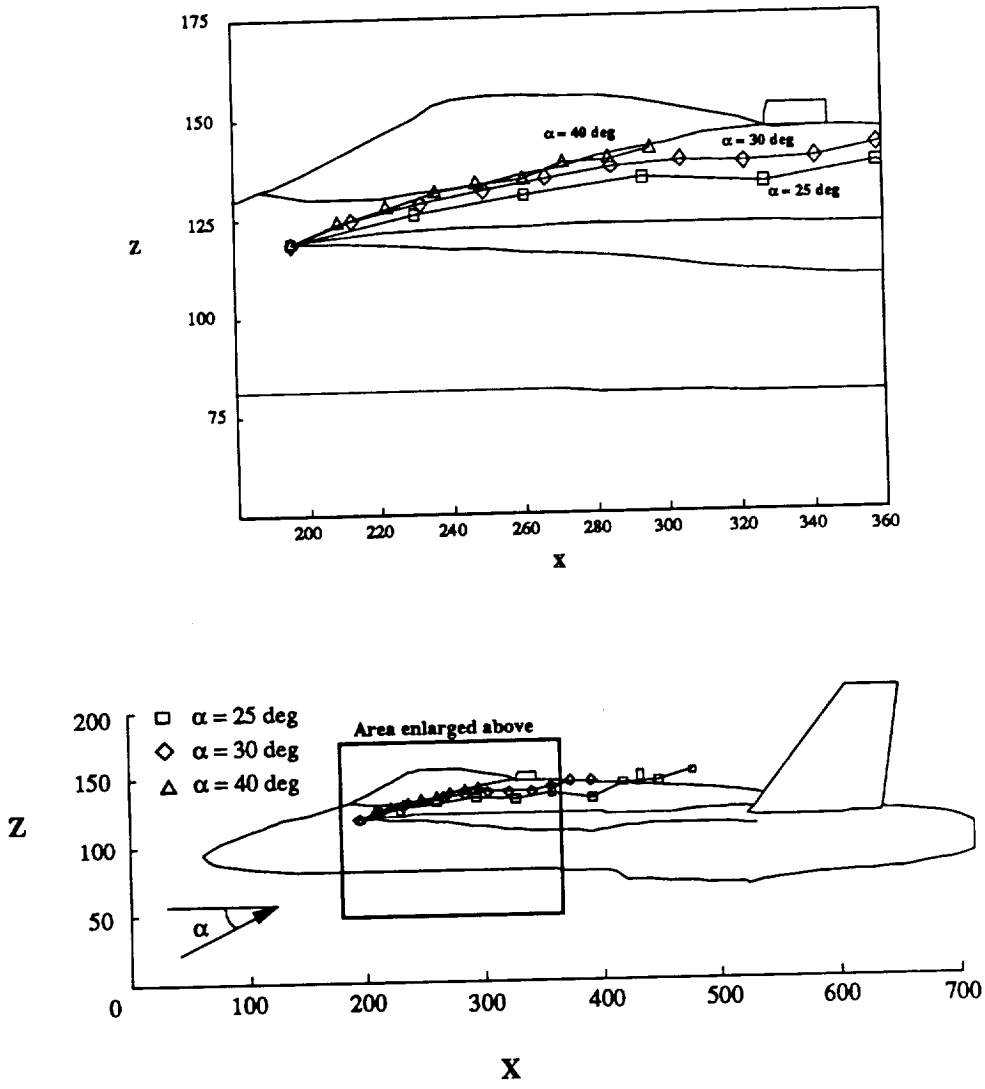

Figure 27. Effect of Angle of Attack (α) on the Vertical Location of the LEX Vortex Core. Angle of Sideslip $\beta = 0$ Degrees

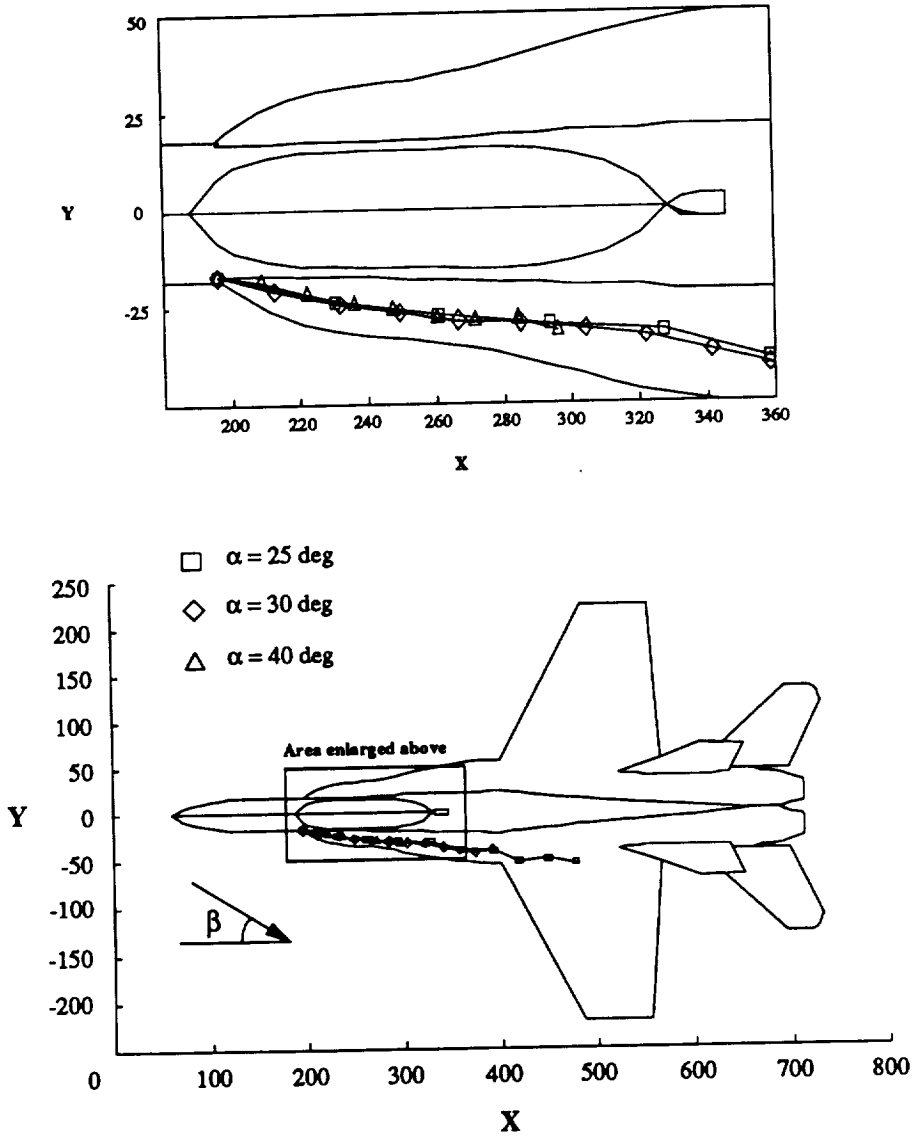

Figure 28. Effect of Angle of Attack (α) on the Lateral Location of the LEX Vortex Core. Angle of Sideslip β = 0 Degrees

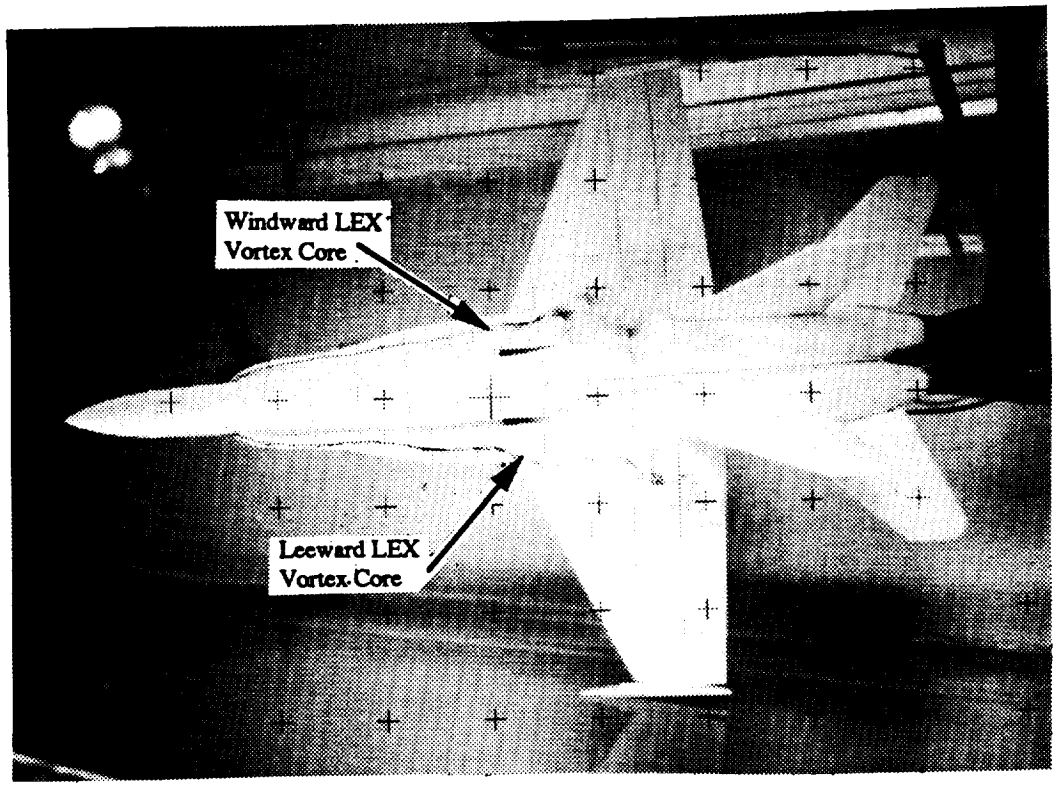

Figure 29. Effect of Angle of Sideslip on the Lateral Location of the LEX Vortices. Alpha = 25 Degrees; Beta = 5.5 Degrees

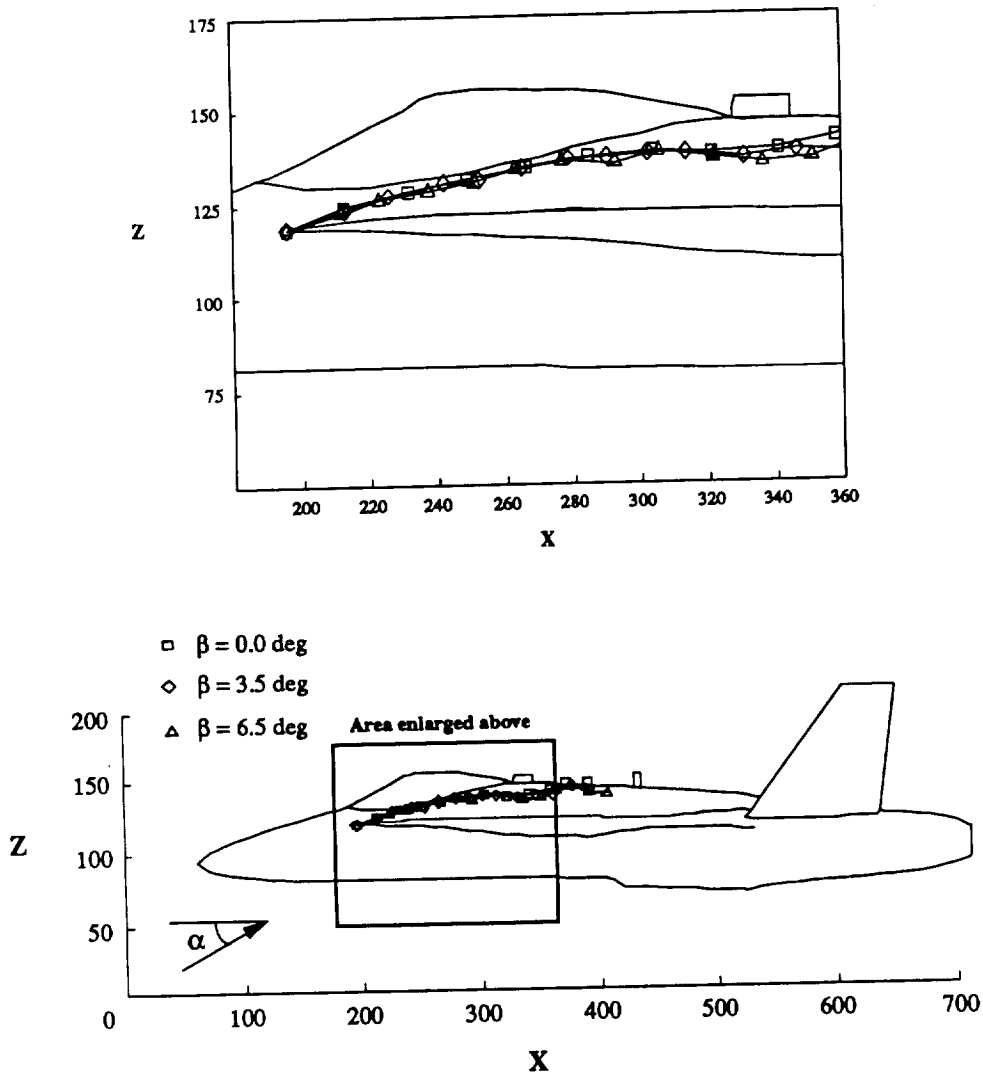

Figure 30. Effect of Angle of Sideslip (β) on the Vertical Location of the Leeward LEX Vortex Core. Angle of Attack α = 30 Degrees

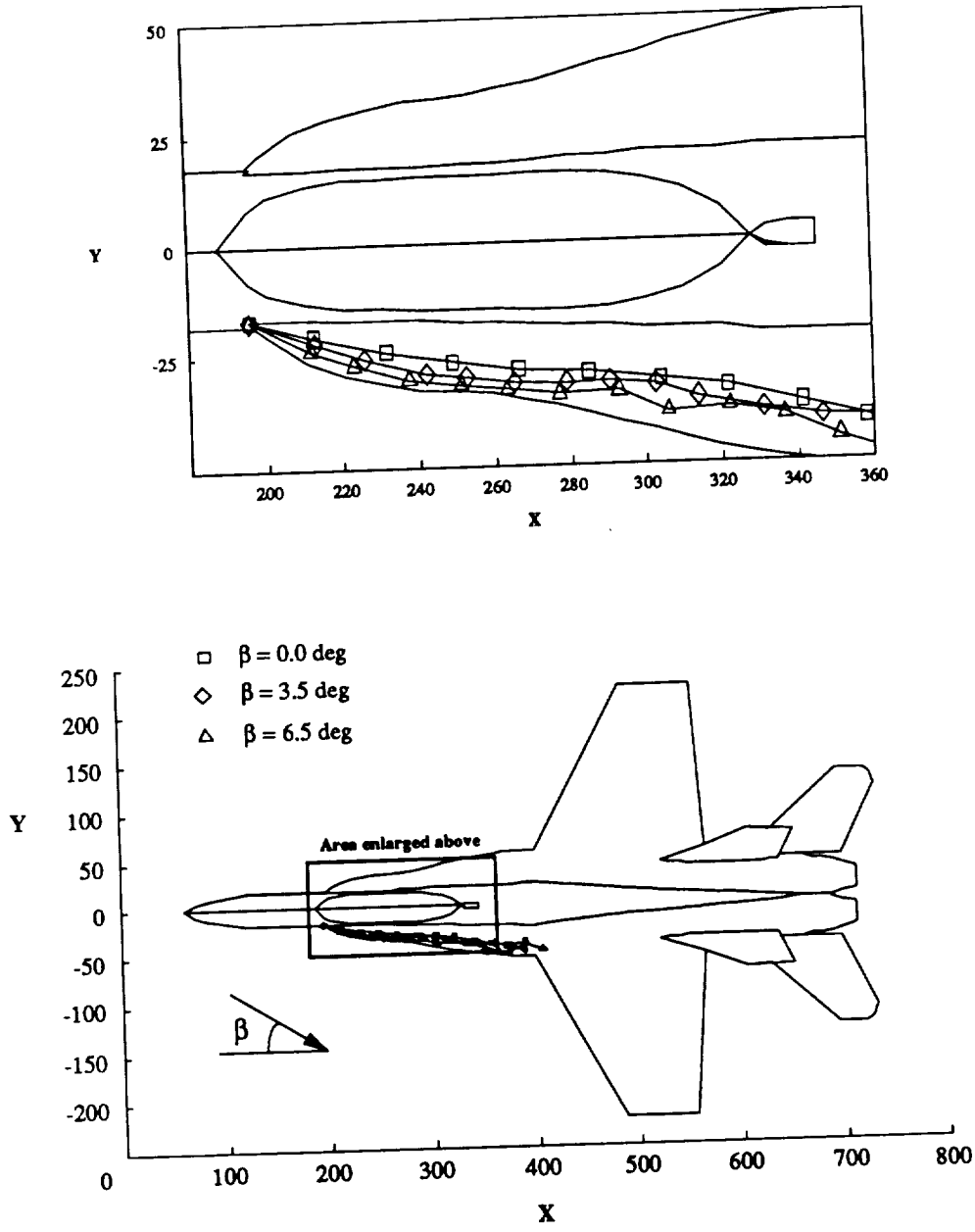

Figure 31. Effect of Angle of Sideslip (β) on the Lateral Location of the Leeward LEX Vortex Core. Angle of Attack α = 30 Degrees

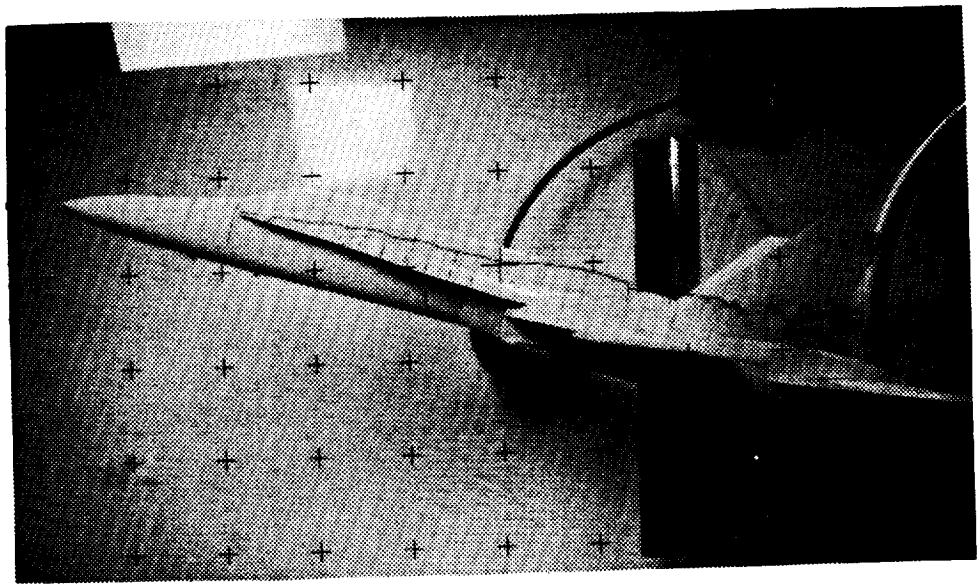

a) Alpha = 15 Degrees; Beta = 0 Degrees

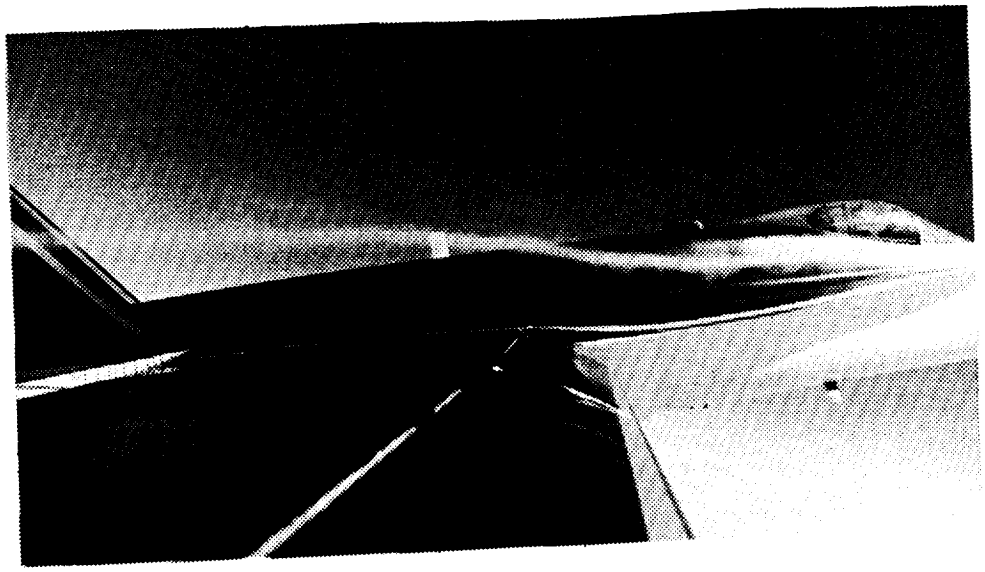

b) Alpha = 15.8 Degrees; Beta = 0.2 Degrees

Figure 32. Comparison of the LEX Vortex Core Location Between Water Tunnel and Flight Results

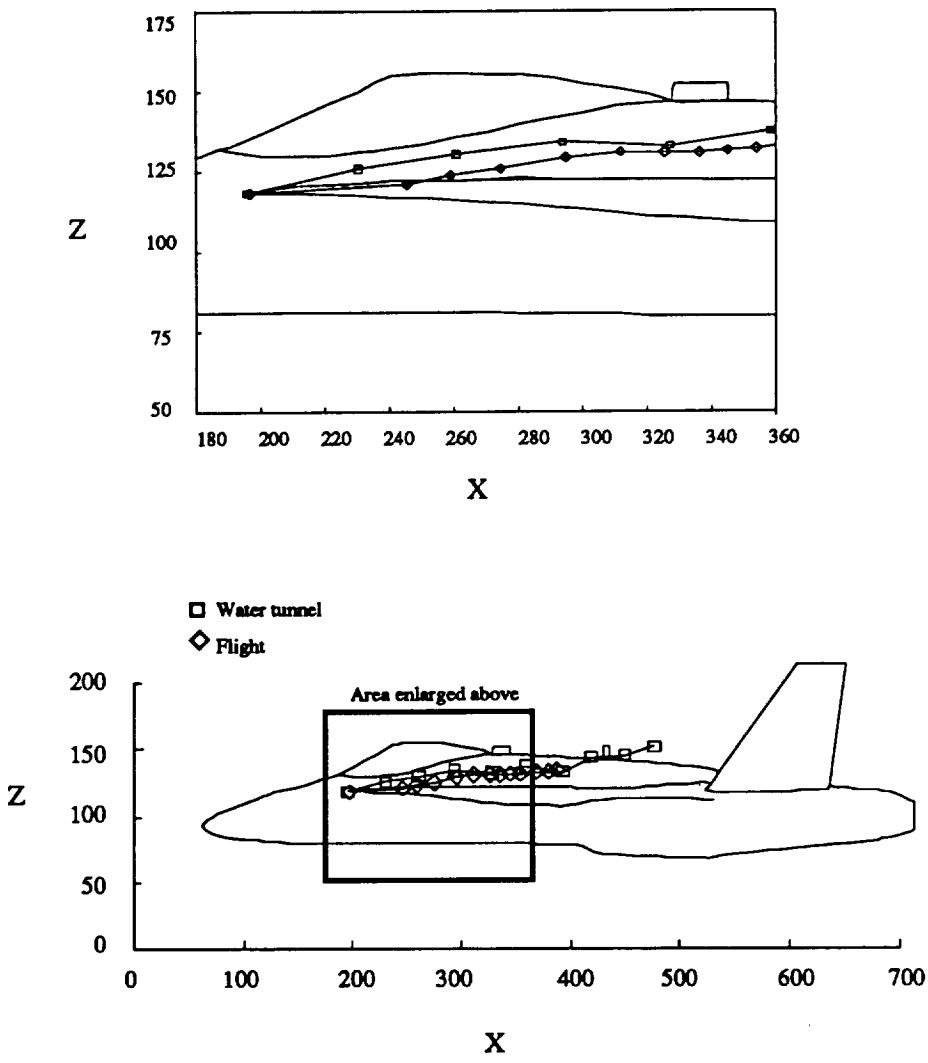

Figure 33. Comparison of the LEX Vortex Core Vertical Location Between Water Tunnel and Flight Data. Angle of Attack α = 25 Degrees; Angle of Sideslip β = 0 Degrees

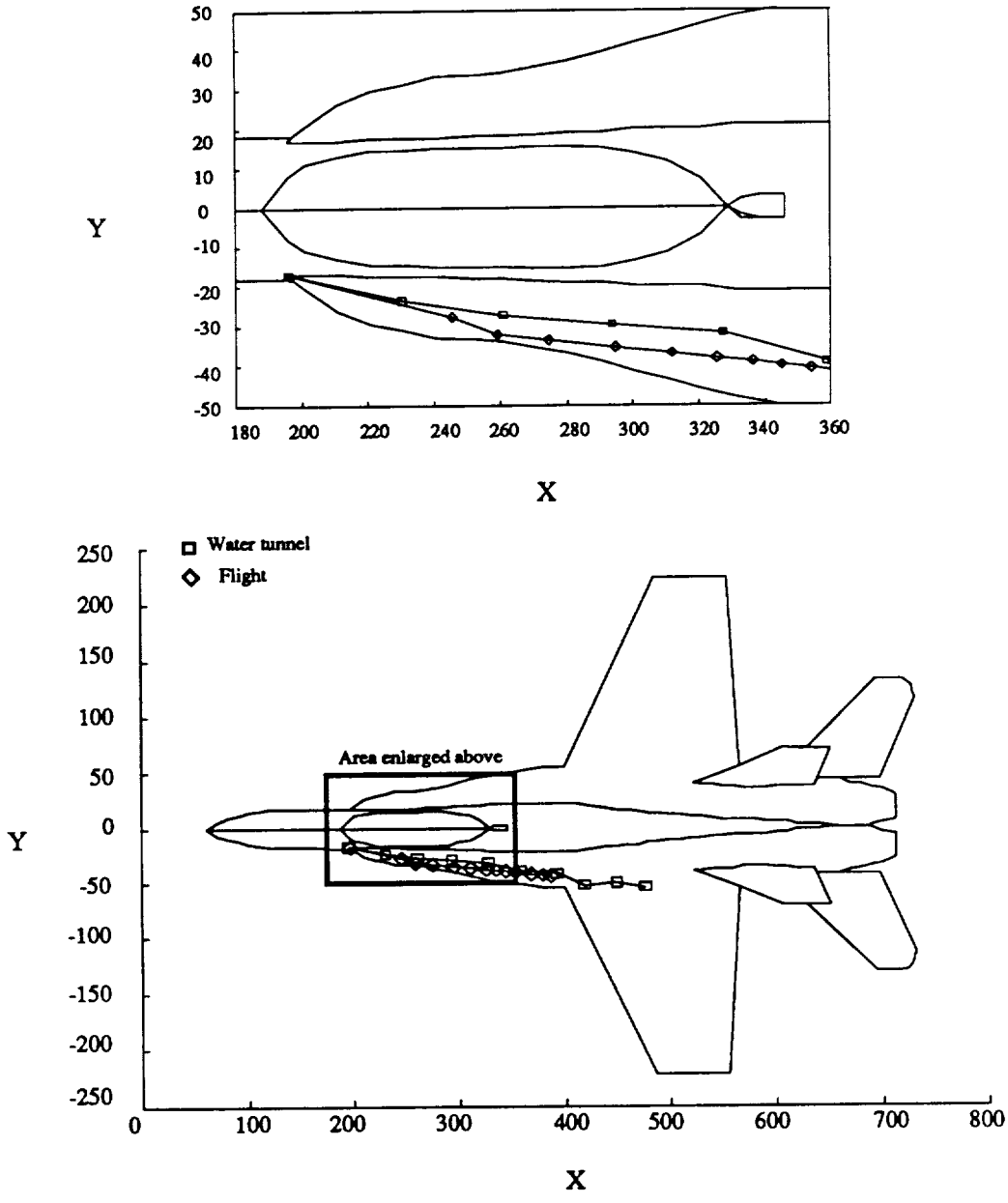

Figure 34. Comparison of the LEX Vortex Core Lateral Location Between Water Tunnel and Flight Data. Angle of Attack α = 25 Degrees; Angle of Sideslip β = 0 Degrees

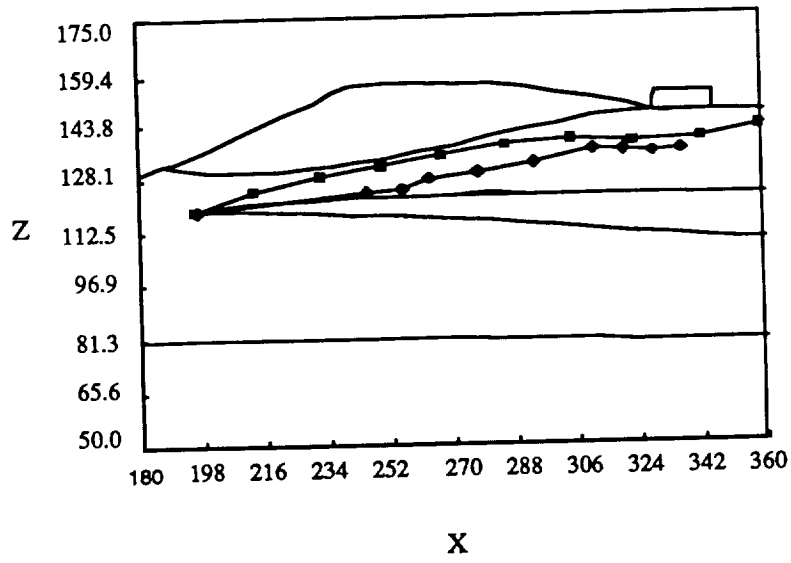

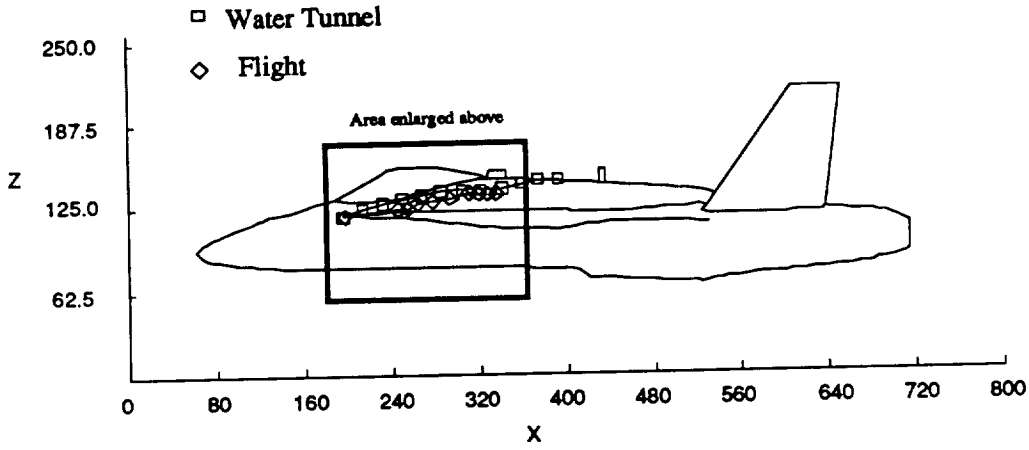

Figure 35. Comparison of the LEX Vortex Core Vertical Location Between Water Tunnel and Flight Data. Angle of Attack α = 30 Degrees; Angle of Sideslip β = 0 Degrees

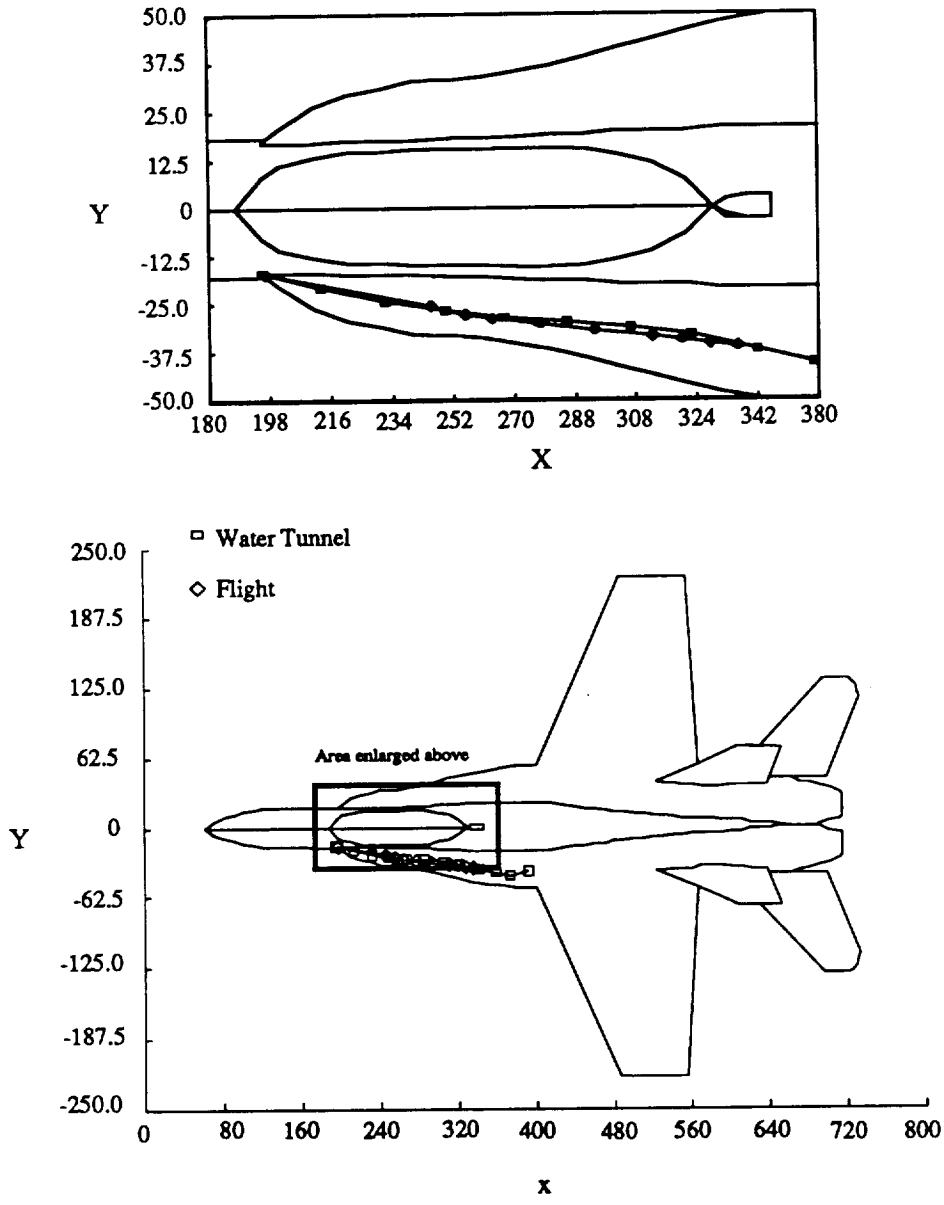

Figure 36. Comparison of the LEX Vortex Core Lateral Location Between Water Tunnel and Flight Data. Angle of Attack α = 30 Degrees; Angle of Sideslip β = 0 Degrees

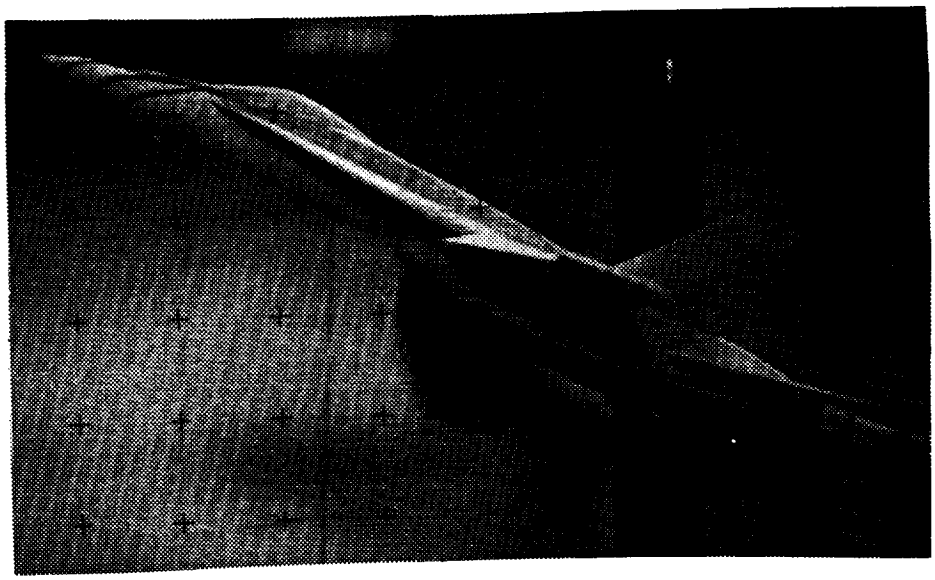

a) Side View

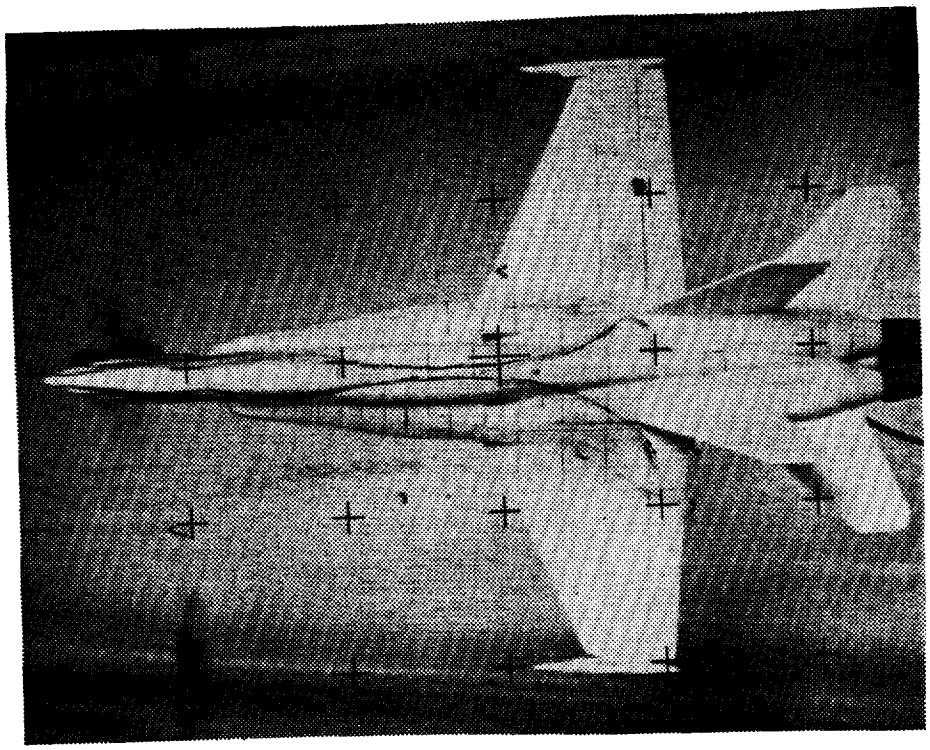

b) Top View

Figure 37. Location of Forebody Vortices. Alpha = 25 Degrees; Beta = 0 Degrees

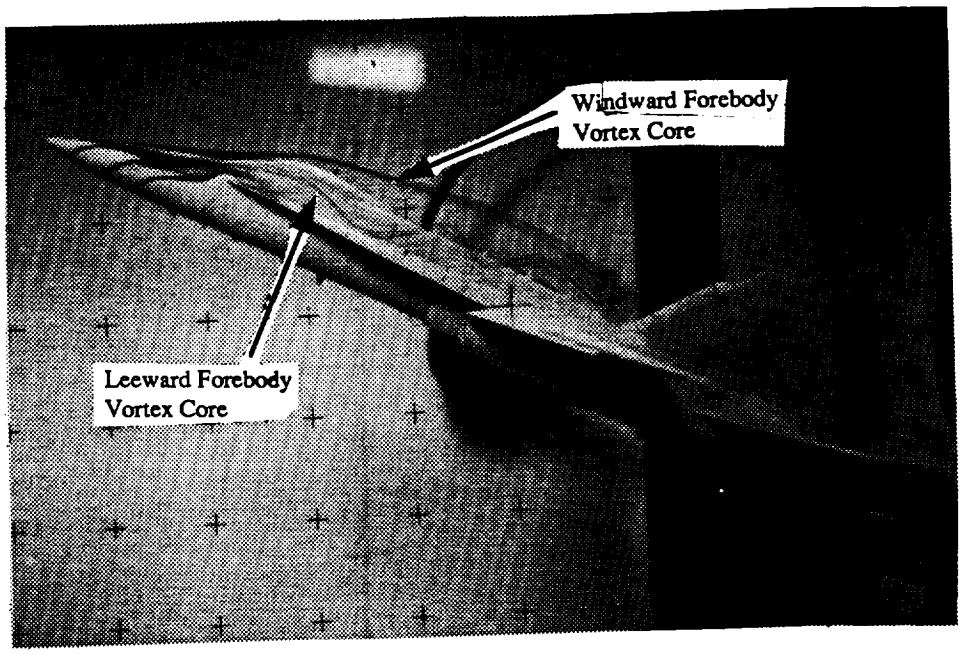

a) Side View

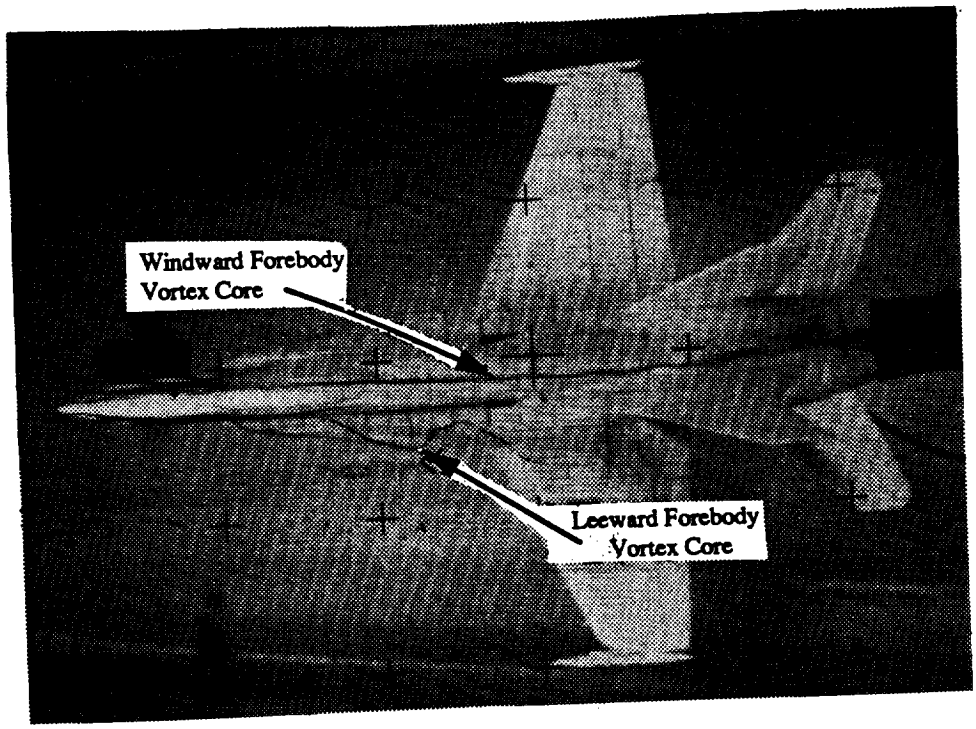

b) Top View

Figure 38. Location of Forebody Vortices (Effect of Angle of Sideslip). Alpha = 25 Degrees; Beta = 4.0 Degrees

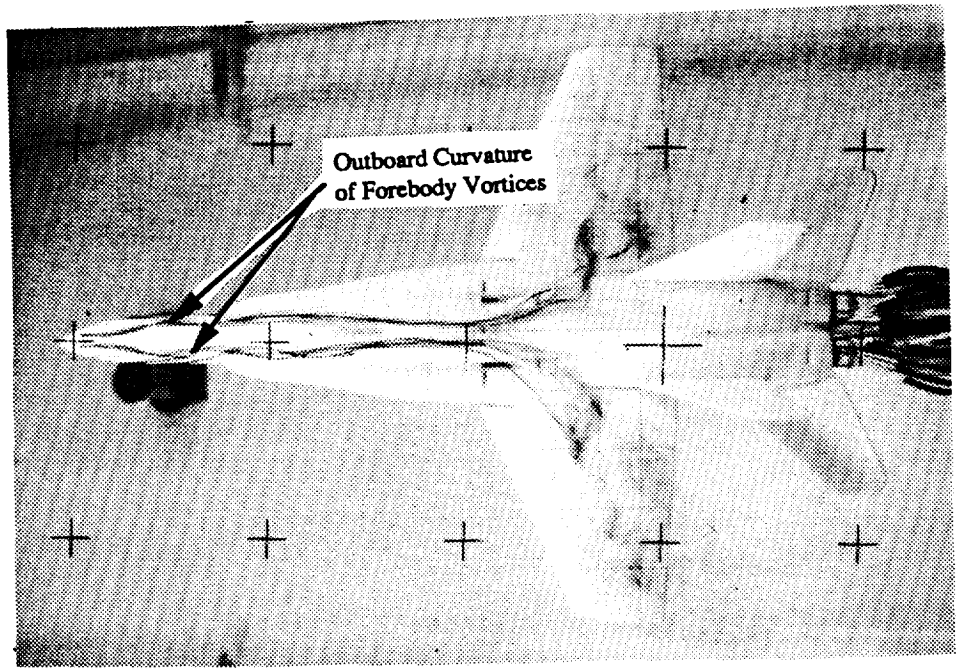

a) 48A Model

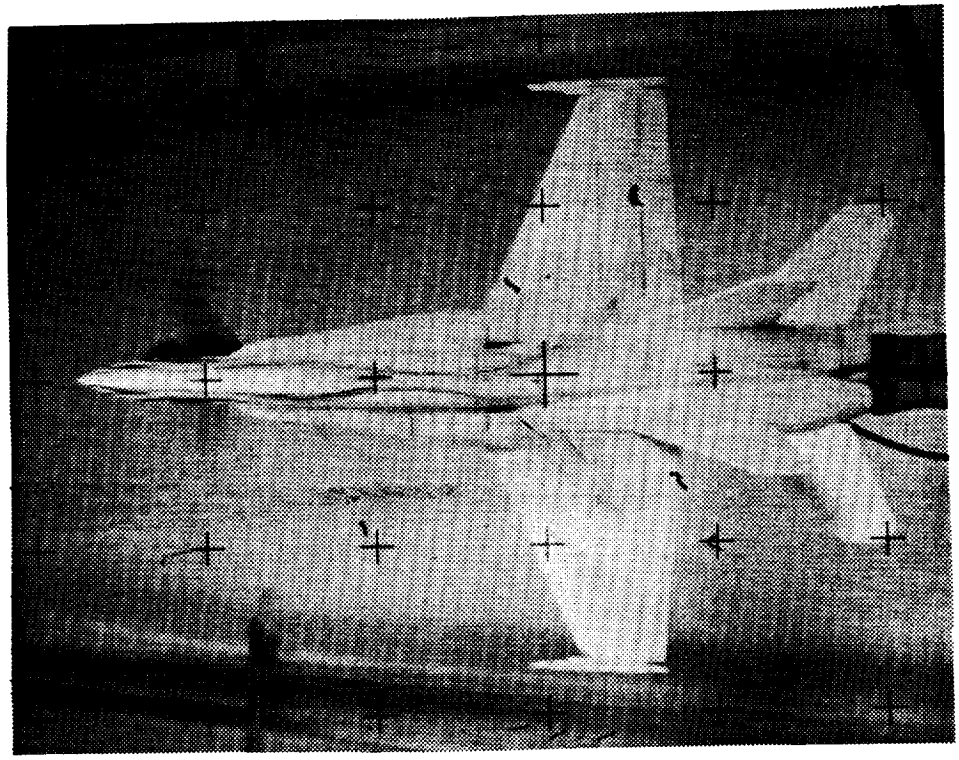

b) 48C Model

Figure 39. Location of Forebody Vortices (Effect of Forebody Geometry). Alpha = 30 Degrees; Beta = 0 Degrees

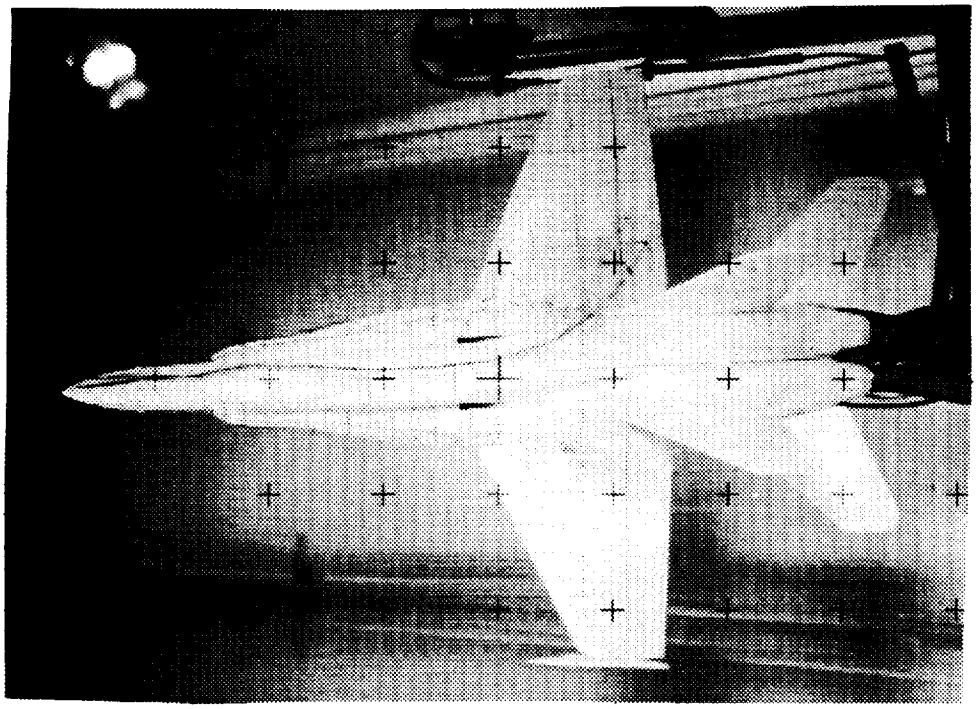

a) 32A Model

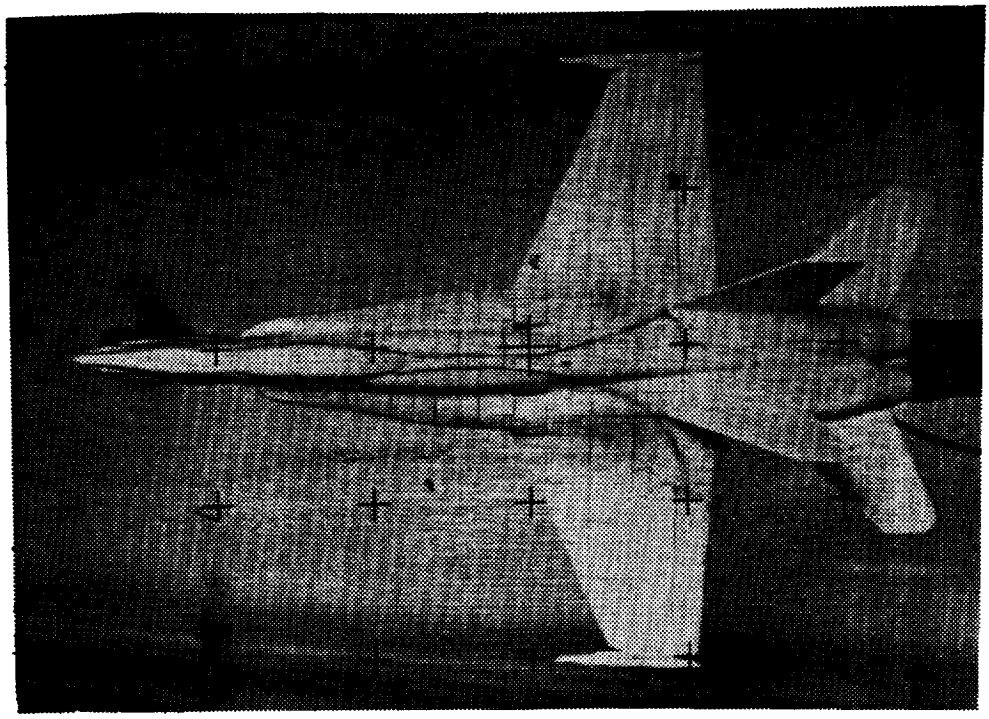

b) 48C Model

Figure 40. Location of Forebody Vortices (Effect of Model Scale). Alpha = 25 Degrees; Beta = 0 Degrees

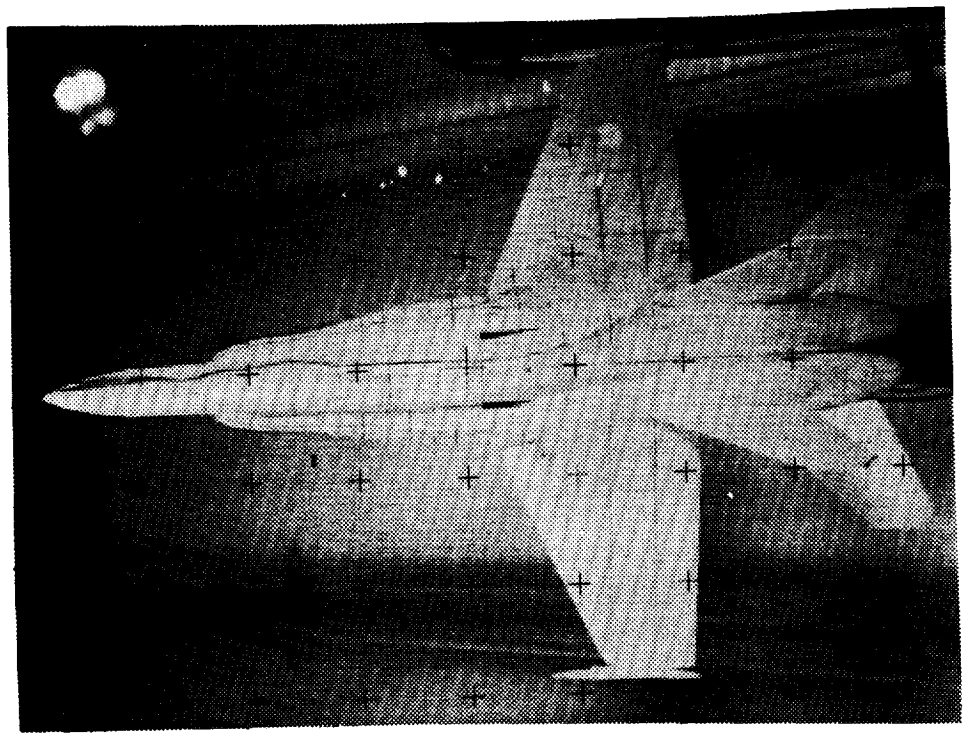

a) 32A Model

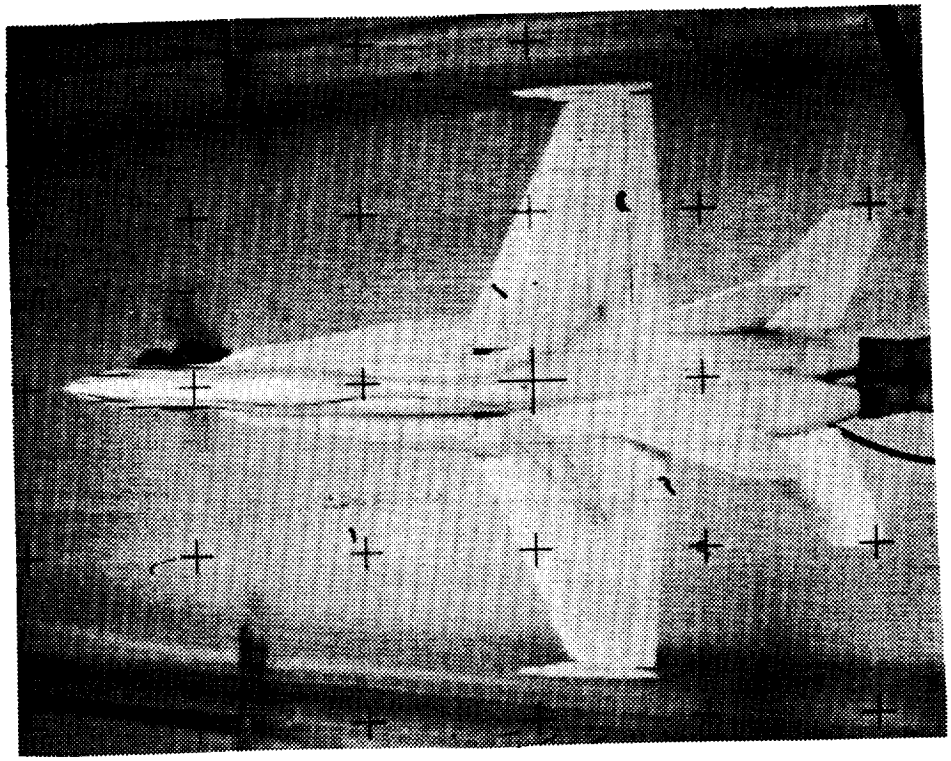

b) 48C Model

Figure 41. Location of Forebody Vortices (Effect of Model Scale). Alpha = 30 Degrees; Beta = 0 Degrees

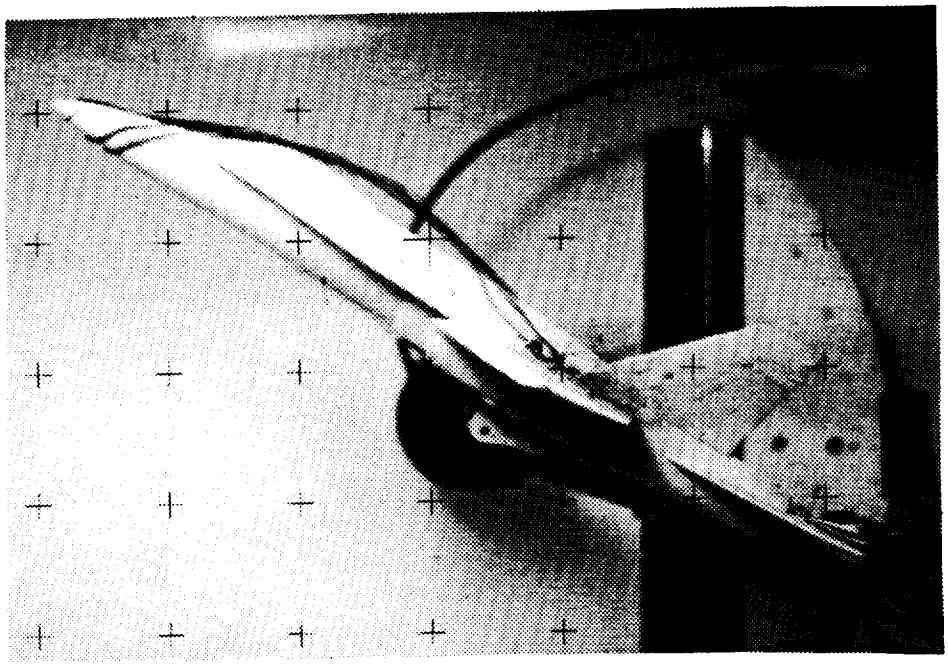

a) 48A Water Tunnel Model

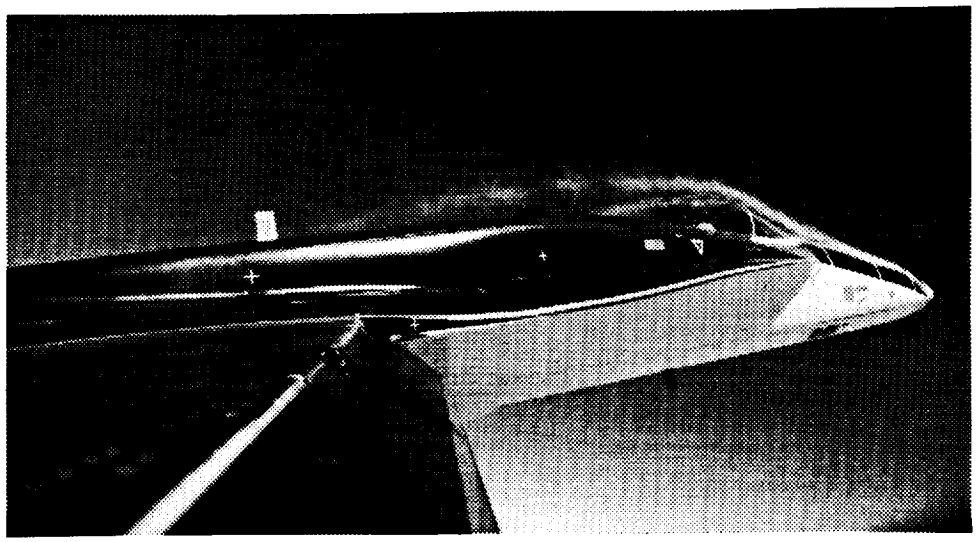

b) F/A-18 HARV

Figure 42. Comparison of Forebody Vortex Location Between Water Tunnel and Flight Results [Ref. 23]. Alpha = 30 Degrees; Beta = 0 Degrees

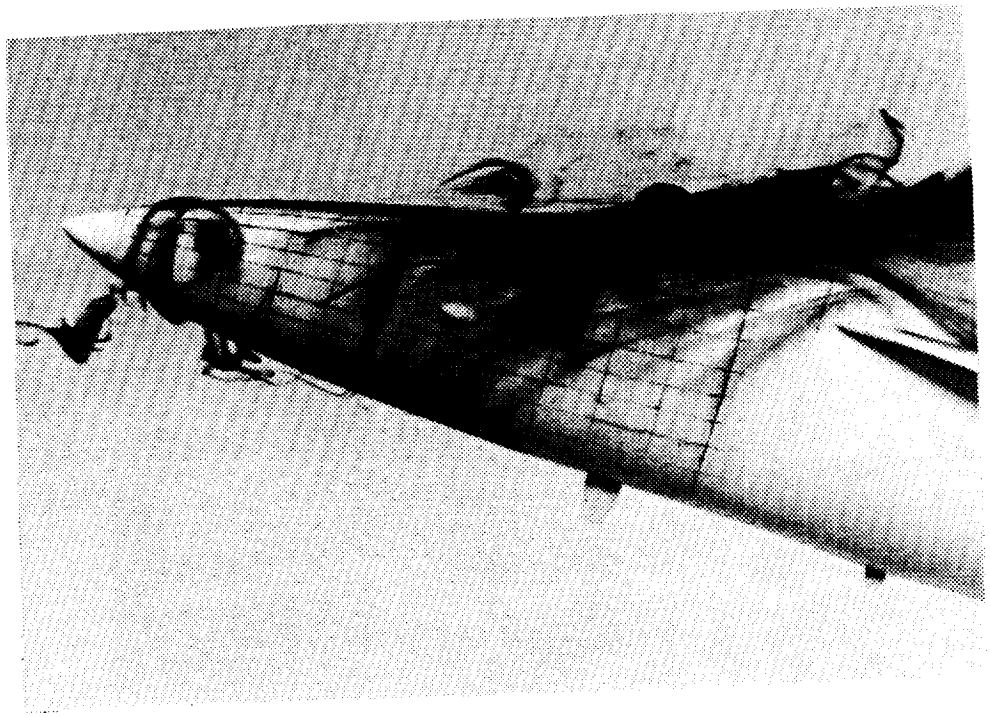

a) Side View of the Forebody

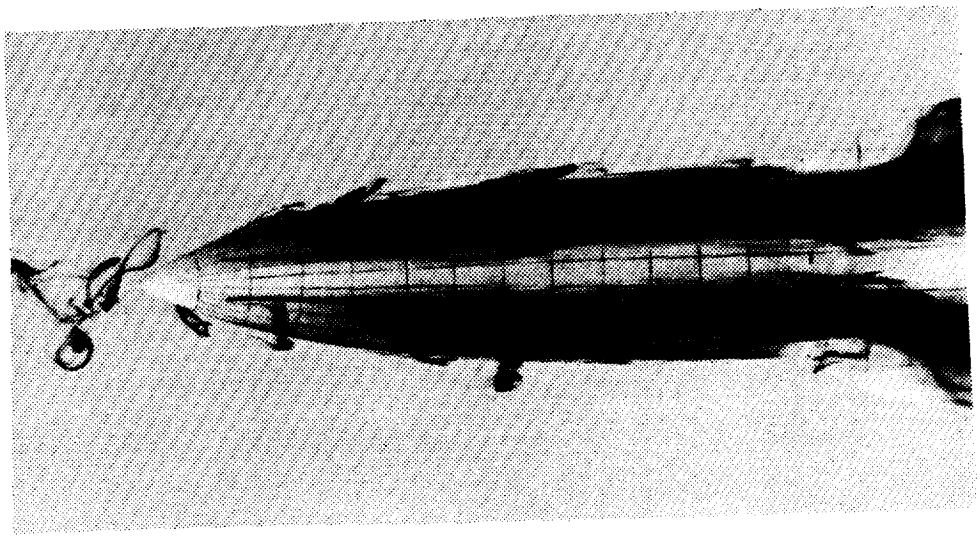

b) Top View of the Forebody

Figure 43. Forebody Surface Flow Visualization. Alpha = 20 Degrees; Beta = 0 Degrees

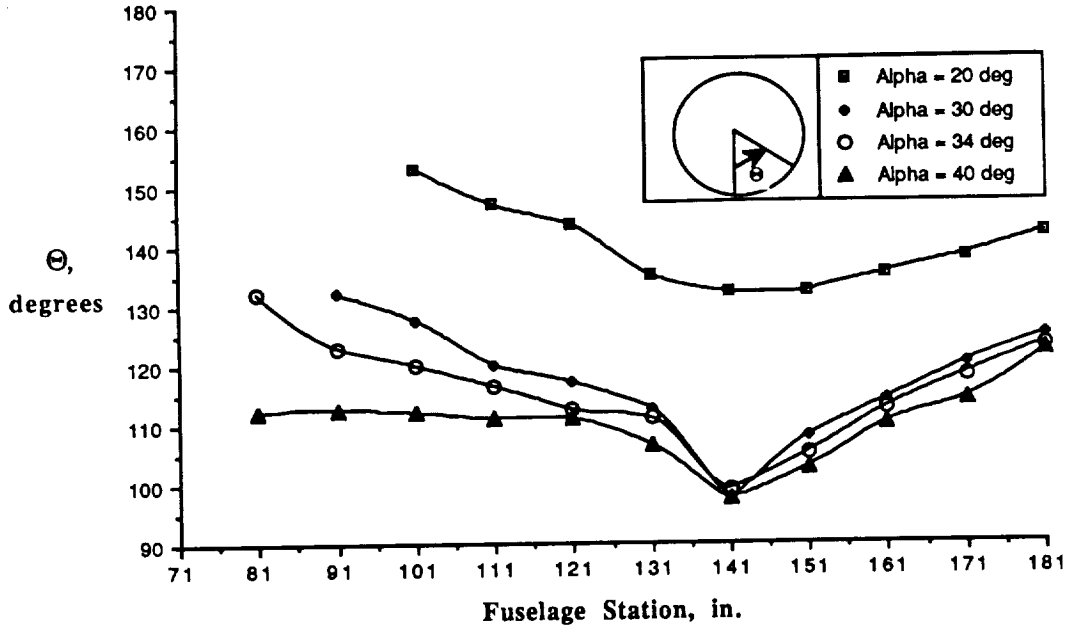

Figure 44. Effect of Angle of Attack on the Location of the Forebody Primary Separation Line

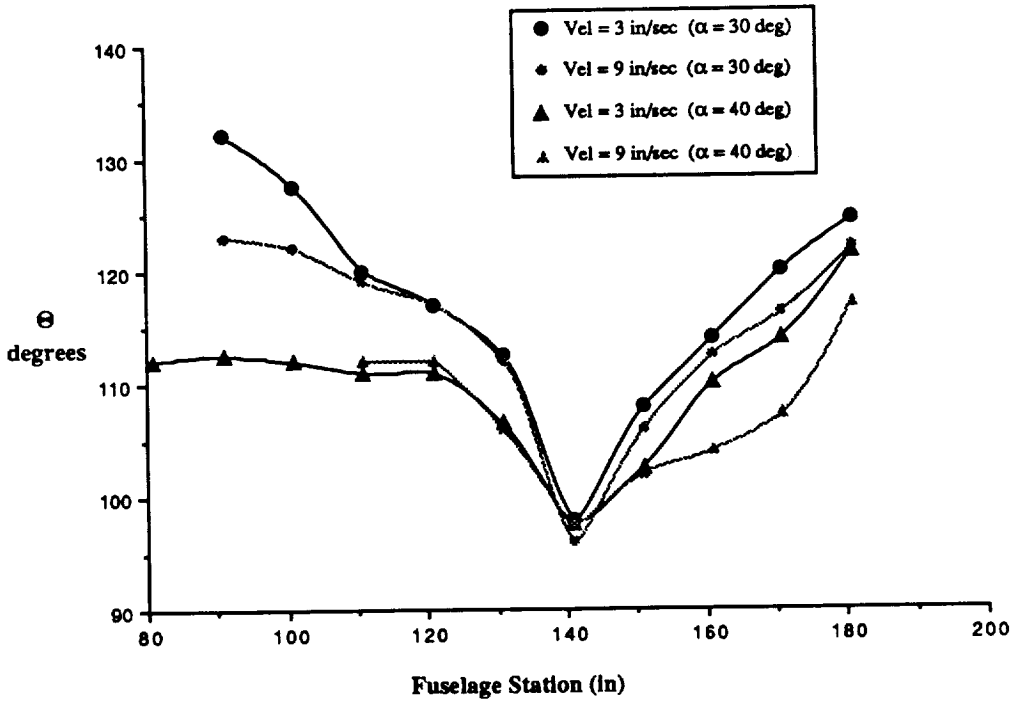

Figure 45. Effect of Reynolds Number on the Location of the Primary Separation Lines of the Forebody

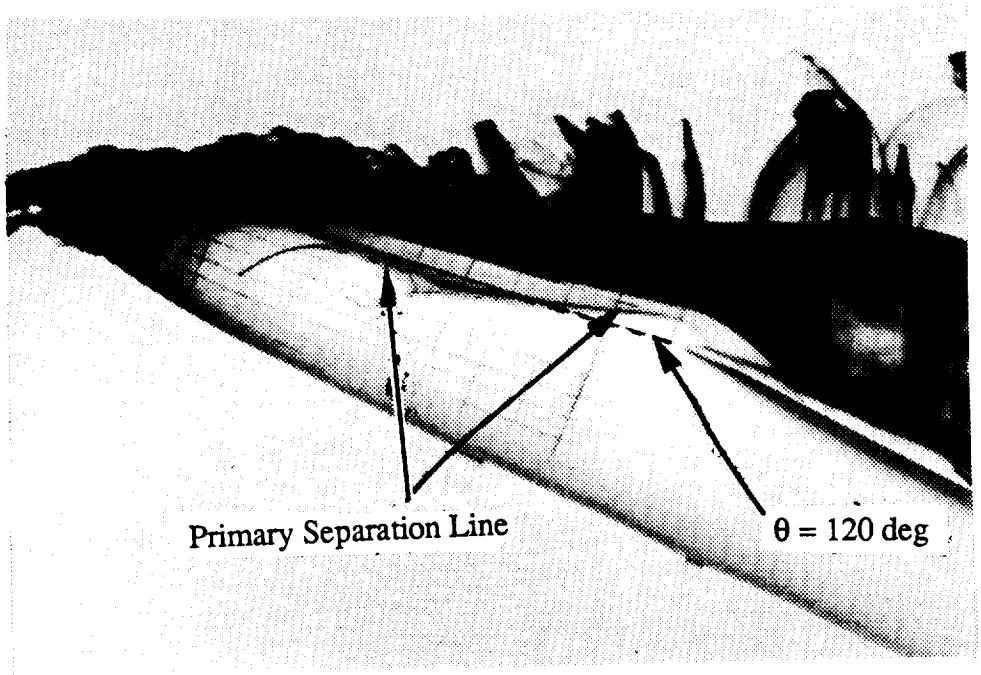

a) Water Tunnel Result

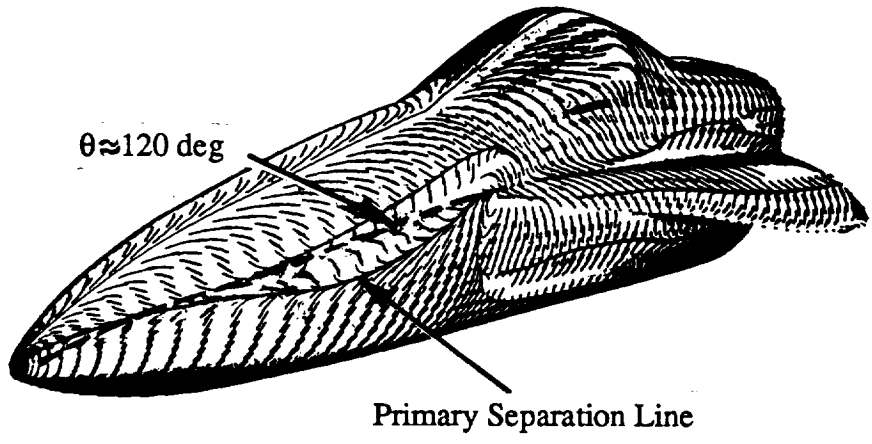

b) CFD Solution

Figure 46. Comparison of the Location of the Primary Separation Line Between Water Tunnel Results and a Laminar Flow CFD Prediction [Ref.34]. Alpha = 30 Degrees; Beta = 0 Degrees

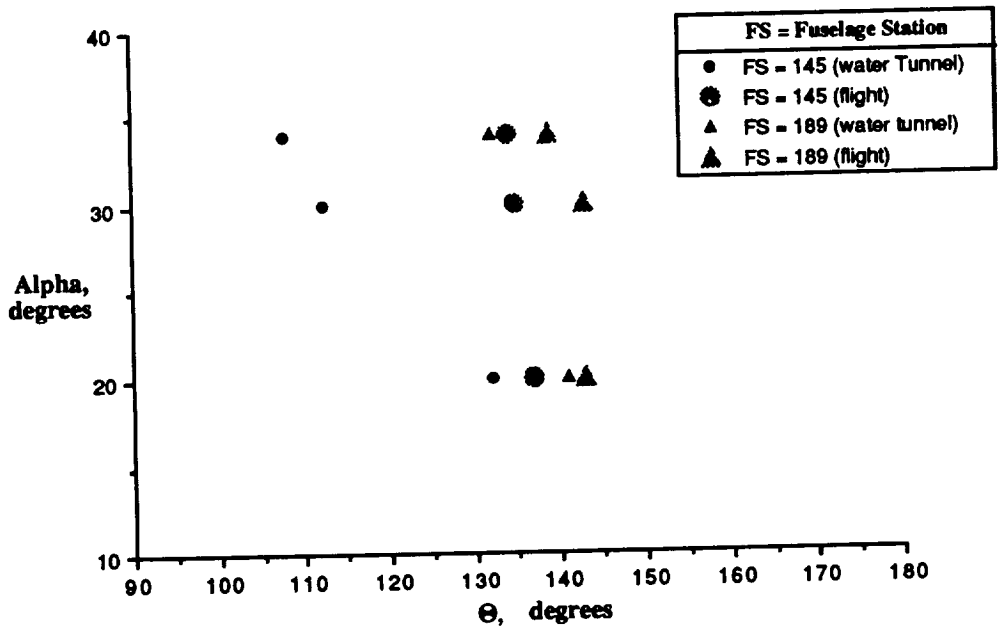

Figure 47. Location of Separation Lines From Water Tunnel and Flight Results

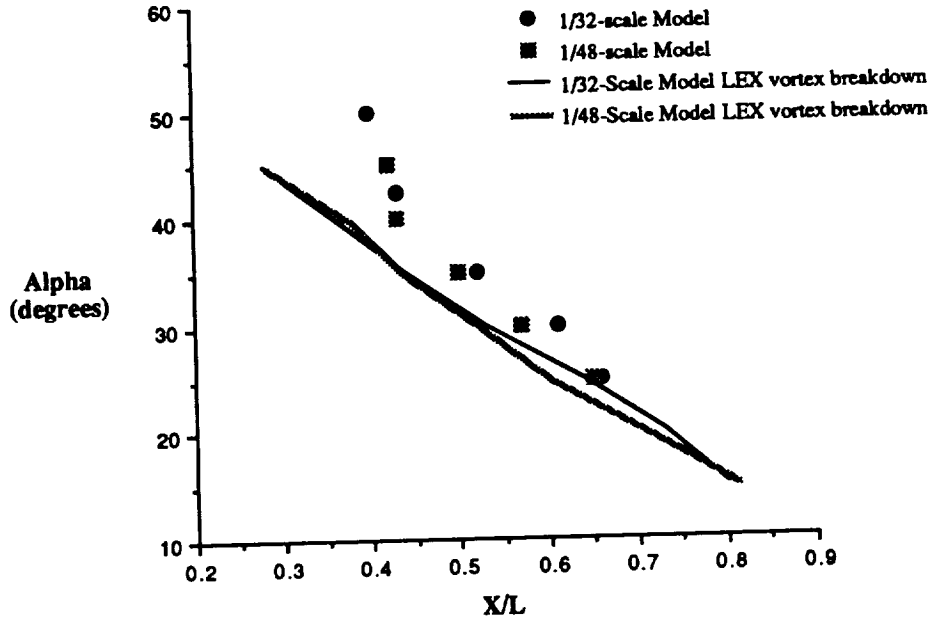

Figure 48. Longitudinal Location of LEX/Forebody Vortex Interaction and LEX Vortex Breakdown

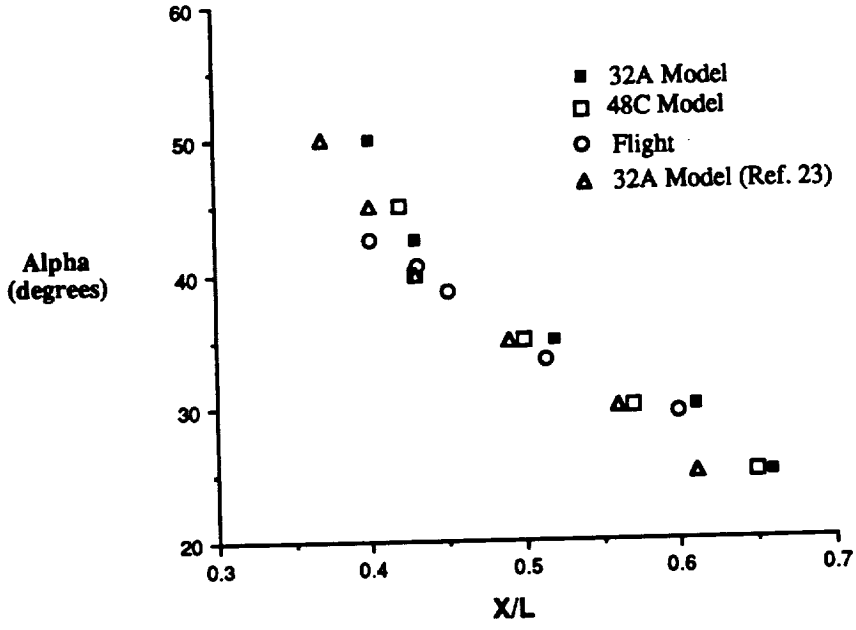

Figure 49. Longitudinal Location of LEX/Forebody Vortex Interaction From Water Tunnel and Flight Results

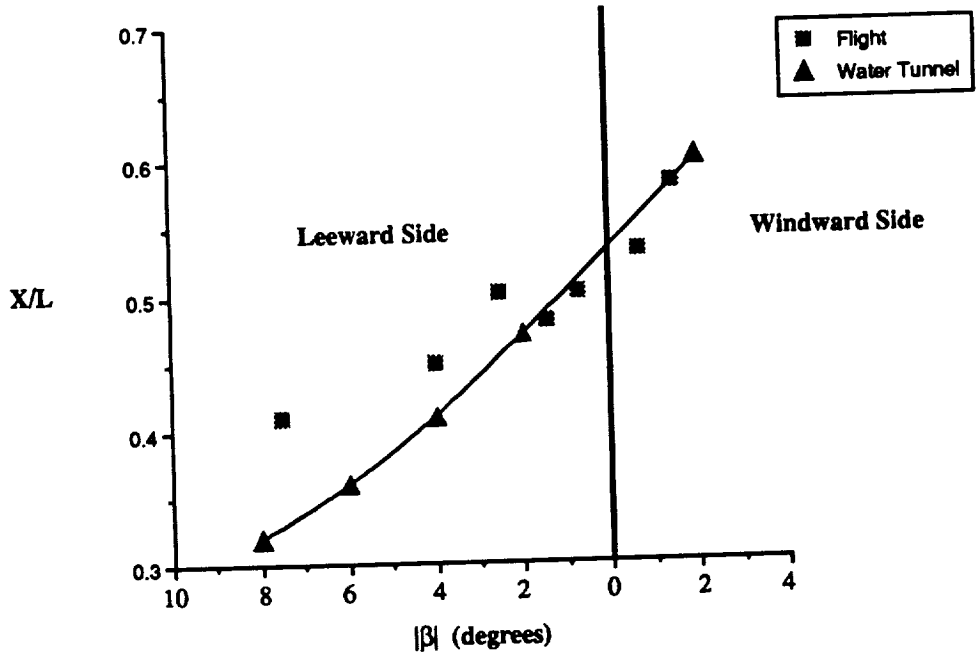

Figure 50. Comparison Between Flight-measured and Water Tunnel Results of the Longitudinal Location of the LEX/Forebody Vortex Interaction as a Function of the Angle of Sideslip β (α = 33 Degrees)

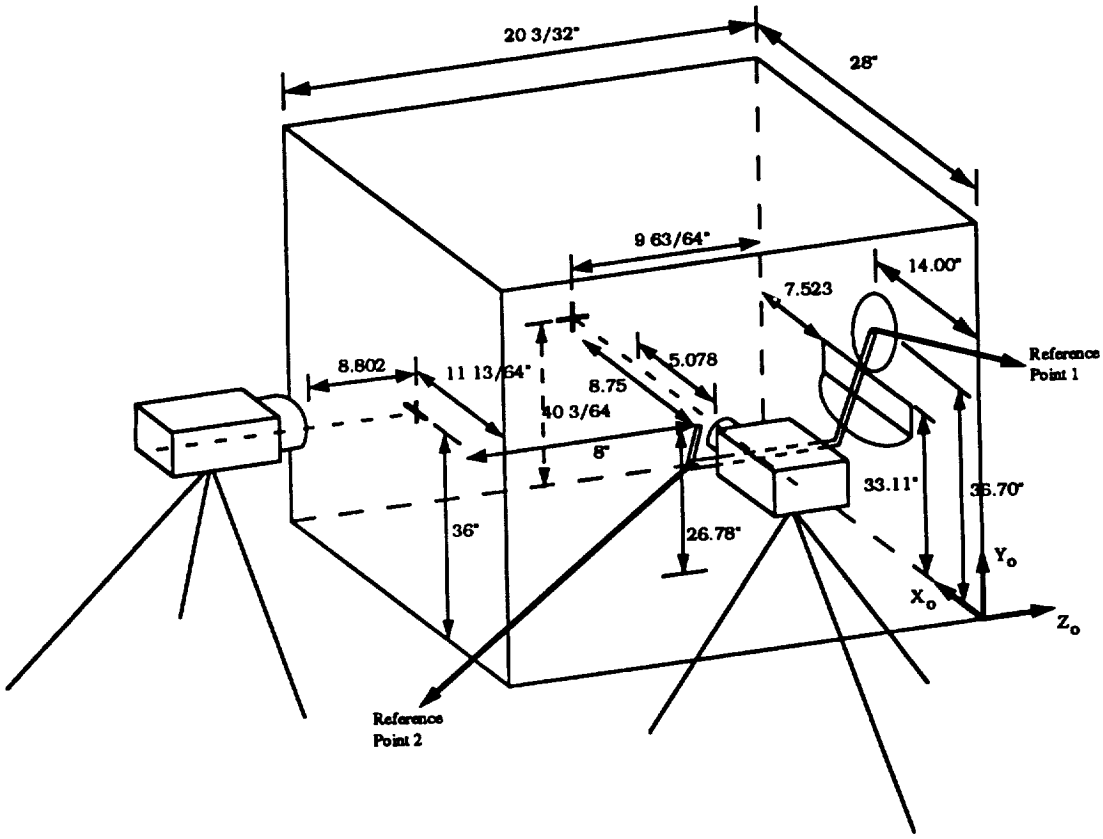

Figure B.1. Location of Cameras and Dimensions Needed for the Vortex Path Reconstruction Technique

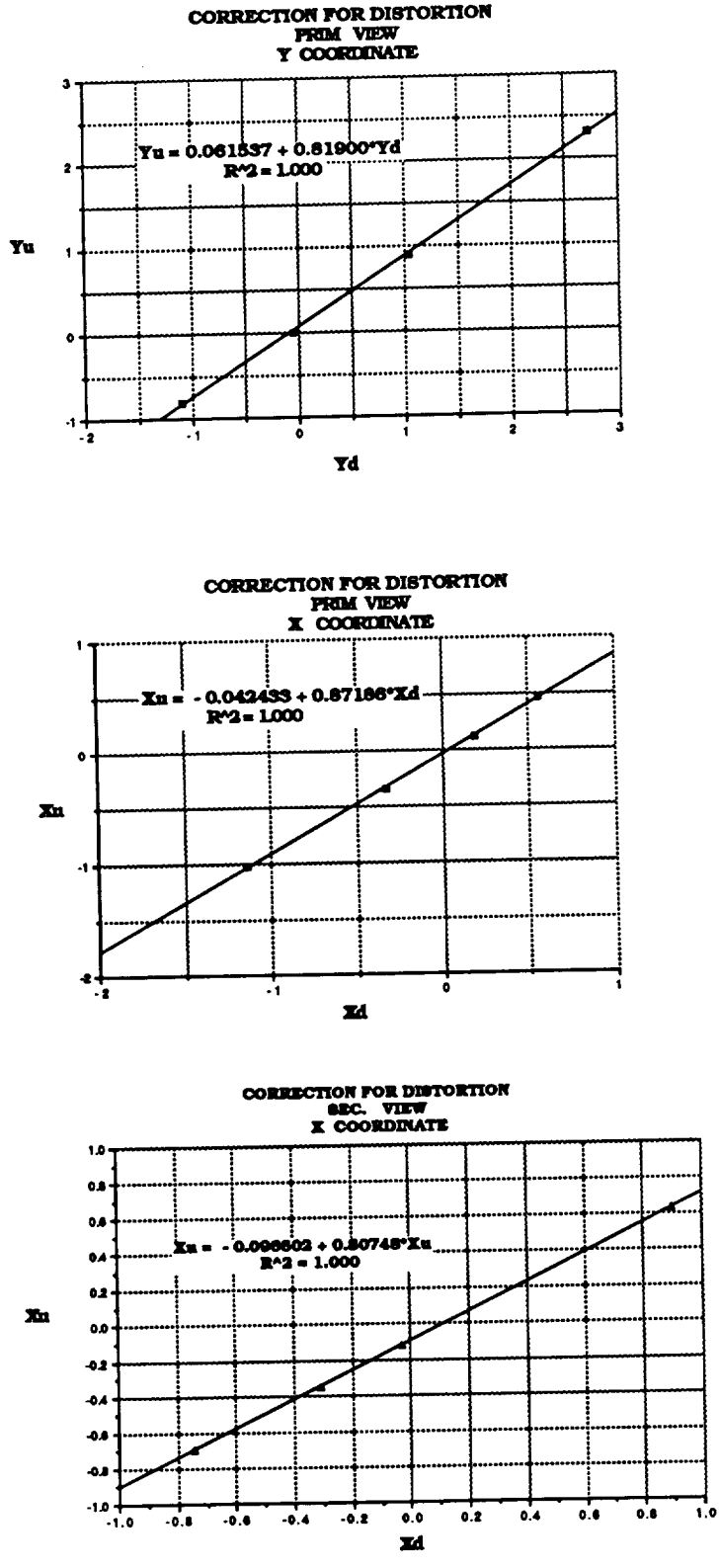

Figure B.2. Relationships Between Distorted (d) and Undistorted (u) Picture Coordinates (All Coordinate Values in Inches)

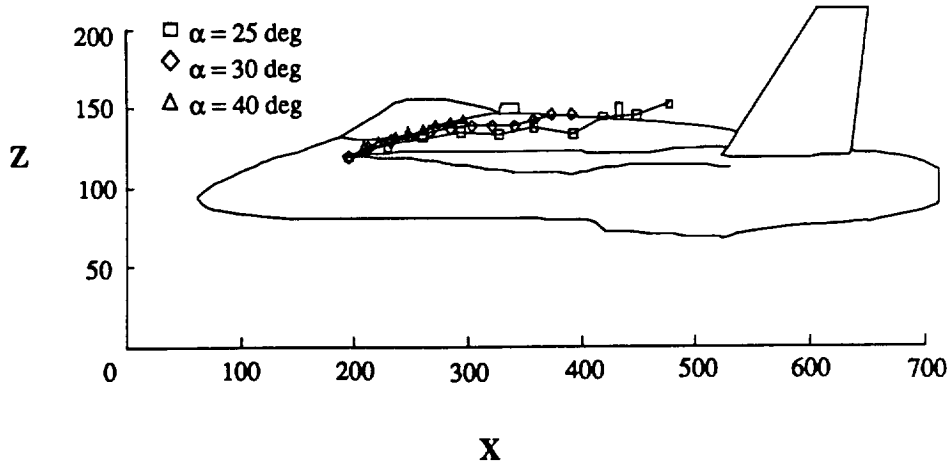

Figure B.3. Example of Results Obtained From the Vortex Path Reconstruction Algorithm